Doctoral Thesis

Predictive modeling and experimental analysis of the drilling process of Carbon Fiber Reinforced Polymer composite laminates

Jaewoo Seo

Department of Mechanical Engineering
(Mechanical Engineering)

Ulsan National Institute of Science and Technology

2021

Predictive modeling and experimental analysis of the drilling process of Carbon Fiber Reinforced Polymer composite laminates

Jaewoo Seo

Department of Mechanical Engineering
(Mechanical Engineering)

Ulsan National Institute of Science and Technology

Predictive modeling and experimental analysis of the drilling process of Carbon Fiber Reinforced Polymer composite laminates

A thesis/dissertation submitted to
Ulsan National Institute of Science and Technology
in partial fulfillment of the
requirements for the degree of
Doctor of Philosophy

Jaewoo Seo

12/10/2020

Approved by

Advisor
Hyung Wook Park

Predictive modeling and experimental analysis of the drilling process of Carbon Fiber Reinforced Polymer composite laminates

Jaewoo Seo

This certifies that the thesis/dissertation of Jaewoo Seo is approved.

12/10/2020

Signature

Advisor: Hyung Wook Park

Signature

Thesis Committee Member : Young-Bin Park

Signature

Thesis Committee Member : Namhun Kim

Signature

Thesis Committee Member : Sang hoon Kang

Signature

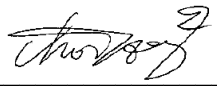

Thesis Committee Member : Hae-Jin Choi

ABSTRACT

Predictive modeling and experimental analysis of the drilling process of Carbon Fiber Reinforced Polymer composite laminates

Jaewoo Seo

Doctor of Philosophy in Engineering

Ulsan National Institute of Science and Technology

Carbon fiber reinforced plastic (CFRP) is promising composite material which is a combination of carbon fiber and polymer matrix. CFRP has been actively utilized in the aerospace, automobile, and sport goods due to their superior mechanical properties. High strength-to-weight ratio is one of the biggest advantages of CFRP composite laminates which contribute to development of lighter structural component with abundant strength and stiffness. Although CFRP materials are fabricated in the near-net shape, they still demand the post processing such as drilling, trimming and surface finishing processes to be used as a final product. Among them, the drilling is the most frequently used process for assembly and joining of the components. However, anisotropic and non-homogeneous characteristics of CFRP composite make the drilling process much more difficult than general metallic materials. Above adversities include the reduced life of drill bit with excessive tool wear by materials and leads to defect occurrence in the composite workpiece. Therefore, investigation of optimal process parameters is essential to overcome the adverse effect which can be appeared during drilling process and to make high quality CFRP hole.

This study aims at predictive modeling of drilling process of CFRP composite to understand mechanism of force and defect generation. Predictive modeling can be divided into two sections, analytical and numerical studies for a deeper understanding of the process.

First, experimental studies were conducted to investigate to figure out the process parameters affecting the drilling process of CFRP composites. Machining process involved with multiple factors, such as machine tool dynamics, tool geometry, material properties, and cutting conditions. Especially,

fiber volume fraction, and thermo-mechanical properties of CFRP composite was also considered in the study. Cutting force, and delamination were observed with dynamometer, optical microscope and computational tomography image. It was observed that both thrust force and delamination were intensely related to the feed, and diameter of drill bit. Fiber volume fraction also contribute to the magnitude of cutting force and force changes in time domain. Support plate showed prevention effect of delamination without affecting the cutting force and tool wear.

Second, an analytical investigation of the drilling forces for unidirectional CFRP composites according to different machining parameters. Analytical modeling focused on the prediction of thrust force, which was a force generated in the drilling feed direction. Process parameters were selected considering the geometry of drill bit, cutting conditions, and material properties for the accurate calculation. In the analytical modeling in light of drill bit, the chisel edge region is classified as an extrusion operation and the lip is considered as an orthogonal small-element cutting region. The chipping, pressing, and bouncing regions of the lip are incorporated into this thrust force model. In addition, the analytical model includes the thermophysical properties of CFRP by incorporating softening of the material due to heat generation during the cutting processes. Based on the developed model, the thrust force curve for all drilling stages is analyzed in time-domain considering both cutting conditions and material properties. Comparison between predictions and experiments was performed on three CFRP samples (USN 150Y, USN 150B, and USN150E) with different fiber volume fractions and sixteen cutting conditions. It was observed that the predicted forces can capture the trend of the experimental data with the error of the minimum and maximum percentage error for USN 150Y was 12 to 29%, 19 to 36% for USN 150B, and was 16 to 33% for USN 150E. Time-domain analysis and fluctuation evaluation were also used to better understand the mechanism of thrust force during CFRP drilling.

Finally, investigation of the delamination of CFRP composites laminates during the drilling process has been conducted. When drilling the CFRP laminates, delamination is one of the severe defects that degrade the quality of CFRP products. However, delamination is the damage propagation inside the material which demand numerical analysis to observe stress-strain behavior. Therefore, finite element model of CFRP drilling was developed using commercial FE software to simulate the damages generated in the cohesive zone between the interface of laminates. Drilling simulation and tests were conducted to analyze effect of feed, spindle speed, and back-up plate on delamination as well as the thrust force. Before the delamination analysis, calculated thrust force results were validated by the experimental results to assure the accuracy of simulation. Delamination of the FE model were assessed by the evaluating damage criterion value of cohesive zone between the composite laminate plies. Quantified delamination factors of simulation were compared to the experimental results which acquired and processed by computational tomography image and image processing techniques and showed good agreement.

TABLE OF CONTENTS

LIST OF FIGURES

LIST OF TABLES

NOMENCLATURE

A_d	area of delaminated area
A_0	area of hole
$D_{\max}$	Diameter of circular delaminated zone
D_0	Diameter of hole
F_d	Delamination factor
E_3	young's modulus of CFRP in transverse direction
v_{13}	Poisson's ratio of CFRP
R_1	radius of drill bit
dF_{chi}	elemental cutting force of chisel edge
dF_{chr}	elemental cutting force of chisel edge in radial direction
dF_{cha}	elemental cutting force of chisel edge in axial direction
dF_x	cutting force in orthogonal cutting system
w	web thickness of drill bit
K_{ch}	coefficient of chisel edge
n	spindle speed[revolution/sec]
f	feed[mm/rev]
γ_0	rake angle of the cutting lip region
γ_w	chisel edge angle
γ_f	feed angle
r_{chi}	radius of the chisel edge
ε_d	Point angle of drill bit

ψ	rake angle of the chisel edge
τ_1	shear strength perpendicular to the fiber direction
τ_2	shear strength parallel to the fiber direction
θ	equivalent fiber orientation
a_c	clearance angle of the tool
β	friction angle of the rake face of the tool
ϕ	shear angle of the cutting element of the cutting lip section
θ_r	helix angle of the drill bit varying along the cutting lip section
ϕ_1	web angle in the direction normal to the axis of the drill bit
θ_h	helix angle of the drill bit
r_e	radius of the fillet of the cutting lip
μ	friction coefficient between the tool and the workpiece
$P(T)$	mechanical property at the temperature T
P_0	mechanical property at the room temperature
V_f	fiber volume fraction of CFRP
T_g	glass transition temperature
T_d	decomposition temperature

1. Introduction

1.1. Research background and motivation

Over the past decades, there have been extensive use of composite materials replacing general metallic materials. Especially, Carbon Fiber Reinforced Polymer (CFRP) composite material lead the development of technologies of aerospace, defense, automotive, and sport goods sectors with their superior mechanical properties such as high strength-weight-ratio, higher corrosion resistance, and improved fatigue performance. [1-4] For example, the amount of composite materials used in Boeing 787 Dream-liner estimated to over 50% of the airplane weight. Gradual increase of global demand of carbon fiber has been reported by Carbon Composites e.V (CCev) and the AVK as shown in Fig. 1-1. According to their report, 95% of carbon fiber utilized in the form of CFRP composite material in various industries. In addition, annual growth of CFRP market is forecast to at least 13% with the extensive use and cost reduction. [5, 6]

CFRP composite materials are generally fabricated in the near net shape with various production process, however, they still require post-processing to be the final product/component. Post-process includes the hole making, edge trimming, and surface finishing. Among them, hole machining has been extensively required to the fabricated CFRP components to assemble and join to the other components. [7-16] To ensure the strong and precise riveted and bolted joints for the joining/assembly operation, high quality machined holes are essential without the damage and defects on the machined material. There have been several unconventional attempts to machine hole such as, water-jet machining, laser machining, and electrical discharge machining. [17, 18] Mechanical drilling process has been the common and reliable process to make hole with high productivity and relatively low cost in the manufacture industries. [19, 20] However, mechanical drilling operation exposed to the adverse effect by anisotropic, un-homogenous, and highly abrasive characteristics of CFRP composite materials. [7, 8, 21-23] As shown in Fig. 1-2, various defects, such as fiber pull-out, dimensional error, spalling, and delamination can be generated by drilling process. Delamination is the most severe defects occurred in the material related to the fractures into layers, and that degrade the strength and decrease life of

composite materials. To avoid the delamination and make high quality hole, understanding of drilling mechanism and prediction of optimal process parameters for drilling process are essential. In previous studies, the CFRP drilling with drill bit has been experimentally studied. [7, 9, 23-26] Those studies investigated the effect of process parameters (such as spindle speed, feed, drill bit geometry, and material properties) to the machined hole. However, understanding of mechanism and observation of behavior of workpiece during the process was unable. In addition, there have been few studies to predict the mechanical behavior of workpiece during the drilling process. Therefore, an understanding of the process through predictive model is required for high quality and defect free drilling process.

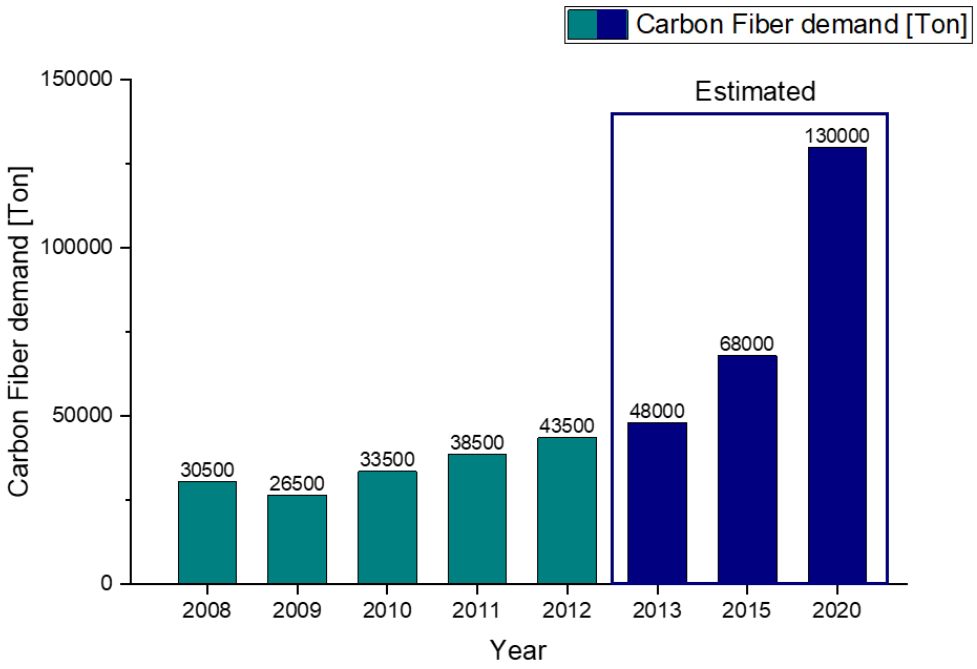

Figure 1-1. Global demand growth of CFRP material

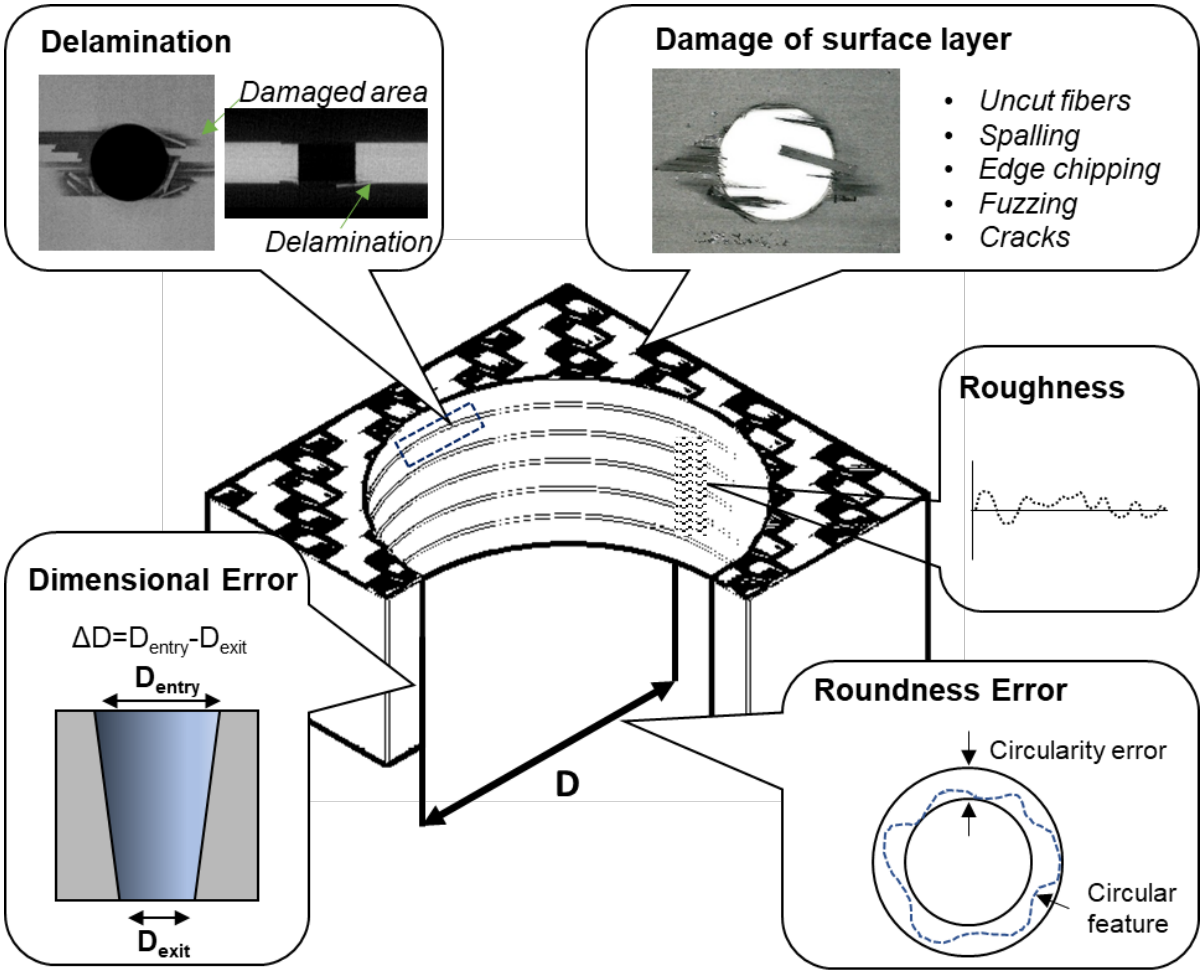

Figure 1-2. Quality criteria of machined hole of CFRP

1.2. Research objectives

The overall objectives of this study are to investigate the effects of process parameters on the cutting forces, and delamination, and to develop the predictive model to simulate force change on drilling process and behavior of damage propagation in the CFRP composite laminates. Ultimately, this study aims at developing the accurate delamination prediction model validated by the various experimental conditions. More detailed objectives of this study are as follows:

- ✓ To investigate the effect of process parameter to the cutting force and delamination occurred during the CFRP drilling process, and find the major process parameter such as, drill bit geometry, material properties, and cutting conditions.
- ✓ To develop the analytical model with understanding of fundamentals of CFRP drilling mechanism for reliable cutting force simulation for whole drilling process considering the major process parameters.
- ✓ To develop the numerical model to predict the damage propagation and delamination for CFRP composite laminates with finite element method with appropriate material constitutive and damage model construction.
- ✓ To validate the accuracy of prediction models and establish the appropriate assessing method for quantified delamination considering the damage behavior inside the composite materials.

1.3. Outline of This Work

This thesis is composed of a total of six chapters. Chapter 1, 2, and 6 are the introduction, the overview of CFRP drilling characteristics and mechanism, and summary, respectively. Major research achievements and discussions are presented in Chapter 3, 4, and 5.

Chapter 3 investigated the effect of process parameters on the CFRP drilling process. In this chapter, tool geometry, material properties, and cutting conditions were selected as the major process parameters which need to be observed. Cutting force and delamination ratio results were acquired to figure out the effect of process parameters. Major parameter for the predictive method were chosen based on the parameter analysis from experiment.

Chapter 4 investigated the effects of major process parameters on cutting force using the analytical model. Fundamental cutting model was studied and implemented to the drilling motion of drill bit considering the tool geometry, and cutting conditions. Material characteristics of composite material was also implemented to simulate force changes during the whole process.

Chapter 5 investigated the effect of major process parameters on the cutting force and damage behavior in the CFRP materials using numerical model. Finite element method was employed to observe the material behavior during the drilling process. Constitutive material and damage model were constructed to implement material characteristics of CFRP composite laminates.

Finally, the end part of the chapter 4, and 5 investigated the accuracy of the predictive models with experimental validation. The cutting force changes during the whole process time calculated by both analytical and numerical model was validated with varying cutting conditions. In addition, the method to assess the delamination was developed by using minimum damage value for FE results. The experimental delamination factor results were acquired by computational tomography image and calculated through the image processing technique, thereby validating the delamination factor of the predictive model. The outline of this thesis to achieve the research purposes as shown in Figure 1-2.

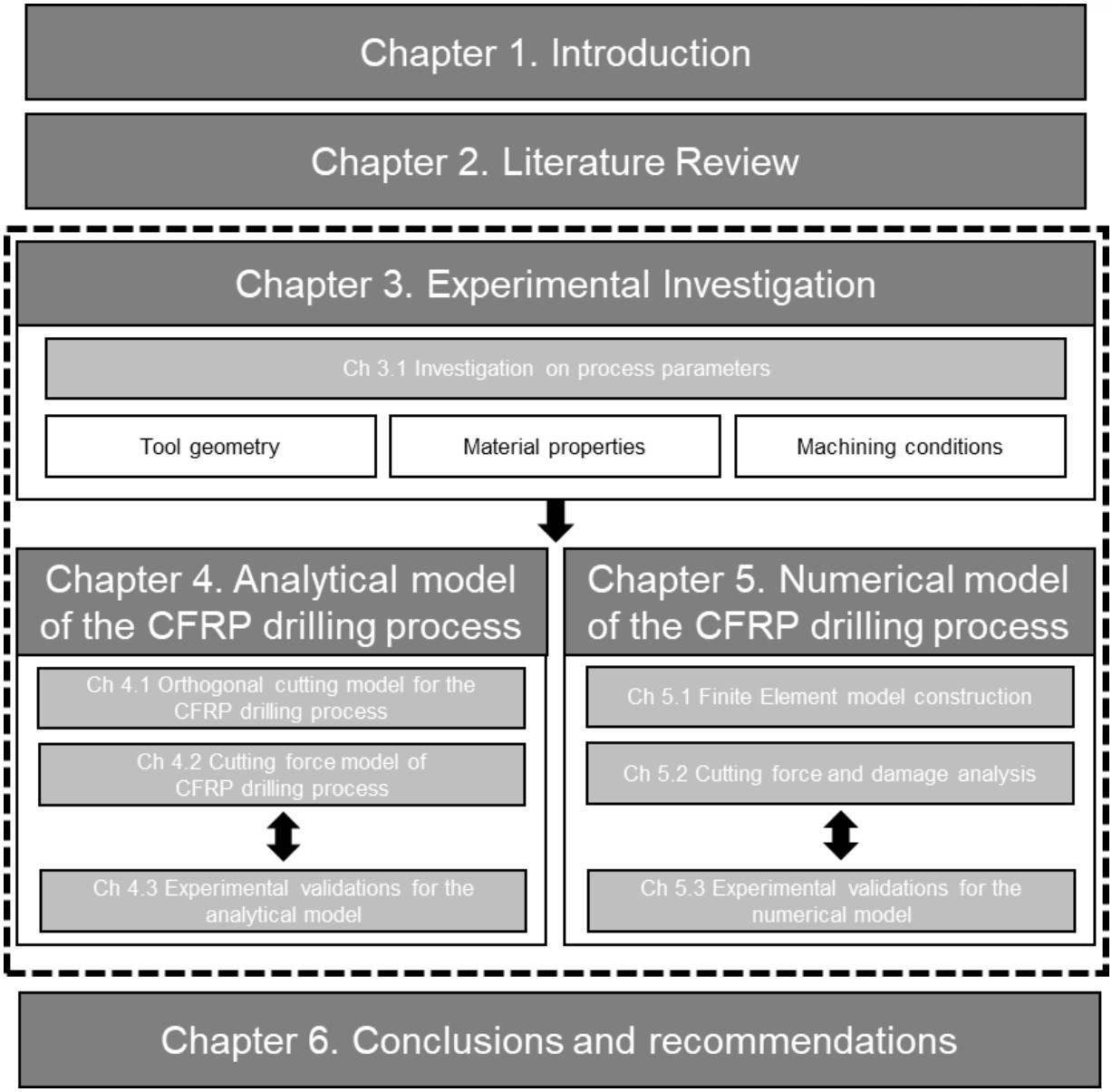

Figure 1-3. Research outline

2. Literature reviews

2.1. Machining characteristics of CFRP materials

2.1.1. Carbon Fiber Reinforced Polymer (CFRP)

In general, machining of CFRP is a difficult due to materials' inhomogeneity properties and anisotropic structure [1, 2, 7, 27]. In addition to the adverse mechanical properties, CFRP has low thermal conductivity and low specific heat capacity, excessive rise of temperature during the machining process that concluded to material softening and thermal degradation. [9, 28, 29] Thus, the machining of the CFRP can be associated with unwanted defects on machined workpiece and severe tool wear[30-46]. Generally, thrust force during CFRP drilling process reaches maximum point at the exit of workpiece, which delaminate the drill-exit surface. Some of the important characteristic of CFRP which influences the strength of the CFRP materials are fiber volume fraction and the resin content. But very limited investigations have been reported which can give a clear understanding about the machining performance of CFRP composite of varying fiber volume fraction. Hence an exhaustive study is required which can give a clear understanding about the change in the force generation and delamination that occurs during the drilling of CFRP of varying volume fraction.

2.1.2. Experimental analysis on CFRP drilling

Various experiments have been conducted by researchers, investigating influence of parameters such as spindle speed, feed, drill bit geometry, and material properties to cutting force and delamination. Experimental studies on the CFRP drilling process were conducted since the early 2000s. [7, 22, 47, 48] Davim et al. studied about the influence of process parameters using statistical analysis with the experimental results. [7] Cutting velocity and feed rate were chosen as the input variables, and observed the power, specific cutting pressure, and delamination factor [21, 24, 47] Regression model was developed using the diameter of drill bit and feed as the the major factor. Abrao et al. also investigated the effect of the tool geometry and material properties on thrust force and delamination, and the feed rate was the major factor in every drill bit type. [21] Gaitonde et al. investigated influence of cutting speed, feed rate, point angle in high-speed drilling condition. [47] Grilo et al. investigated the influence of three distinct drill (SPUR, R950, and twist drill) geometries to the delamination factor. SPUR drill showed the best performance in specific cutting conditions. [26] After that, Gaugel et al. [40] studied the influence of tool wear to the delamination factor with novel tool wear analysis method. Diamond coating on the drill bit showed contribution to quality of composite materials. Recently, Caggiano et al. developed monitoring

system and optimization algorithm to find the optimal process parameters for tool life and hole quality. [43] In Table.2-1, influence of process parameters to output variables were summarized. Based on the literature studies, the feed, and spindle speed were selected as major factors, and in case of tools, twist drill bit was used. In addition, the fiber volume fraction was considered in this study to investigate the effect of the material properties. Recently process parameters of optimized using soft computing techniques such as fuzzy logics and neural network models. [49-66] Those computing techniques can be adapted due to development of monitoring and sensor technologies. [45, 46, 51, 67-73] Advanced cutting process such as vibration assisted, ultrasonically assisted, and using novel design cutting have been adapted by several researchers to improve the quality of process and workpiece. [74-81]

2.1.3. Assessment of delamination

Delamination assessment is generally done by using the concept of delamination factor. First method to evaluate the delamination was introduced by Chen.[2] The delamination factor they proposed was defined as the ratio of the maximum diameter of delamination zone to the diameter of the hole which can be expressed as below:

$$F_d = \frac{D_{\max}}{D_0}$$

However, with the conventional method for delamination quantification, the contribution of damaged area, and crack propagation were ignored. New methods have been proposed by researchers to compensate for the drawbacks of the conventional method. 2-dimensional, and 3-dimensional delamination assessment were established considering damage propagation of drilling induced delamination on the CFRP. [4, 82-84] Mohan et al. proposed the delamination assessment considering contribution of damaged area. [85] Faraz et al. also proposed the area based delamination assessment in similar method. [30] Davim et al. proposed the new delamination factor which considers the both crack length and damaged area, and several researchers adapted the adjusted delamination factor in the experimental studies. [4, 86] However, 2-dimensional delamination factor which considers the area contribution has been actively utilized in the studies developing predictive model for the intuition of proposed method. A summary of the proposed methodologies of delamination factors is expressed in Table 2-2.

For the reliable assessment of delamination, appropriate measurement of delamination is essential. General method for the delamination measurement was conducted by using optical microscope, which was the most economical and easiest method. However, with the development of non-destructive measurement technologies, several researchers introduced the assessment techniques. Tsao and Hocheng measured the delamination by ultrasonic C-Scan using ultrasound energy. [87] Kourra

et al. used the X-ray radiography to measure damaged zone inside the composite materials with acceptable accuracy. [88] Furthermore, Computational Tomography(CT) image was achieved by Lopez-Puente et al. [48] and Haeger et al. [89] for 3dimensional measurement. High resolution 3D image could be acquired by using CT, and damage inside the CFRP composite can be observed in more detail.

Table 2-1. Summary of experimental studies on CFRP drilling process

Work material	Drill bit geometry	parameters	Analysis tool	Output variables	Ref.
Woven CFRP	Twist drill, Brad & Spur drill	Cutting speed (m/min), Feed (mm/rev)	ANOVA	Power (W), Specific cutting pressure (N/mm^2), Delamination factor	Davim [86]
GFRP	Twist drill(3types), Brad & Spur drill	Cutting speed(m/min), Feed(mm/rev)	ANOVA	Thrust force(N), Tool wear, Delamination	Abrao et al. [21]
Woven CFRP	Twist drill(4types)	Point angle(θ), Cutting speed(m/min), Feed rate(mm/min)	ANOVA	Delamination factor	Gaitonde et al. [47]
Woven CFRP	Twist drill(4types)	Spindle speed(RPM), Feed rate(mm/min),Point angle(θ)	Artificial Intelligence model(ANN)	Delamination factor	Karnik et al. [90]
Woven CFRP	Twist drill, Brad & Spur drill	Spindle speed(RPM), Feed rate(mm/min)	Image Processing tool(Sherlock software)	Delamination factor	Grilo et al. [26]
UD CFRP	Twist drill	Spindle speed(RPM), Feed rate(mm/min), Coated/non coated	Image processing tool(Zeiss Axiovision software)	Delamination, Tool wear	Gaugel et al. [40]
MD CFRP	Twist drill	Spindle speed(RPM), Feed(mm/rev)	Machine learning	Tool wear	Caggiano et al. [43]

Table 2-2. Summary of delamination of assessment and measurement method

Dimension	Name	Assessment method	Measurement	Ref.
1D	Conventional delamination factor	$F_d = \frac{D_{\max}}{D_0}$	Optical microscope	Chen [2], Davim [86], Gaitonde et al. [47], Karnik et al. [90], Abhishek et al [91],
2D	Two-dimensional delamination factor	$F_d = \left(\frac{A_D}{A_0}\right)\%$	Digital scanning	Faraz et al. [30]
2D	Delamination factor	$F_d = \frac{A_D}{A_0}$	Digital scanning	Mohan et al. [85], Melentiev et al. [92]
Combined	Adjusted delamination factor	$F_{da} = F_d + \frac{A_d}{(A_{\max} - A_0)}(F_d^2 - F_d)$	Optical microscope	Davim [86], Grilo et al. [26], Rubio et al. [4]
2D	Delamination factor	$F_d = \frac{A_D}{A_0}$	CT scanning	Giasin et al. [93]
3D	Delamination area	Damaged area and Crack analysis	CT scanning	Tsao and Hocheng [87], Saoudi et al. [94], Durao et al [25], Haeger et al [89],Lopez-Puente et al. [48]

cj2.2. Analytical modeling in composite material drilling

There have been several tries to develop cutting force model for CFRP materials in machining processes. [95-97] Some of the first attempts to develop a thrust force model for the machining of CFRP

was done by Chandrasekharan et al., where a mechanistic model was developed for the drilling of fiber reinforced composite.[1] Coefficients for specific cutting pressure was calculated empirically, which was further included with the geometrical parameters of a drill bit to predict the thrust force. Langella et al. used a mechanistic approach to develop thrust and torque prediction model in semi-empricial method. [98] The lip region was considered as a very small region of orthogonal cutting operations for the development of the model. Although the model was first of its kind, but its dependency on the coefficients calculated empirically makes it usage very limited. Guo et al. tried to develop a model for prediction of thrust force and torque generated during the drilling of CFRP composite. The model treats the machining using chisel edge region as an extrusion operation. The lip region was considered as an oblique cutting zone where three distinct tool-workpiece interactions, i.e. Chipping, Pressing and bouncing phenomenon takes place. [99] Model developed by them mostly considers the cutting force model developed by the Zhang et al. [100] Although the model could be used to predict the thrust and torque forces generated during drilling operations, inclusion of additional drill bit geometry details, such as the helix and normal rake angles, could improve the model accuracy. Karpat et al. developed a milling model that introduced a coefficient quantifying the variation in force generated according to fiber angle, and considers the force generated in radial and tangential directions. [101] Cheng et al. also developed a model of the thrust force and torque generated when drilling CFRP/Al laminates. [102] Although their model could calculate the forces that occurred when the drill was moved from the CFRP to Al regions, it did not account for the chisel and lip cutting processes. Meng et al. developed a semi-empirical model that computed the variation in thrust force that occurs at the drill bit lip based on input force coefficients. [103] the model showed its effectiveness in capturing the force variations, but more exhaustive model is required which can capture these variations at the chisel edge and the lip region during the drilling operation. Cheng et al. tried to develop a thrust force model for drilling-countersinking of CFRP/Al stacks. The whole machining operation was divided into different regions i.e. chisel edge, cutting edge of drilling, cutting edge of rimming, and cutting edge of countersinking. [104] Maegawa et al. used the cutting force model to develop a model for milling operation by considering

the tool wear. Polycrystalline diamond and tungsten carbide tool were used to validate the model and to understand the cutting mechanism taking place for unidirectional CFRP composite by considering the tool wear. [105] Jahromi and Bahr adopted a different approach for the development of model for orthogonal cutting of CFRP. Energy based modelling approach was used to develop the model which was specifically used for the CFRP with 90-degree to 180-degree fiber orientation.[106] It can be learned from the above discussion that most of the developed model takes care of the material properties by using the specific cutting coefficient. Since these coefficients were developed using empirical relations, hence it may not provide a proper understanding about the machining requirements needed when different types of CFRPs are treated. Some of the models which takes care the material properties by using modulus and shear strength of the material, should also be further modified and tested to make it more applicable for generic cases of CFRP machining conditions. Inclusion of more geometrical parameters of drill-bit geometry can further enhance the applicability of the model for CFRP machining prediction.

2.3. Numerical modeling in composite material drilling

Finite element analysis and simulation were implemented to the machining area to derive a computational model predicting the mechanical behaviors of workpiece [18, 25, 28, 39, 107-110]. Finite element method has been actively used in this area because direct experimental approach to understand machining process is expensive and time consuming. One of the initiative studies of analysis on machining of FRPs using finite element method was carried out by Ramesh et al. [111], when the existing of FE models focus on the metal cutting process. Previous studies were constrained to orthogonal cutting process to understand mechanism of FRP cutting process [35, 112-114]. Mahdi et al., developed a FE model for orthogonal cutting of FRPs considering the chip breaking phenomenon [112]. They predicted cutting force in 2D model according to the cutting condition. Cheng et al., performed the micro scale cutting simulation on the UD CFRP considering thermal-mechanical coupling [115]. Failure modes for fibers, matrix and the interface were investigated using simple damage-based fracture method.

Numerical simulation and experimental validation were conducted according to the fiber orientation comparing cutting and thrust force. Abena et al., proposed the zero thickness cohesive elements based on a traction-separation law to achieve accurate simulation of CFRP orthogonal cutting process with understanding of fiber-matrix interface.[116]

Although there have been many developed analytical models to calculate the cutting forces, however, some studies have shown that numerical model plays a key role in the analysis of mechanisms for drilling process and the prediction of damage in the workpiece. Durao et al., carried out the initiative finite element model to analyze delamination during drilling of carbon/epoxy composite laminates.[25] In referred paper, thrust forces in two different drill bit geometries were simulated and validated by the experimental data. 3D finite element model was applied to simulate delamination onset and growth incorporating with cohesive mixed-mode damage model and showed good agreement. However, in this study the influence of cutting parameters was not considered. Since that 3D FE simulation of the drilling process of FRPs is very complex, so the previous studies have been applied the commercial FE software. [111-113, 117-122] Al-wandi et al., performed the finite element and experimental study to evaluate the delamination occurred during CFRP drilling process by presenting equivalent adjusted delamination factor [123]. ANSYS-Explicit was applied to simulate the process using the ply-based modeling method. Singh et al., also performed an experimental and finite element approach to study drilling characteristics of UD-GFRP composite laminates and found that both thrust force and delamination factor depends on the drill point angle and the feed rate [22]. Wu et al., carried out the FE model to predict the drilling force and torque using the Deform-3D finite element simulation software. [117] Giasin et al., analyzed the drilling process of GLARE composite laminates using ABAQUS/Explicit. Quality of the processed hole was examined in various perspectives which includes surface roughness, burr height, hole size, error of circularity and delamination [124].

Table 2-3. Summary of FE model for CFRP machining process

Work material	Machining operation	Simulation software	Simulation results	Ref.
CFRP and GFRP	Orthogonal cutting	ABAQUS/Explicit	Cutting force(N), damage propagation	Santiuste et al. [125]
CFRP	Orthogonal cutting	AdvantEdge 3D	Fracture analysis	Usui et al. [113]
CFRP	Milling	ABAQUS/Explicit	Damage and cutting force	Rentsch et al. [126]
Woven GFRP	Drilling	ANSYS DYN	Thrust force(N)	Nilanjan Das et al. [127]
UD GFRP	Drilling	ANSYS	Thrust force(N), Delamination	Singh et al. [22]
GLARE	Drilling	ABAQUS/Explicit	Thrust force (N), Torque (N-m)	Giasin et al. [124]
CFRP	Drilling	ABAQUS/Explicit	Thrust force(N), Delamination	Isbilir and Elaheh[18, 119]

3. Experimental investigations on CFRP drilling process

3.1. Introduction

Quality of drilled hole of CFRP composite laminate and productivity are determined by various process parameters. [29, 36, 38, 46, 105, 110, 123, 124, 128-140] In this study, experimental studies were conducted to investigate to figure out the process parameters affecting the drilling process of CFRP composites. Machine tool dynamics, tool geometry, material properties, and cutting conditions are the parameters need to be observed. Machine tool contributes to the vibration and positional accuracy parameters of the machining process. [141-150] Vibration is determined by the machine tool dynamics, which is related to the performance of the machine tool and tool holder combination. Drilling tool is the major factor which investigated by previous researchers. [3, 4, 7, 21, 22, 30, 48, 82, 90, 98, 151-153] In case of twist drill bit, point angle and diameter of the drilling tool affects the force and delamination generated during the drilling process. [21, 98, 99, 127, 131, 154-156] Fiber orientation, matrix properties, fiber properties, and fiber volume fraction are the parameters for the composite properties. [103, 113, 157-161] For the fiber orientation, there are uni-directional(UD) CFRP, which is arranged in the one direction, multi-directional(MD) CFRP, which is the laminate stacked by carbon fiber plies with different angles, and woven CFRP. The fiber volume fraction refers to the amount of carbon fiber in the composite laminate, which affects the material properties. Especially, fiber volume fraction, and thermo-mechanical properties of CFRP composite was also considered in the study. There are spindle speed, feed, and the fixture conditions for the cutting conditions, and feed affects the force and delamination of the CFRP. Additionally, appropriate fixture design is the one important factor that prevent the defect occur during the machining process. [87, 137, 162, 163] Cutting force, and delamination were observed with dynamometer, optical microscope and computational tomography image. It was observed that both thrust force and delamination were intensely related to the feed, and diameter of drill bit. Fiber volume fraction also contribute to the magnitude of cutting force and force changes in time domain. Support plate showed prevention effect of delamination without affecting the cutting force and tool wear. [133, 164, 165]

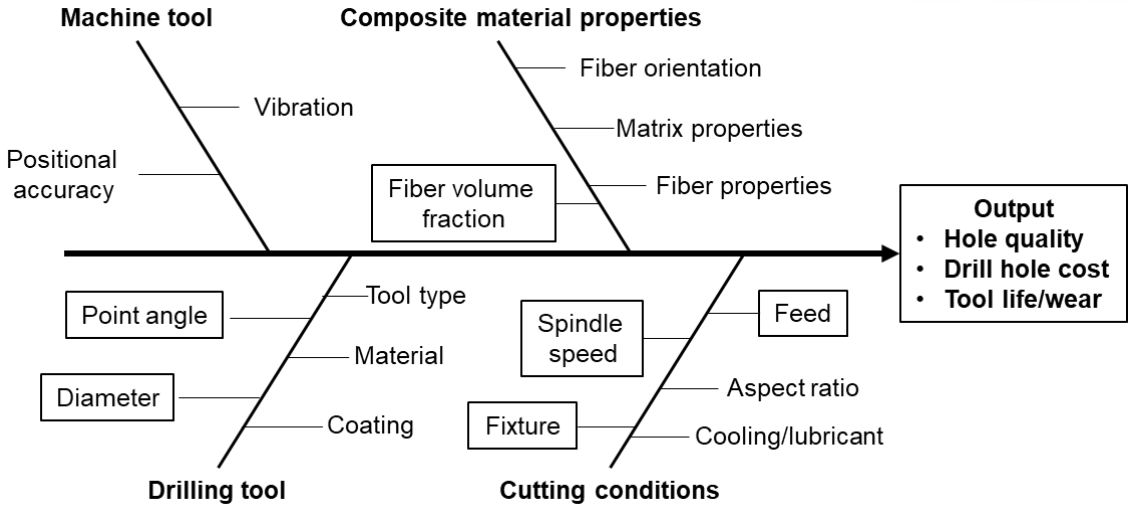

Figure 3-1. Process parameters in the CFRP drilling process

3.2. Investigation on thrust force according to the fiber volume fraction

Thrust force is the major force component affects the quality of drilled hole, and it is the force generated in feed direction of the drilling process. [33, 94, 136, 166] As shown figure 3-1, parameters of the drilling quality and productivity controlled by the several process parameters. Machine tool performance, composite material properties, drilling tool, and cutting conditions are the major factors. In this work, fiber volume fraction, and fiber orientation of the composite materials were considered. 3 types of uni-directional CFRP were chosen in this experiment. Fiber volume fraction contributes to the thermo-mechanical properties of composite materials. Drilling tool was fixed to twist drill bit which has 9mm of diameter with 135° of point angle, and It was manufactured by the Kennametal Inc. Drilling experiment was conducted according to the varying spindle speed and feed. The magnitude of the force was measured with the dynamometer (9257B) manufactured by Kistler Inc. Sampling rate of the dynamometer was 1000hz for the measurement. Temperature elevation due to drilling process was also measured with the thermocouples equipped to the CFRP composite materials as shown in figure 3-2. Software and DAQ manufactured by National Instrument Inc. were used for the temperature measurement. Machining center manufactured by Hermle Inc. was utilized for the drilling experiment. Detailed summaries of the equipment are expressed in the table 3-1, and table 3-2. Spindle speeds for

the drilling experiment were from 3000RPM to 9000RPM which are the adequate speed in general use

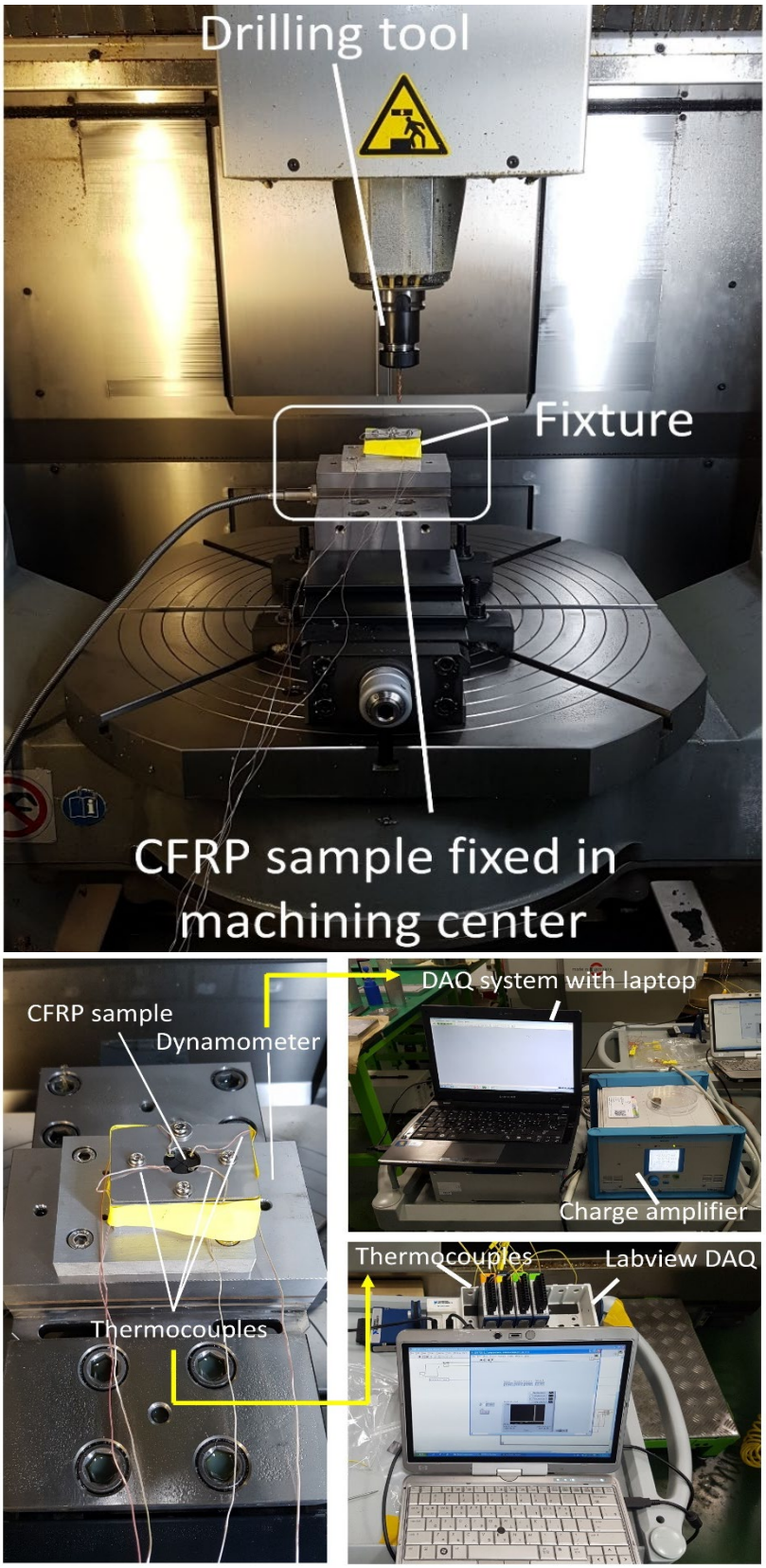

Figure 3-2. Experimental setup for drilling test

of drilling process.

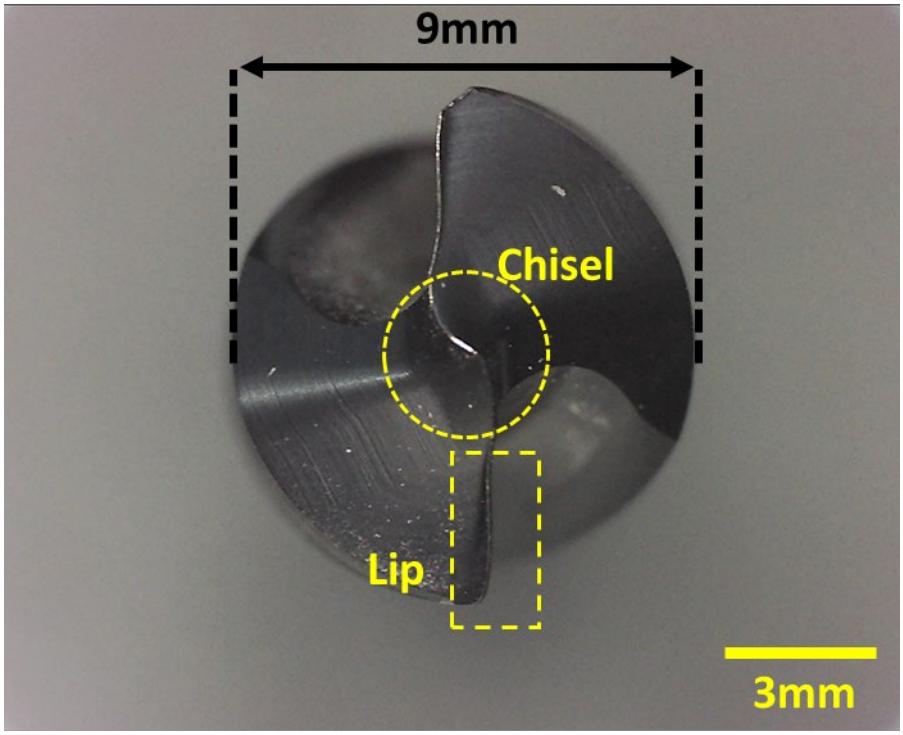

Figure 3-3. Optical microscopic image for drill bit

Three different unidirectional carbon fiber composite materials with varying volume fraction, namely USN 150(66%), USN 150(57%) and USN 150(49%) (SK chemicals) was used for the experiments. Each sample was cured using autoclave at 125℃ for 90 minutes under 5bar pressure. The detailed material properties for the three CFRP composites are displayed in the table 3-1. The material properties of the CFRP composite were calculated using the rule of mixture. Each of the composite material was tested for the four set of speed and feed rate, varying each parameter one at a time. Hence, in total 48 experiments were conducted i.e. 16 experiments for each type of CFRP sample. The experimental thrust force results obtained were analyzed in this section.

The effect of increase in volume fraction on maximum thrust force is shown in the figure 3-5. under different speeds and feed rates. It can be seen form the Fig 3.4 to Fig 3.6 that when the feed rate was increased from 0.02 mm/rev to 0.08mm/rev, a steep increase in the thrust force was observed. It

can be attributed to the increase in the amount of material removed per unit time with the increase in the feed rate which might have resulted in the load on the cutting lip. This trend is similar for all the three CFRP material under four different speeds of 3000 rpm, 5000rpm, 7000rpm and 9000rpm. It can be seen from the respective figures (Fig 3.4 to Fig 3.6) that the thrust force is highest for the specimen USN 150E (Vf=67%) as compared to specimens USN 150Y (Vf= 49%) and USN 150B (Vf=57%). This might have occurred because of the increase in the overall strength of the material due to the presence of high content of fiber. Hence the force requirement for deforming and removing the material also got increased. It can also be seen from the results shown in figures (Fig 3.4 to Fig 3.6) that when the fiber volume fraction of the specimens was increased from 49% to 57%, the rise in the force is not linear. In fact, the differences in the thrust force between the two specimens were very minimal and no specific trend was observed. This deviation might have resulted because of the nonlinear change in the material properties like strength and modulus, when the fiber volume fraction was increased from 50% to 70%. It was observed from the work of Amuthakkannan et al. that when the fiber volume fraction got increased from 48% to 75%, the non-linearity in the change in the modulus of the fiber composite material becomes more prominent. [167] This nonlinear change in the strength was also reported in the work of karam where this change was attributed to the misorientation and inhomogenous fiber spread. [168] This nonlinear change in the material property might have resulted in the nonlinear rise in the thrust force during drilling. Hence when the fiber volume fraction gets increased within very narrow range (49% to 57%), the variation in the force generation might be very minimal and nonlinear. The experimental thrust forces values obtained were then compared with the predicted mean thrust force of the model at the end moment of stage 2.

Table 3-1. Material properties of CFRP according to the volume fraction of fiber

	USN 150(66%)	USN 150(57%)	USN 150(49%)
Content of fiber %	75	67	60
Fiber volume fraction % (V_f)	66	57	49
Young's modulus, E_1 (GPa)	160	138	121
Young's modulus, E_3, E_2 (GPa)	10.13	8.02	6.8
Shear strength, τ_1 (Mpa)	99	89	79
Shear strength, τ_2 (Mpa)	75	63	54
Poission's ratio, υ_{13}	0.28	0.31	0.33
Glass transition temperature (℃)	126		
Decomposition temperature (℃)	405		

Table 3-2. Drill bit geometrical parameters

Diameter of drill (mm)	9
Chisel edge thickness (mm)	0.49
Point angle (degree)	135
Clearance angle (degree)	11
Helix angle (degree)	30

Table 3-3. Machining parameters for drilling test

Cutting condition	Spindle Speed (rpm)	Feed (mm/rev)
1	3000	0.02
2	5000	0.02
3	7000	0.02
4	9000	0.02
5	3000	0.04
6	5000	0.04
7	7000	0.04
8	9000	0.04
9	3000	0.06
10	5000	0.06
11	7000	0.06
12	9000	0.06
13	3000	0.08
14	5000	0.08
15	7000	0.08
16	9000	0.08

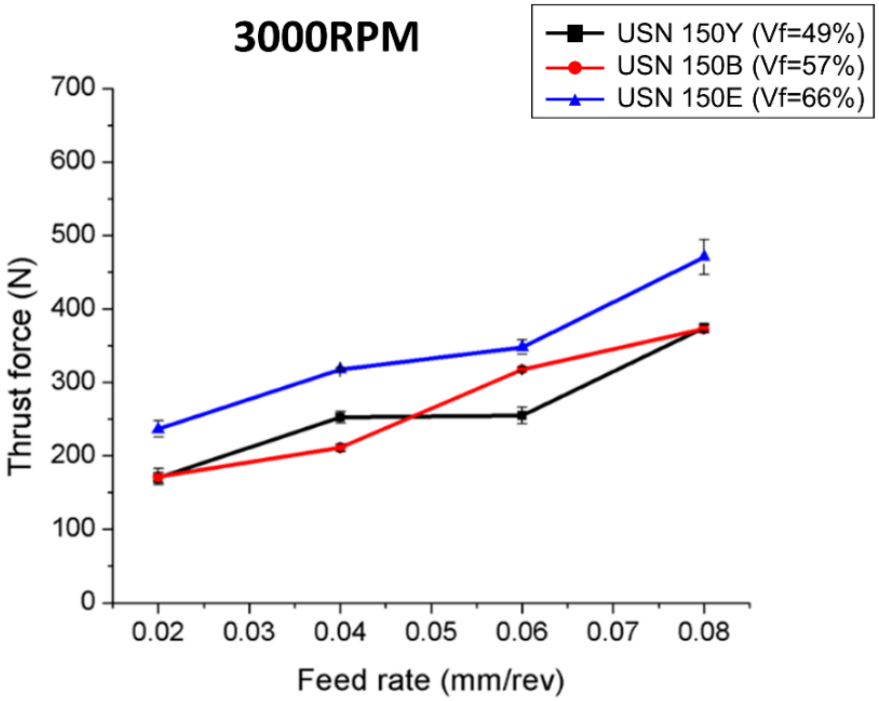

Figure 3-4. Thrust force according to the feed and fiber volume fraction at spindle speed of 3000RPM

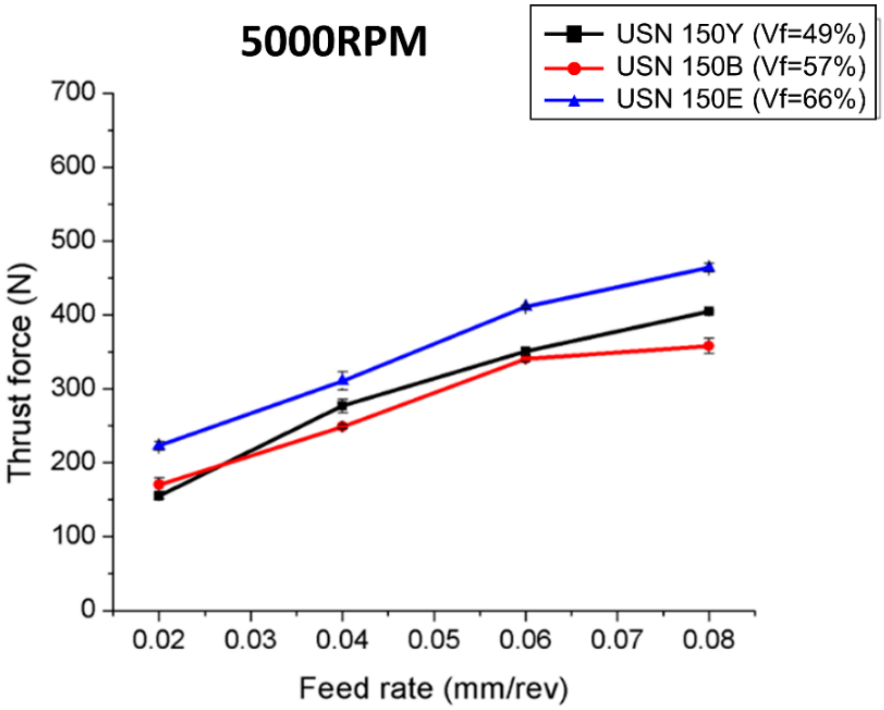

Figure 3-5. Thrust force according to the feed and fiber volume fraction at spindle speed of 5000RPM

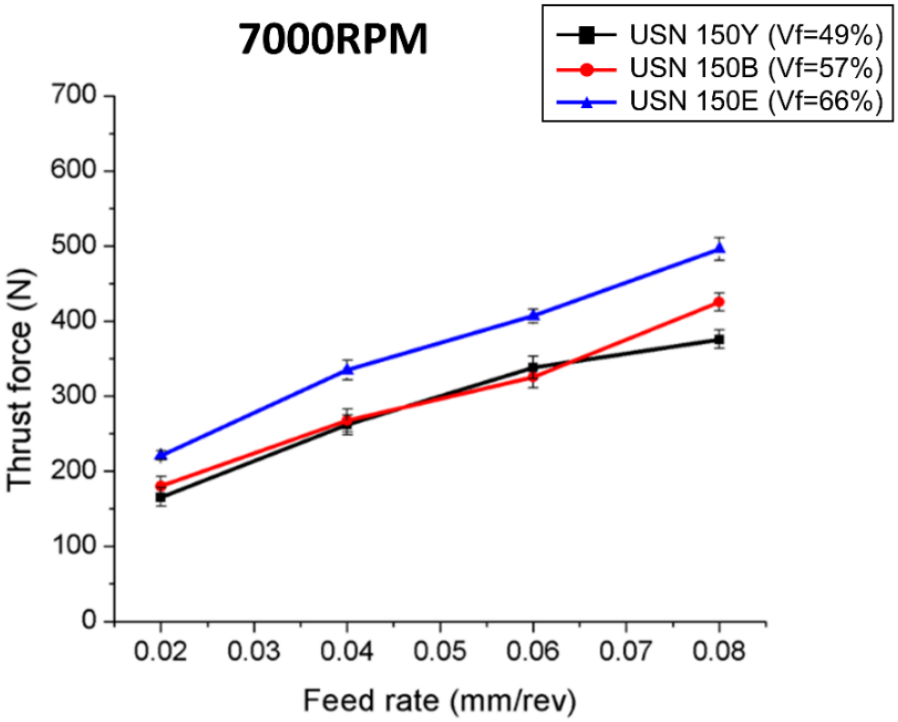

Figure 3-6. Thrust force according to the feed and fiber volume fraction at spindle speed of 7000RPM

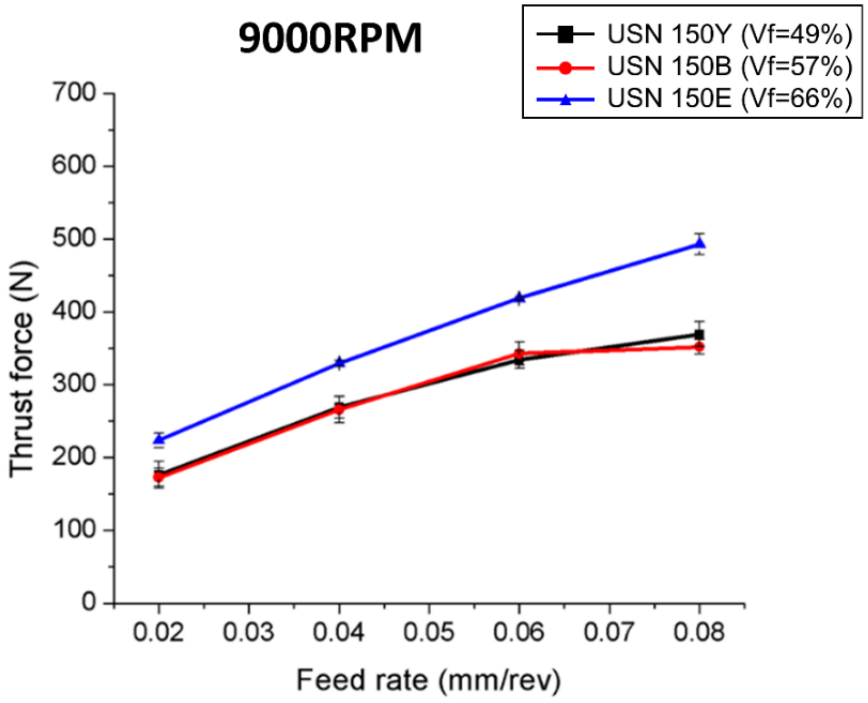

Figure 3-7. Thrust force according to the feed and fiber volume fraction at spindle speed of 9000RPM

3.3. Investigation on delamination

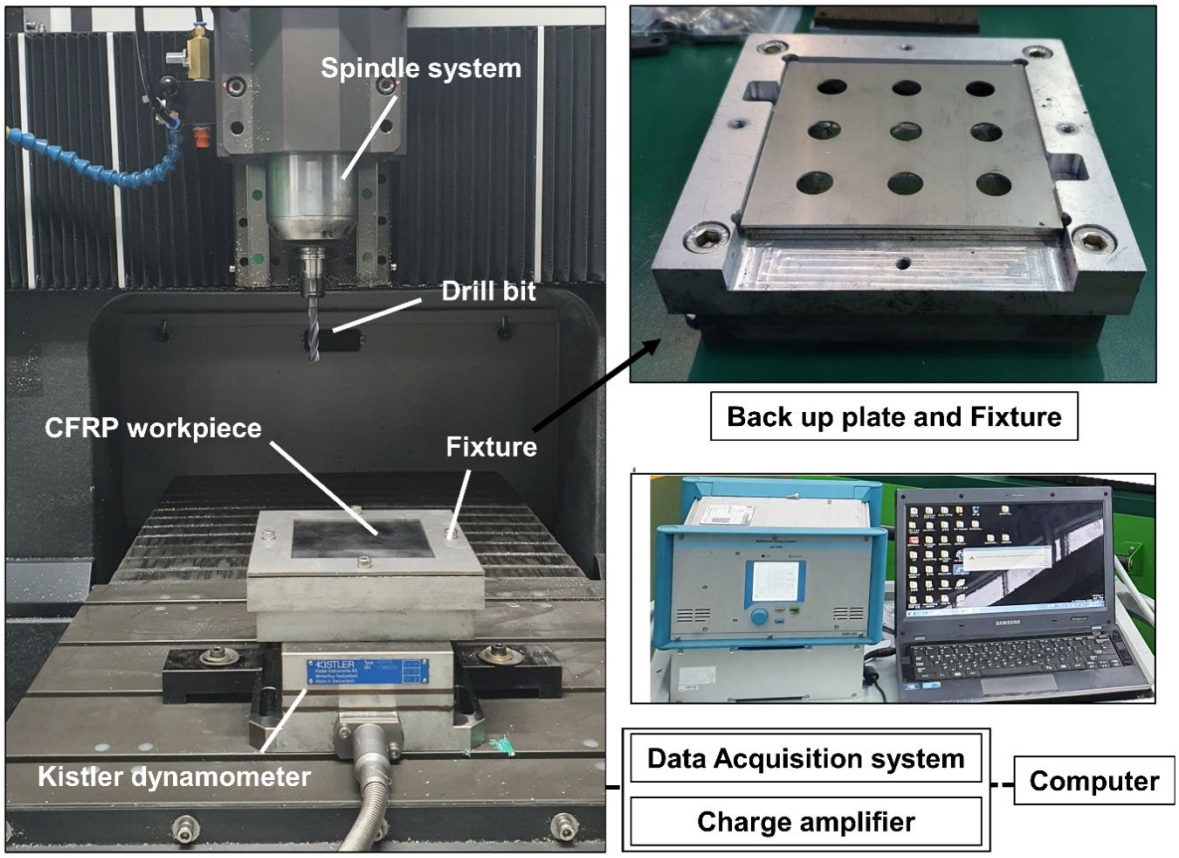

Figure 3-8. Experimental setup for the drilling test with 3axis CNC machine tool

Figure. 3-8 shows the experimental setup for the drilling experimental for delamination investigation. Drilling tests were conducted using a three-axis computer numerical control (CNC) machine tool. Multidirectional carbon fiber composites tested in this work were fabricated by prepreg with T300 reinforced fiber and epoxy resin supplied by the SK chemicals in Korea. CFRP laminates were cured in an autoclave at 125°C for 90minutes with 5 bar pressure. Workpiece was 3mm in thickness with 14 plies stacked in fiber orientation with sequence of $[(0/0/90/90)_3/0/0]_s$. The geometric parameters of the drill bit (solid carbide drill; Kennametal, Ltd.) used in the experiments are given in Table 3. Dry drilling tests were conducted under 13 different sets of spindle speeds and feeds to investigate effect of machining parameters, and the machining parameters used are described in Table 3-4. Workpiece was fixed on the fixture and 9 holes with different machining parameters were drilled. The experiments were

conducted using a 9257B dynamometer (Kistler Holding AG), which sampled at a rate of 1 kHz. The thrust force generated during the drilling process was measured and recorded using a charge amplifier and data acquisition system. Delamination due to the drilling process occur both side of entering, and exit surface of CFRP composite material. Figure 3-9 shows the drilled CFRP composite for both entering and exit surface respectively. Delamination occurred at the entering surface is peel-up delamination, and the exit surface is push-out delamination as shown in figure 3-10. In general, delamination occurs more frequently at the exit surface and adversely affects the quality of CFRP product. Therefore, in this work, push-out delamination was analyzed, and inspected non-destructive testing was performed.

The CFRP composite laminates were inspected by using microcomputer tomography (μCT) scanning technique using XT H320 industrial microfocus 3D CT system (Nikon Metrology NV) which has 320 kV microfocus X-ray source. Acquired CT images were transferred to the 3D CT Pro and reconstructed as the valid CT image. VGSTUDIO max (Volume Graphics GmbH) analysis and visualization software for industrial CT data was utilized to investigate the voxel data of CT image as shown in figure 3-11. Thick-slab image function in the software was used to acquire overlapped 2D image of the voxel data. The software's thick slab image function was used to acquire overlapping 2D images of voxel data. For images, volumetric data with a thickness of 0.3 mm was averaged and it is illustrated in the figure 3-12. Delamination factor (Df) in this work denotes ratio of delaminated area to the drilled hole area which is one of the most applied assessment methods in the previous studies. The scanned 2D image was processed in the MATLAB2019 to quantify the delamination factor of each experimental condition. As shown in the figure 3-12, delamination generated in the exit surface of CFRP was restricted to the diameter of hole of the back-plate equipped to the fixture. Figure 3-13, shows the optical image of the exit surface of the CFRP composite at spindle speed of 9000RPM, and feed from 0.02 to 0.18. Delamination propagates according to the fiber orientation of the unidirectional CFRP, and degree of delamination increases gradually as the feed increases. Delamination at the feed above 0.08mm/rev showed a severe quality which need to be suppressed. Drilling tests were conducted

without the back plate.

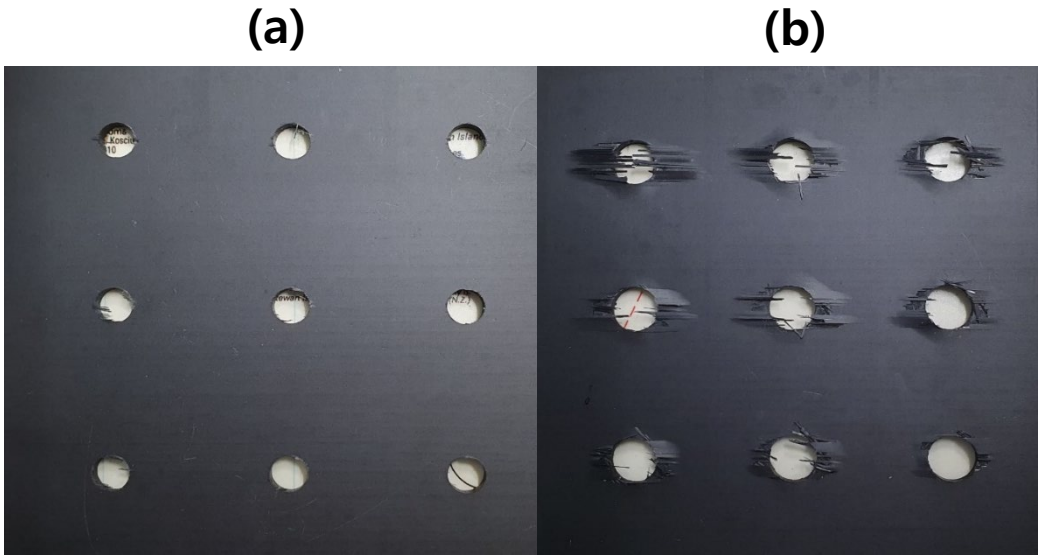

Figure 3-9. Drilled CFRP composite material: (a) entering surface and, (b) exit surface of drilling process

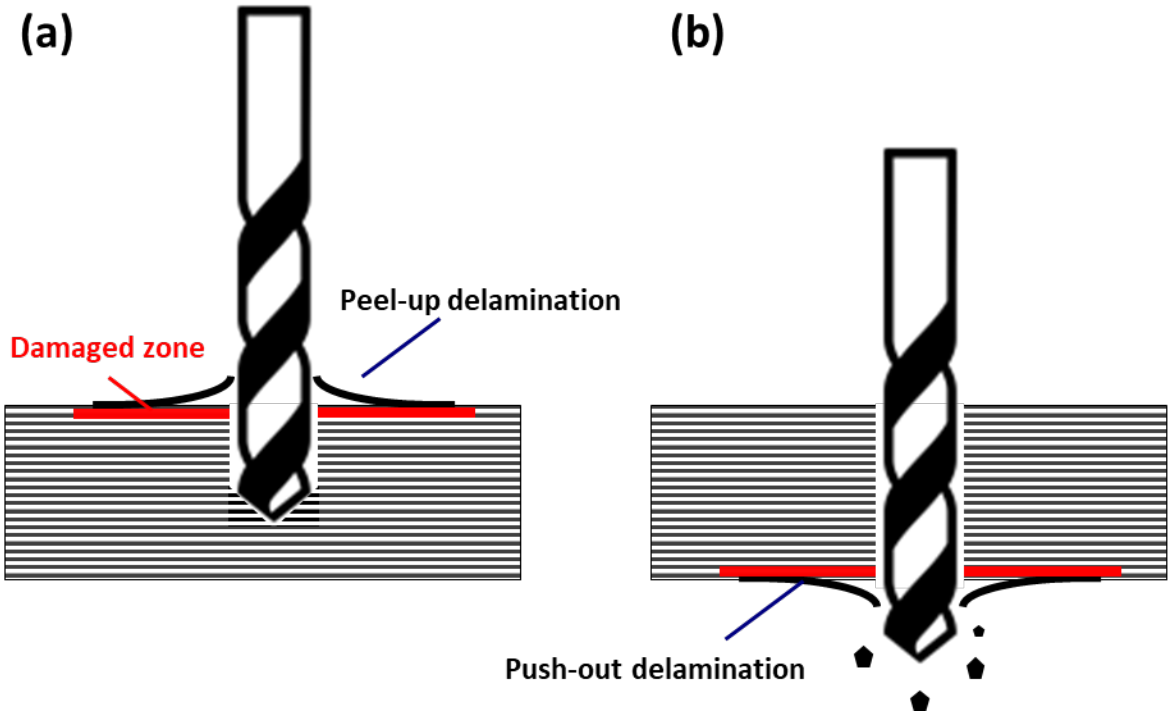

Figure 3-10. Types of delamination: (a)Peel-up delamination at entering surface, and (b)Push-out delamination at exit surface of drilled hole

Table 3-4. Drill bit geometries for delamination investigation

Diameter (mm)	9
Point angle (degree)	135
Helix angle (degree)	30
Clearance angle (degree)	11

Table 3-5. Machining parameters for drilling test for delamination investigation

Cutting condition	Spindle Speed (rpm)	Feed (mm/rev)
1	5000	0.04
2	5000	0.06
3	7000	0.04
4	7000	0.06
5	9000	0.02
6	9000	0.04
7	9000	0.06
8	9000	0.08
9	9000	0.10
10	9000	0.12
11	9000	0.14
12	9000	0.16
13	9000	0.18

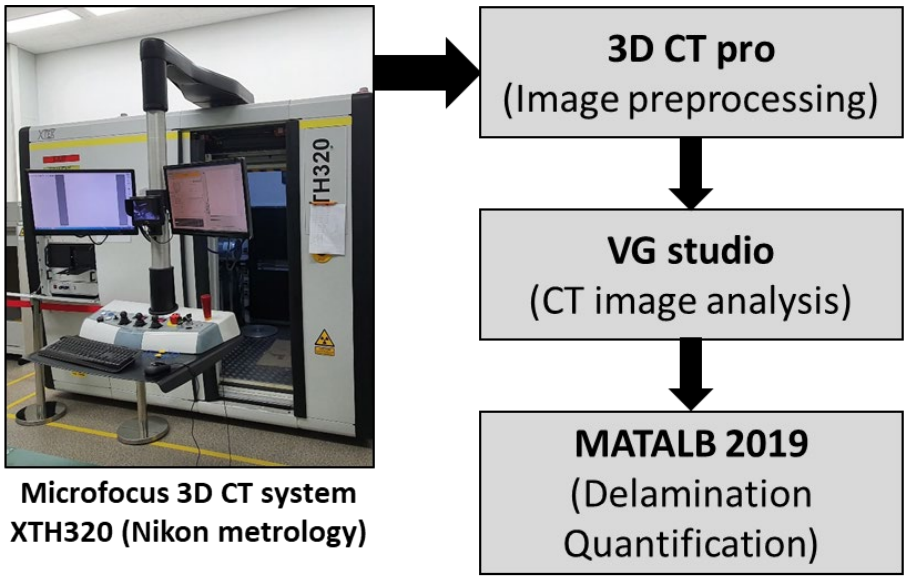

Figure 3-11. CT scan process for drilled hole of CFRP

Table 3-6. Delamination factor of non-backup plate, and backup plate conditions according to the feed

Feed (mm/rev)	Delamination Factor (Non-backup plate)	Delamination Factor (backup plate)	Thrust force (N)
0.02	1.08	1.22	124
0.04	1.27	1.24	180
0.06	1.39	1.31	241
0.08	1.59	1.36	275
0.10	1.95	1.40	333
0.12	1.90	1.34	384
0.14	1.94	1.34	435
0.16	2.04	1.39	487
0.18	2.18	1.47	538

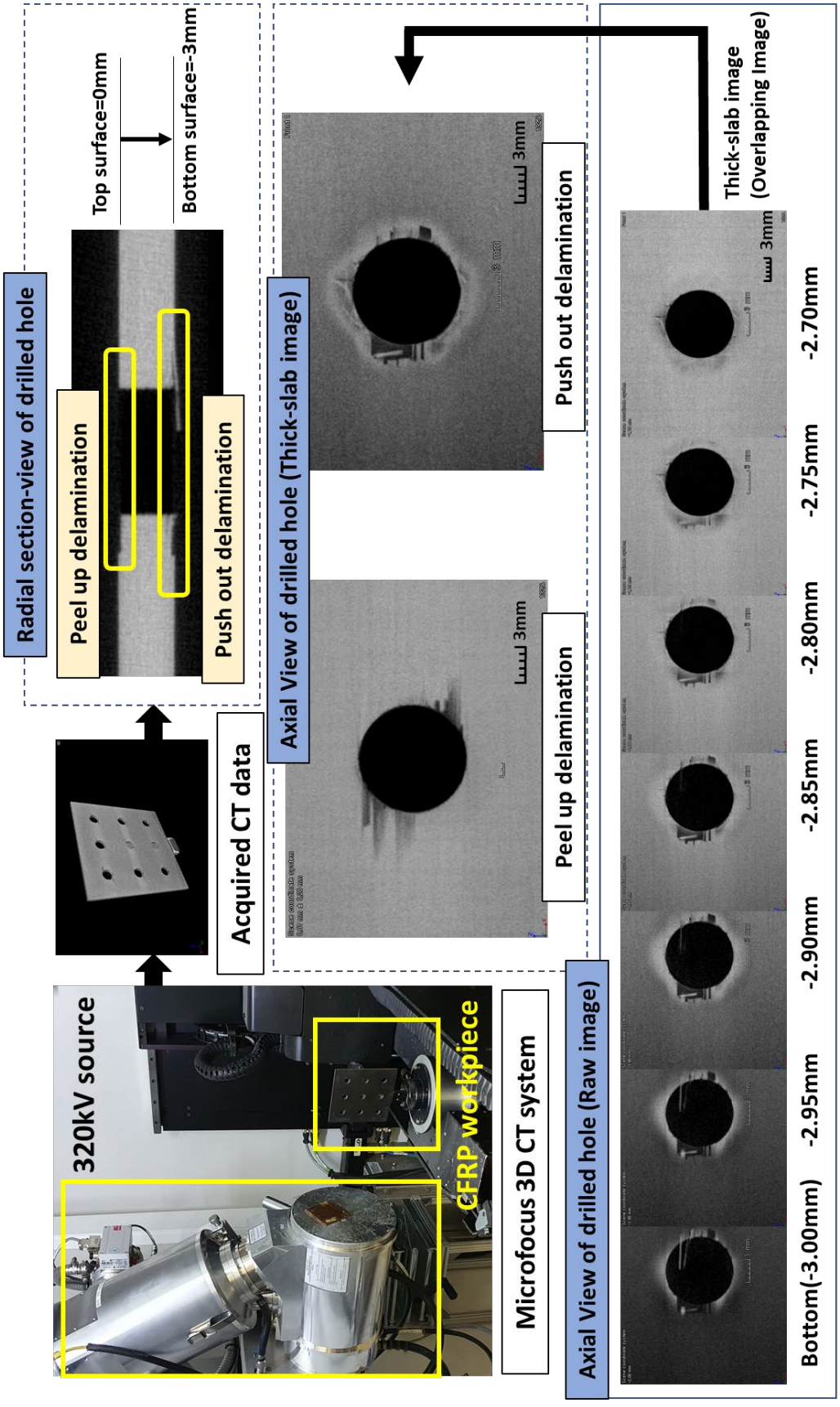

Figure 3-12. CT scan test setup, and image process with thick-slab image

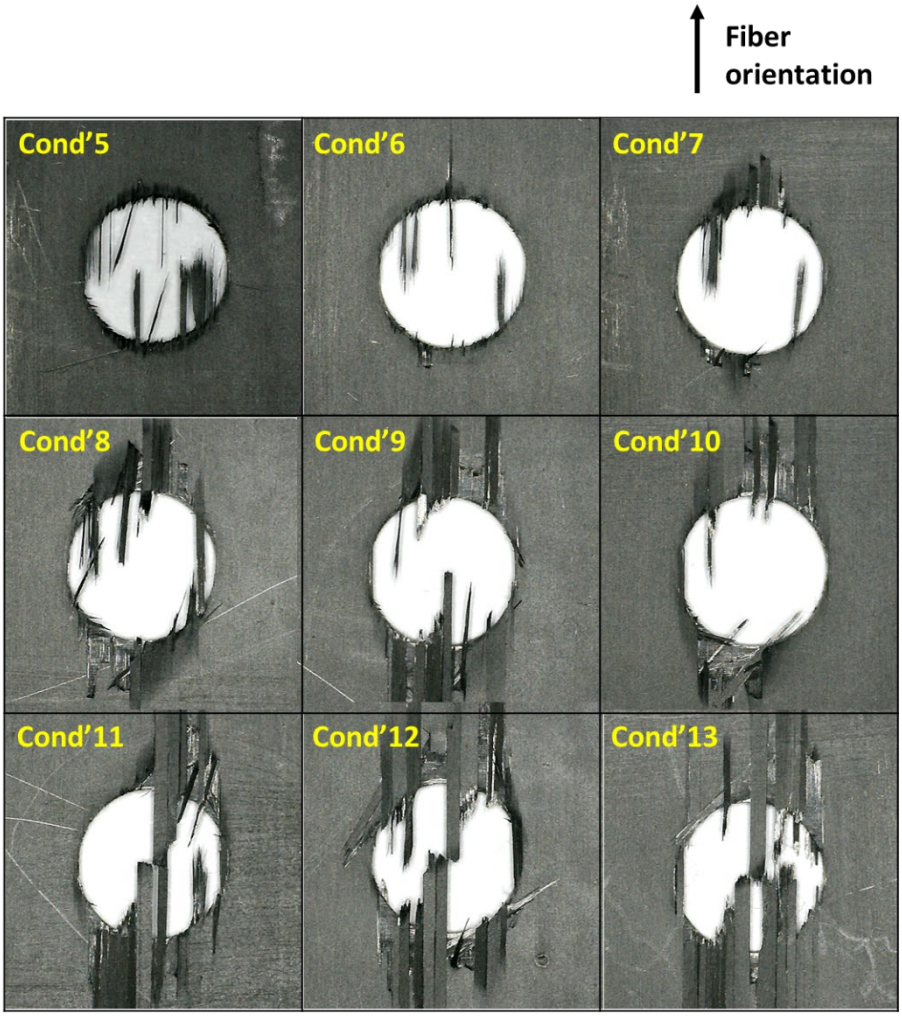

Figure 3-13. Drilled hole of CFRP composite laminate according to the feed conditions

Optical observation of the drilled hole has a limitation which is unable to quantified due to the delaminated surface of composite laminates. For the quantification to the delamination factor, CT image were acquired as shown in figure 3-12. Utilizing the developed Matlab code, CT scanned images of drilled composite material were analyzed as shown in the table 5. Delamination factor of the drilled hole without the backup plate, increases gradually. However, delamination factor increased to the value of 1.4 when the backup plate equipped to CFRP as the backup plate prevent the excessive delamination propagation. CT image of the drilled hole is illustrated in the figure 3-14 and 3-15.

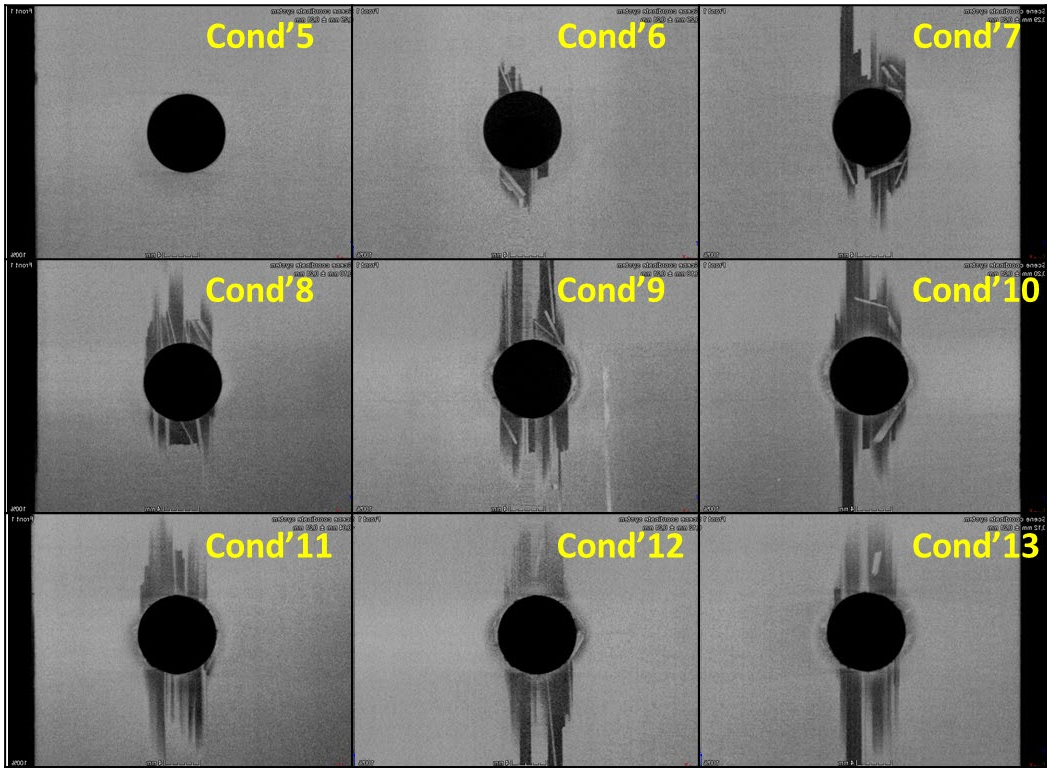

Figure 3-14. CT image of drilled hole without backup plate

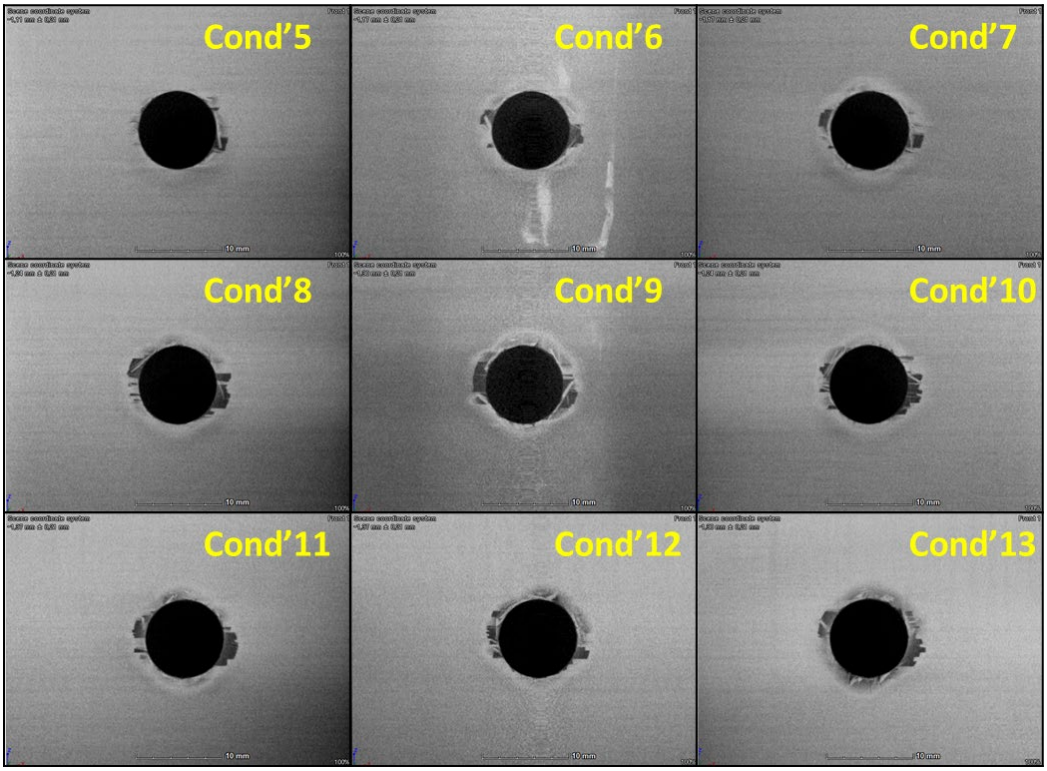

Figure 3-15. CT image of drilled hole with backup plate

3.4. Investigation on drilling process of micro drill bit

This work investigation on the effects of parameters on the hole quality during CFRP micro drilling process. Most of the previous work on CFRP drilling focused on CFRP drilling in macro scale, but more recently, micro hole drilling studies have carried out. This has been due to the increase in demand for micro holes in the aerospace industry. [115, 126, 133, 169-172] In this study, micro hole drilling experiments were carried out with a drill tool with a diameter of 1 mm equipped on the machine tool. The machinability and surface quality according to the feed rate, spindle rotation speed and CFRP type were analyzed. Surface delamination was observed on the surface of the CFRP laminates and the delamination ratio was evaluated according to the cutting conditions. Micro hole drilling of CFRP composites has a complex chip formation mechanism due to the non-homogeneous structure of the material, which makes it difficult to predict machinability. The anisotropic and abrasive nature of the material accelerates tool wear, and composite structures stacked in layers are exposed to defects in the internal structure by external forces. The tool also produces a size effect beyond the conventional size, which results in a nonlinear behavior of the cutting force. Larger ratio of chisel edge further improves thrust force in drilling, while larger aspect ratios of web thickness to drill diameter and drill length over diameter result in tool bending and buckling during drilling.

Table 3-7. Composite material information for micro drilling test

Type	Prepreg	Ply information
Unidirectional	SKYPLEX USN300B	[0deg]X17plies
Multi-directional	SKYPLEX USN300B	[0deg]X9plies+[90]degX8plies
Woven	SKYPLEX WSN3KY	22plies

The work piece materials used in the micro drilling experiments are 3 types of CFRP composite laminate according to the prepreg and ply stacking types. The prepreg used in the CFRP composites are expressed in the Table 3-5.

Workpiece has the thickness of 3mm, 5mm and 10mm and dimensions of 100mm X 100mm. UD and MD CFRP composite laminates are stacked with prepreg named 'SKYPLEX USN300B' which use 'Pyrofil MRC TR50' as carbon fiber material. Woven CFPR composite is made up of 22plies of prepregs. Epoxy resins used for the CFRP composite laminates are 'SKR-K51'. Two fluted solid carbide drill with diameter of 1mm manufactured by 'Union Tool' is used. Tools have 130 degree of point angle with 10mm of flute length with 3mm shank diameter.

Drilling experiments were conducted in 5axes machining center manufactured by Hermle. Milling chuck type tool holder is used to clamp the drill tool for process. Three axes piezoelectric dynamometer, Kistler 9257B, was used for measuring the forces from the drilling experiment. Jig was equipped above the dynamometer to clamp the CFRP composite laminate as shown figure 3-16. Machinability and defect of CFRP composite micro drilling are affected by cutting parameters. Cutting parameters in the experiments are spindle speed (RPM), feed rate (mm/min), Tool type (coated/uncoated) and CFRP material types.

Cutting forces occurred during the micro hole drilling are significantly smaller than those of macro scale drilling. Thrust forces measured from the experiment for woven CFRP composite with spindle speed of 10000, 11000 and 12000RPM with feed rate of 360mm/min were ranged between 8N to 10N. In the same cutting conditions with 8mm diameter of cutting tool shows the thrust force about 90N. 8mm diameter drill bit is manufactured by Kennametal. The work pieces were trimmed to 20mm X 20mm for the inspection. From these experiments, it is noted that delamination on the surface and delamination occurred in the internal structure should be classified separately in the micro drilling process. Non-destructive inspection with CT scan system shows delamination of the internal structure occurred in the macro scale drilling when the micro drilling has no defect. This test conducted in the spindle speed of 10000RPM.

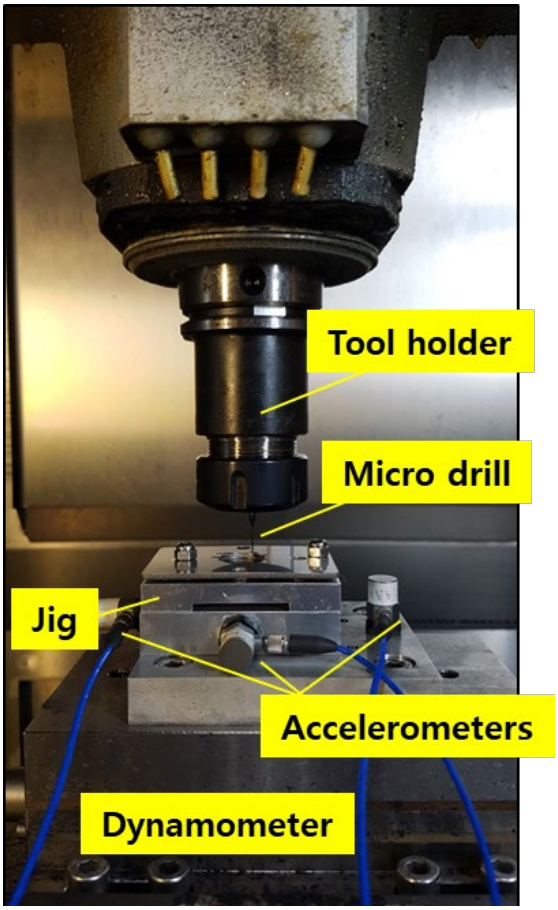

Figure 3-17. Experimental setup for micro drilling test

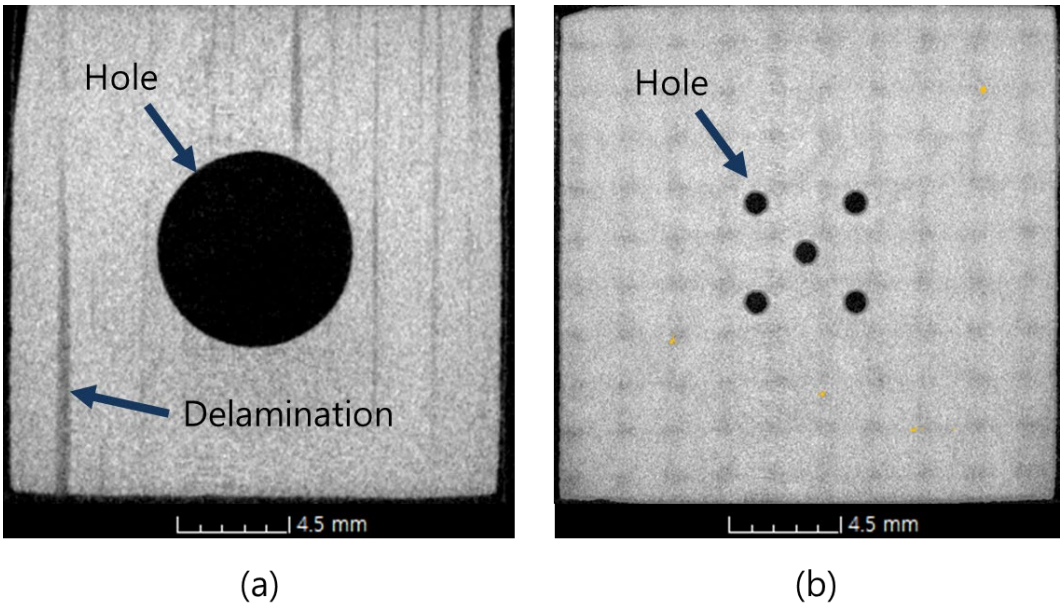

Figure 3-16. CT image of (a) hole with 8mm drill bit (b) hole with 1mm drill bit in same cutting condition

Table 3-8. Thrust force of micro drilling process according to the spindle speed

RPM	10000	11000	12000
Measured thrust force (average of 5holes)	9	8.5	8.3

3.4.1 Machinability of micro drilling process according to cutting condition

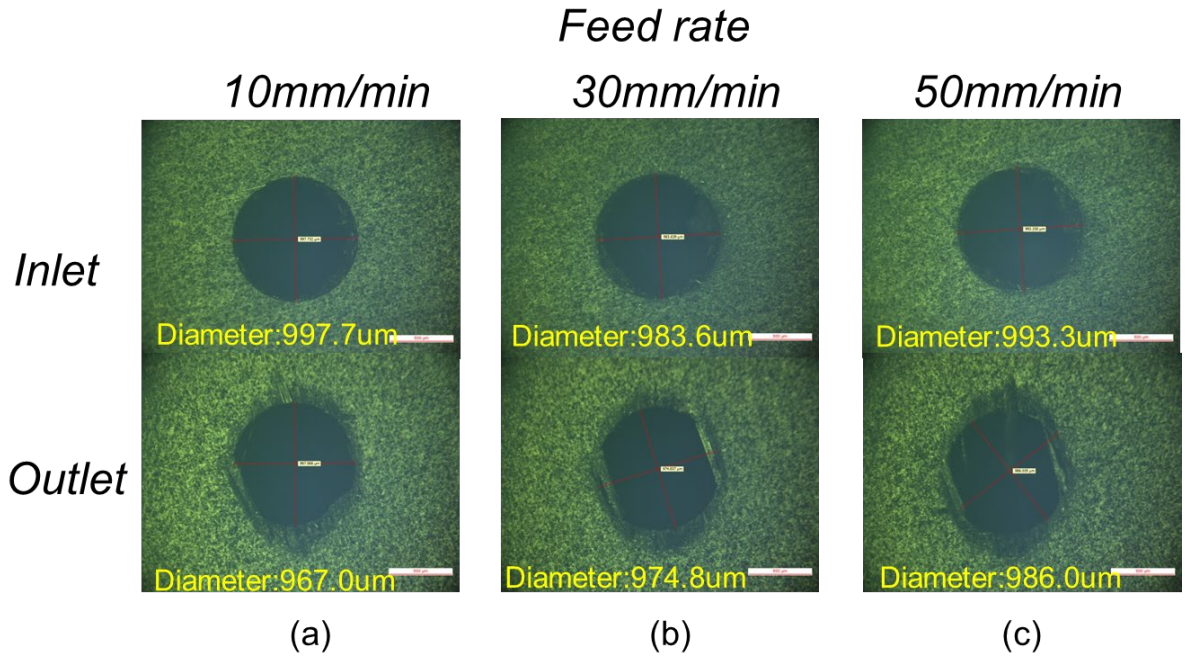

Figure 3-18. Optical microscopic image of machined UD CFRP surface at feed rate of (a) 10mm/min, (b) 30mm/min, and (c) 50mm/min.

hole quality of drilled hole includes the defect as well as the dimensional accuracy. UD CFRP composite laminates with 3mm of thickness was drilled in the spindle speed at 5000RPM according to the change of feed rate with uncoated drill bit as shown in figure 3-18. The machined holes showed a clean entrance at every cutting condition. However, exit surface of CFRP laminates showed the uncut fiber and delamination. Diameter differences between entrance and exit were under 30㎛ at every case.

According to the feed rate the uncut fibers occurred on exit surface were increased. During the CFRP drilling on a macro scale, woven CFRP laminates rarely occurs the uncut fiber. However, in the case of

micro drilling, woven CFRP also generated more uncut fibers as the feed rate increases. In addition, both UD and woven CFRP were rarely affected by the feed rate in the case of the damaged area due to delamination.

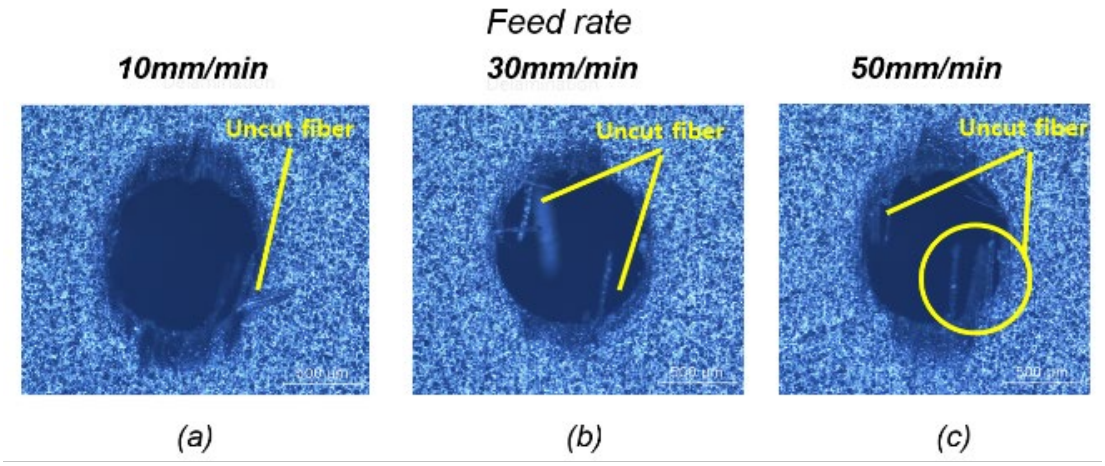

Figure 3-19. Optical microscopic image of machined UD CFRP surface at spindle speed of (a) 6000RPM, (b) 8000RPM, and (c) 10000RPM.

The comparison between uncoated and diamond coated tool in the machinability showed the differences in the results as shown in figure 3-19. Figure shows the exit surface of machined UD CFRP composite laminates according to the spindle speed. Holes machined with diamond coated tool have less uncut fiber and delamination area than holes machined with un-coated tool at the exit region. The drilled hole with un-coated tool have delamination diameter of 1.4, 1.5, and 1.55 mm according to spindle speeds of 6000, 8000, and 10000RPM when the drilled hole with diamond coated tool have no delamination. There is no advanced research to explain quality difference of the hole depending on the coating of the tool, but it is expected that the heat and pressure generated during drilling are relatively smaller for the diamond coated tool and the chip is also discharged faster than un coated tool.

3.4.2 Delamination of micro drilling process

The delamination on the machined CFRP surface can be evaluated through the delamination ratio as shown in figure 3-21. Delamination diameter(D_{max}) is defined as the diameter of circle containing the

delamination of drilled surface of CFRP composite laminates.

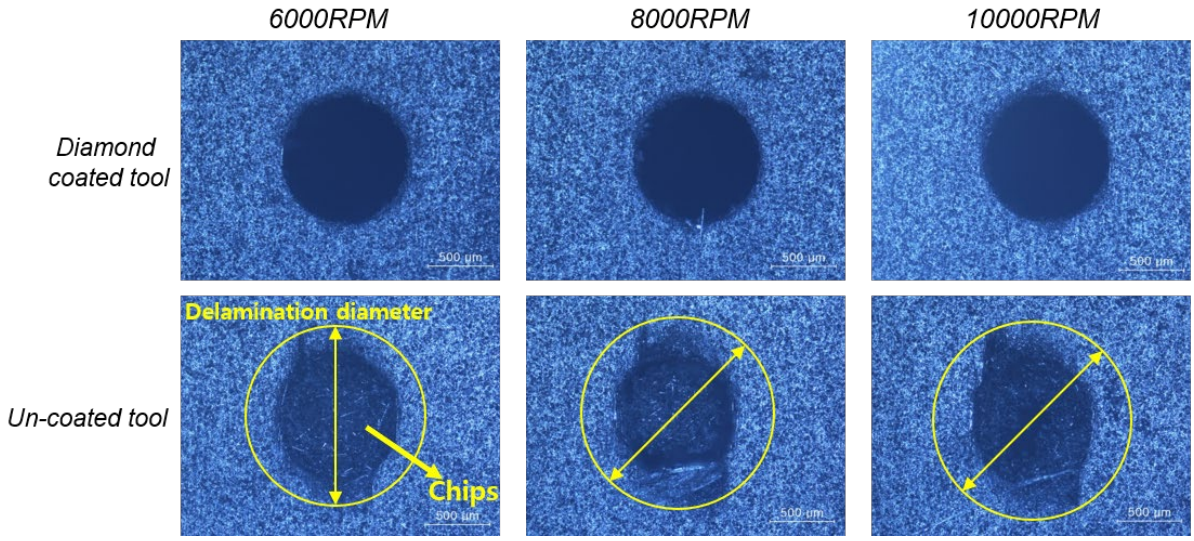

Figure 3-20. Exit surface of CFRP according to the spindle speed, and coating (Diamond coated, un-coated)

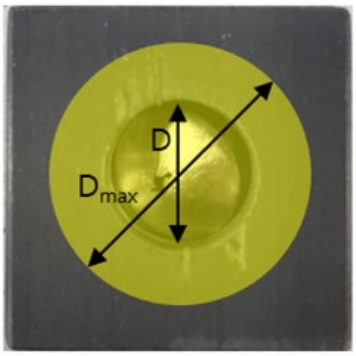

Figure 3-21. Definition of the one dimensional delamination factor

Eq. 3-1

where the F_d is the value of delamination ratio, D_{max} is the measured delamination diameter and D is the hole diameter. The smaller magnitude of delamination ratio means better quality of machined hole.

In every cutting condition, delamination occurred on surface of CFRP composites were inevitable in normal drilling process. To achieve better hole quality, peck drilling process is applied and analyzed in this chapter. Peck drilling is a method of performing drilling by moving several times up and down

without passing through at once like normal drilling. At the same cutting condition, delamination factors of exit region of CFRP composited are compared as shown in figure 3-22. Cutting conditions for the test were diamond coated tool with 1mm diameter in the feed rate of 30mm/min for the UD CFRP. Machined hole with peck drilling shows less uncut fiber as well as the smaller delamination ratio according to the spindle speed.

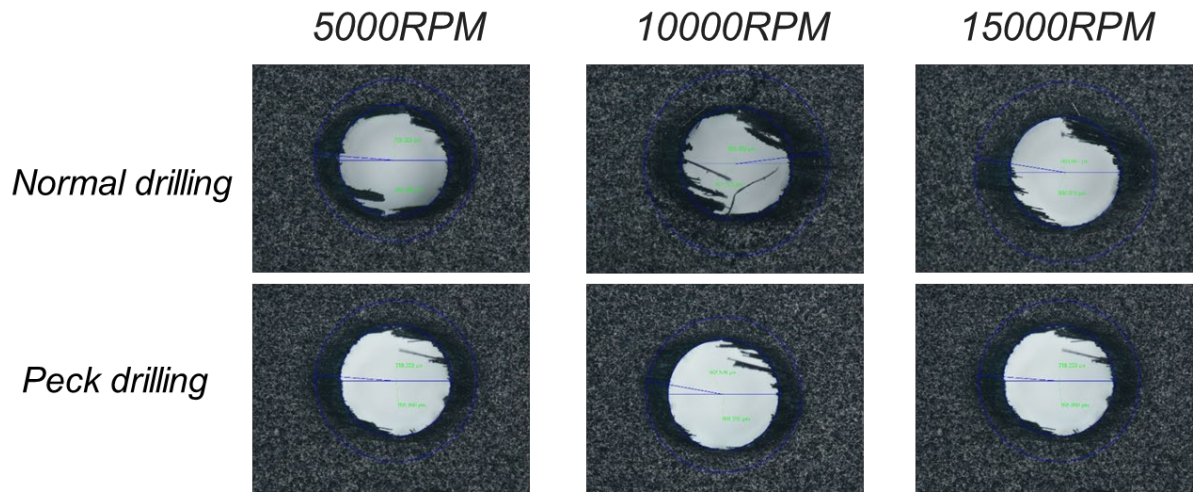

Figure 3-22. Exit surface of CFRP according to the spindle speed, and process types(Normal, Peck drilling)

Unlike a single hole drilling process, the distance between the holes was important in hole patterning. Especially, in the case of UD CFRP, critical delamination occurred between adjacent holes according to fiber orientation. This distance appears to be related to the delamination factor of a single hole and when the distance between the centers of the holes is less than 2.1 mm in the machining conditions under which machining is performed, delamination occurs in which the surface between the hole and the hole is completely peeled off. In micro drilling, both UD and Woven CFRP generated more uncut fibers as the feed rate increased. Coated tools showed better machinability than un coated tools and further research is needed to clarify the reason. Through peck drilling, drilled CFRP laminates showed lower delamination ratio than normal drilling process. Finally, in the micro drilling of UD CFRP, the delamination occurred according to the distance between the hole and the hole, and further study is needed to explain it.

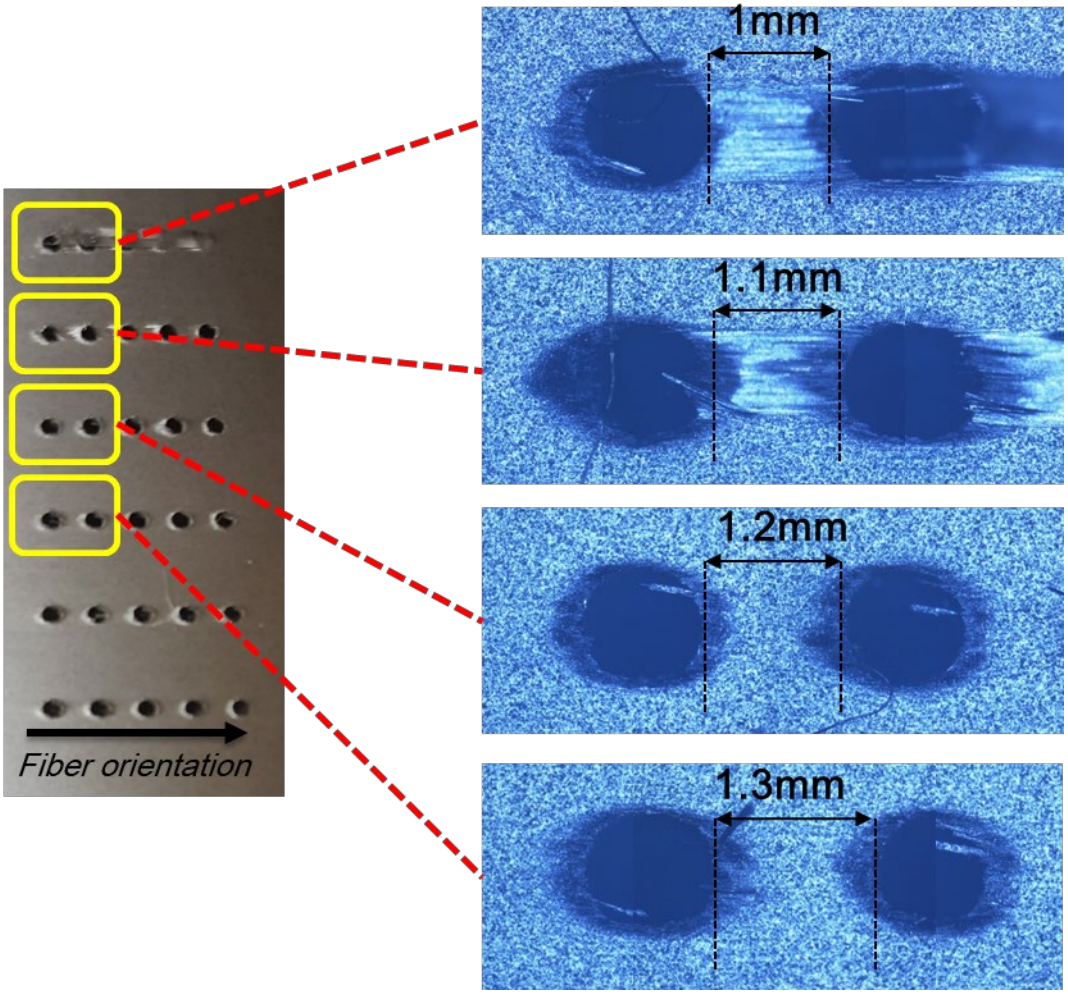

Figure 3-23. Delamination occurred in the hole according to the hole center-to-center distance

Table 3-9. Delamination factor according to the spindle speed(5000,10000,and 15000RPM), and drilling types (Normal, and peck drilling)

Drilling type	5000RPM	10000RPM	15000RPM
Normal	1.44	1.64	1.60
Peck	1.27	1.38	1.44

3.4.3 Investigation on vibration assisted drilling

As mentioned at above work, method of drilling process is another factor affect the quality of machined holes. Vibration assisted drilling process is one of the emerging hybrid processes applied in the machining for difficult-to-cut materials. In this work, ultrasonic machine tool manufactured by DMG mori was utilized for the drilling process as shown in figure 3-24.

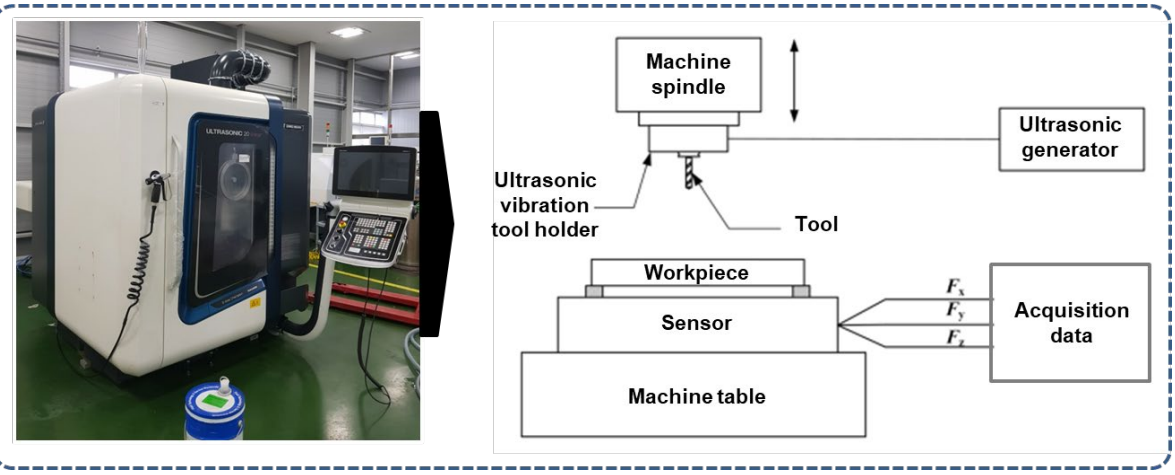

Figure 3-24. Experimental setup for vibration assisted drilling process

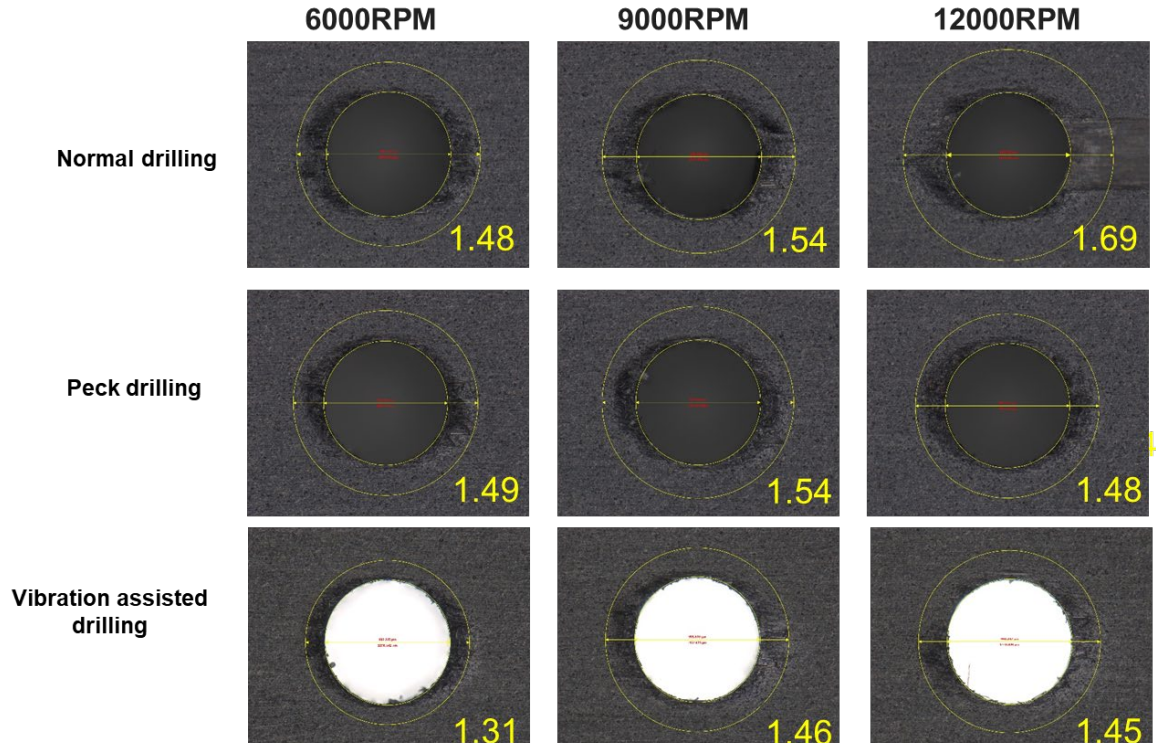

Figure 3-25. Delamination factor of each drilling processes according to the spindle speed

Figure 3-25. shows the exit surface of the machined hole according to the spindle speed, feed rate, and process types. Two fluted solid carbide drill with diameter of 1mm manufactured by 'Union Tool' is used. Tools have 130 degree of point angle with 10mm of flute length with 3mm shank diameter. Vibration assisted drilling showed better results comparing to the normal, and peck drilling processes. Tool vibrates in 30kHz with the approximate amplitude of 0.01mm during the drilling process, and it decreases the delamination. Figure 3-27 shows the result of delamination ratio of both normal and vibration assisted drilling for varying feed rate and spindle speed. Vibration assisted drilling showed the better quality of machined hole for almost every cutting conditions. However, unlike to the drilling process with the macro size drill tool, micro drilling process was not affected by the feed rate. Similar results were also appeared in the drilling tests with the diameter of 0.5mm under same cutting conditions. Vibration assisted drilling showed better surface results in most cutting conditions as shown in figure 3-28. Vibration assisted drilling seems to play the role of lubrication that unable to be used during the CFRP drilling process. Ultrasonic vibration emits the trapped power chips due to the high aspect ratio. However, results according to the cutting conditions tell us that micro drilling process need other approach due to the size effect and nonlinearity of the process.

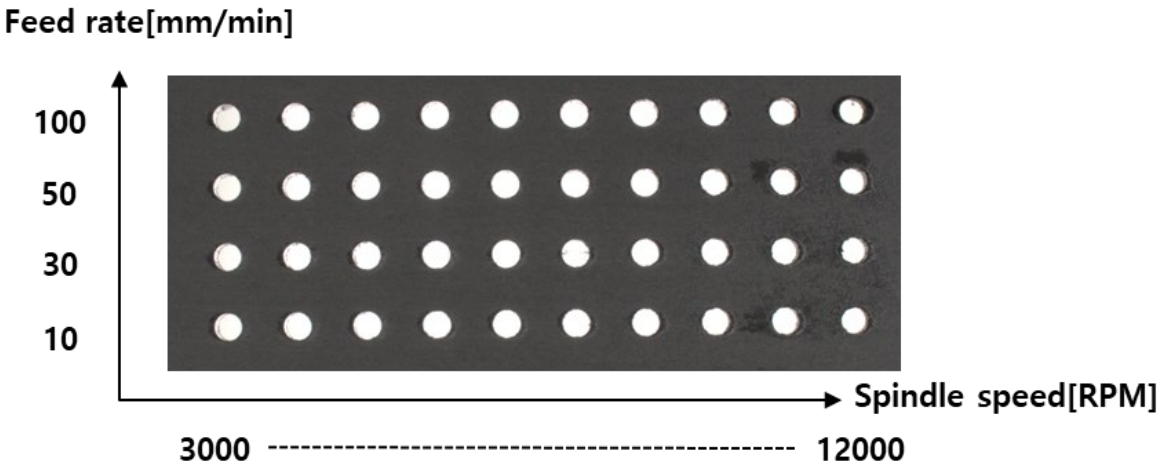

Figure 3-26. Drilled hole with micro drilling process according to the spindle speed and feed rate

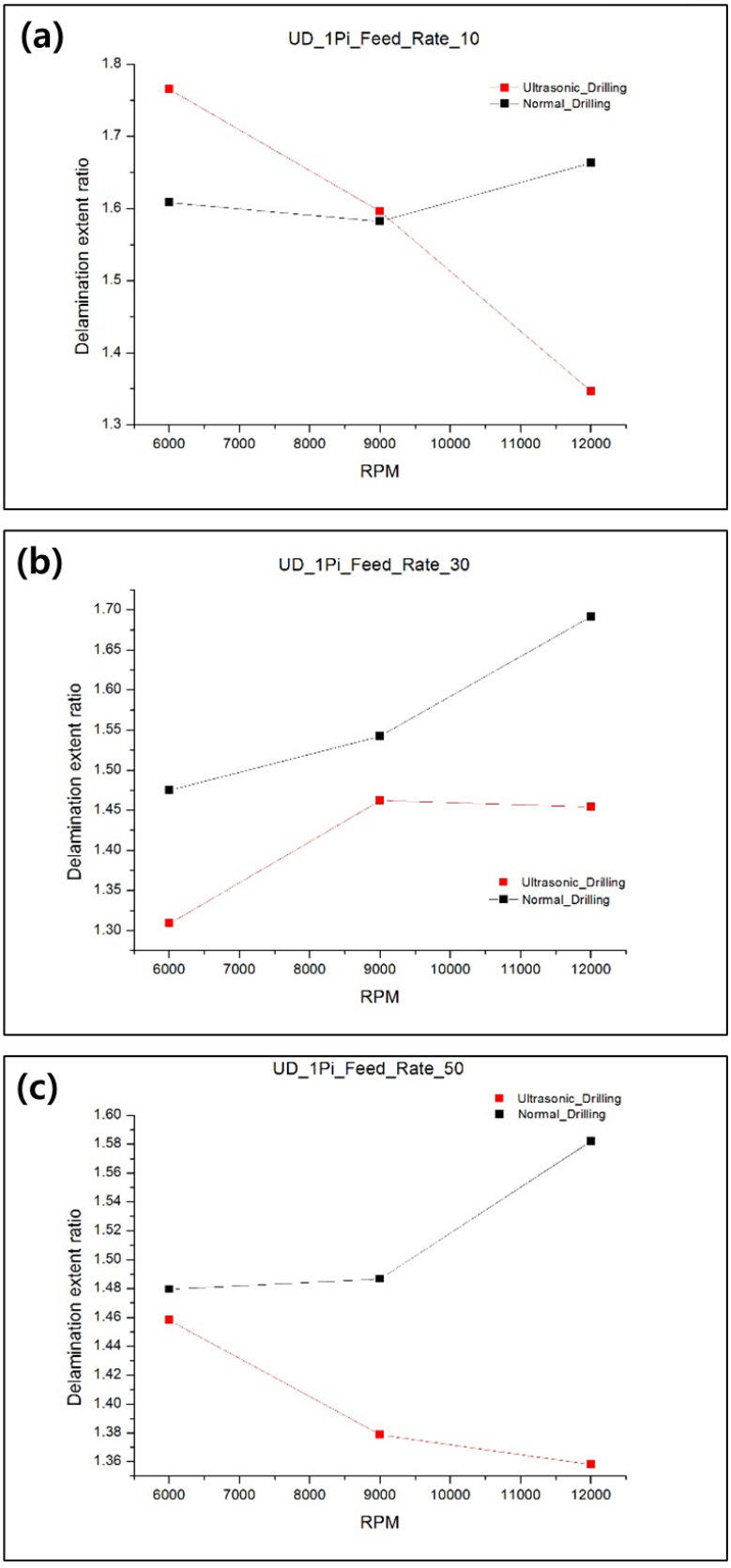

Figure 3-27. Delamination factors according to the spindle speed with feed rate of (a) 10mm/min, (b) 30mm/min, and (c) 50mm/min using 1mm diameter drill bit

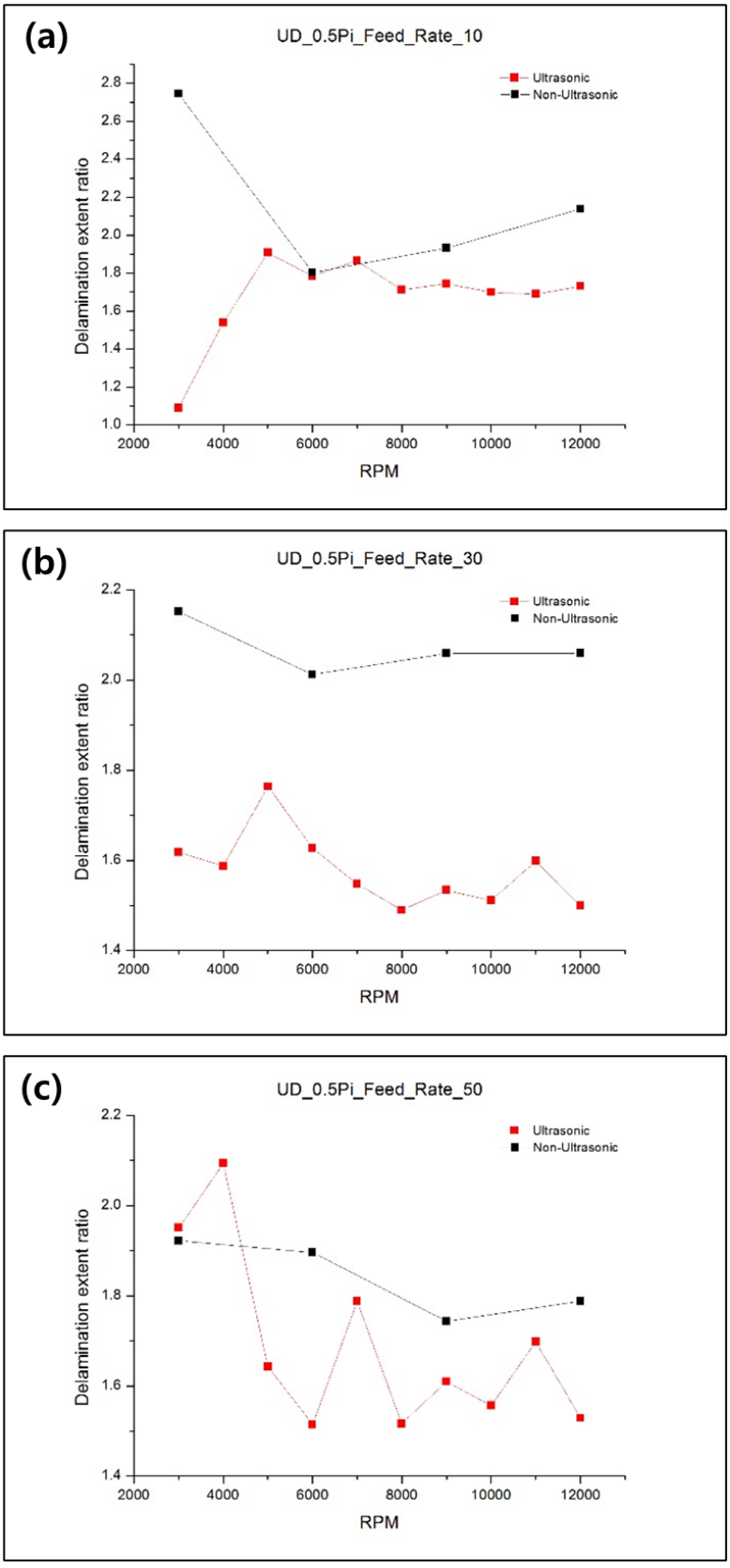

Figure 3-28. Delamination factors according to the spindle speed with feed rate of (a) 10mm/min, (b) 30mm/min, and (c) 50mm/min using 0.5mm diameter drill bit

3.5. Conclusions

In this study, experimental investigations on the process parameters to the CFRP composite drilling process were performed. Various process parameters such as types of composite material, cutting tool, cutting conditions were chosen for the experiment, and analyzed as the result of the thrust force and delamination. The findings and conclusions of this study are summarized as follows:

- ✓ Fiber volume fraction of the CFRP composite material affects the thrust force occurred during the drilling process. Increased fiber volume fraction contributes to the increase of strength for both inter-laminar and fiber orientation, and it causes the thrust force increases under same cutting conditions.
- ✓ Feed of the drilling process strongly affects the thrust force and delamination of the machine hole. Delamination factors were calculated utilizing the processed CT scanned images, and it showed proportional relation to the feed conditions. Backplate during the drilling process prevent the delamination propagation, and delamination area was restricted to the diameter of the backplate.
- ✓ Micro drilling process tests were conducted according to the drilling process types (Normal, Peck, and Vibrated assisted). Machined hole with vibration assisted drilling showed the best performance. However, effect of the micro drilling process was low due to the size effect of the drill bit.

4. Analytical modeling for thrust force during CFRP drilling process

4.1. Introduction

Typically, machining CFRP is a challenging task as it is typically inhomogeneous, and the structure may be somewhat orthotropic. Uncontrolled machining of CFRP can result in fluctuations in cutting force, delamination, and premature tool wear[32-46]. CFRPs can be produced in many forms, differing in extent of machinability. It is known that the fiber volume fraction and resin content of a CFRP have a significant effect on the strength of the polymer; however, few studies have been concerned with the machining performance of CFRPs as a function of fiber volume fraction. Therefore, we present an exhaustive study of the force generation and delamination that occurs when tooling CFRPs while varying the volume fraction. [173]

It can be learned from the above discussion that most of the developed model takes care of the material properties by using the specific cutting coefficient. Since these coefficients were developed using empirical relations, hence it may not provide a proper understanding about the machining requirements needed when different types of CFRPs are treated. Some of the models which takes care the material properties by using modulus and shear strength of the material, should also be further modified and tested to make it more applicable for generic cases of CFRP machining conditions. Inclusion of more geometrical parameters of drill-bit geometry can further enhance the applicability of the model for CFRP machining prediction. [174-177]

This paper focuses on the development of an analytical model for the drilling operation by considering the cutting lip region as a small minute section of orthogonal cutting operation and the chisel edge performing an extrusion operation. The force in the cutting lip section was further modeled by considering the chipping, pressing and bouncing region. Moreover, the fluctuation of forces is also modeled by predicting the minimum and maximum thrust force. Additionally, thermophysical properties of CFRP materials are also considered to predict the full stage thrust force changes in time domain. The prediction capability of the model is further tested for different fiber content of the CFRP

material. Furthermore, the thrust force generated during the drilling operation for three different unidirectional CFRP composite materials with varying volume fractions were compared and analyzed.

4.2. Analytical modelling

Figure 1 shows the complete modeling process. The expected thrust force is calculated based on the input drill bit geometry, CFRP composite material properties, and cutting conditions. A drilling cycle can be divided into four stages; the chisel, lip, and full engagement stages, and the exit stage. The thrust force increases when the chisel edge first enters the material, and continues to increase as the drill lip also engages. The rate of force increase reduces once the bit lip is fully engaged, and the force approaches its maximum value. The thrust force then decreases slowly until the drill bit starts to exit the material. The thrust force decreases sharply when the drill bit breaks out of the material, which continues until the drill bit tip has fully exited the material. The magnitude of the thrust force is strongly affected by material defects, so the proposed model analyzes the maximum and minimum force measured during stages 1 and 2. In addition, the thrust force profile is dependent on the position of the drill bit relative to the composite material; therefore, this model incorporates time-domain analysis so that the complete CFRP drilling process can be understood.

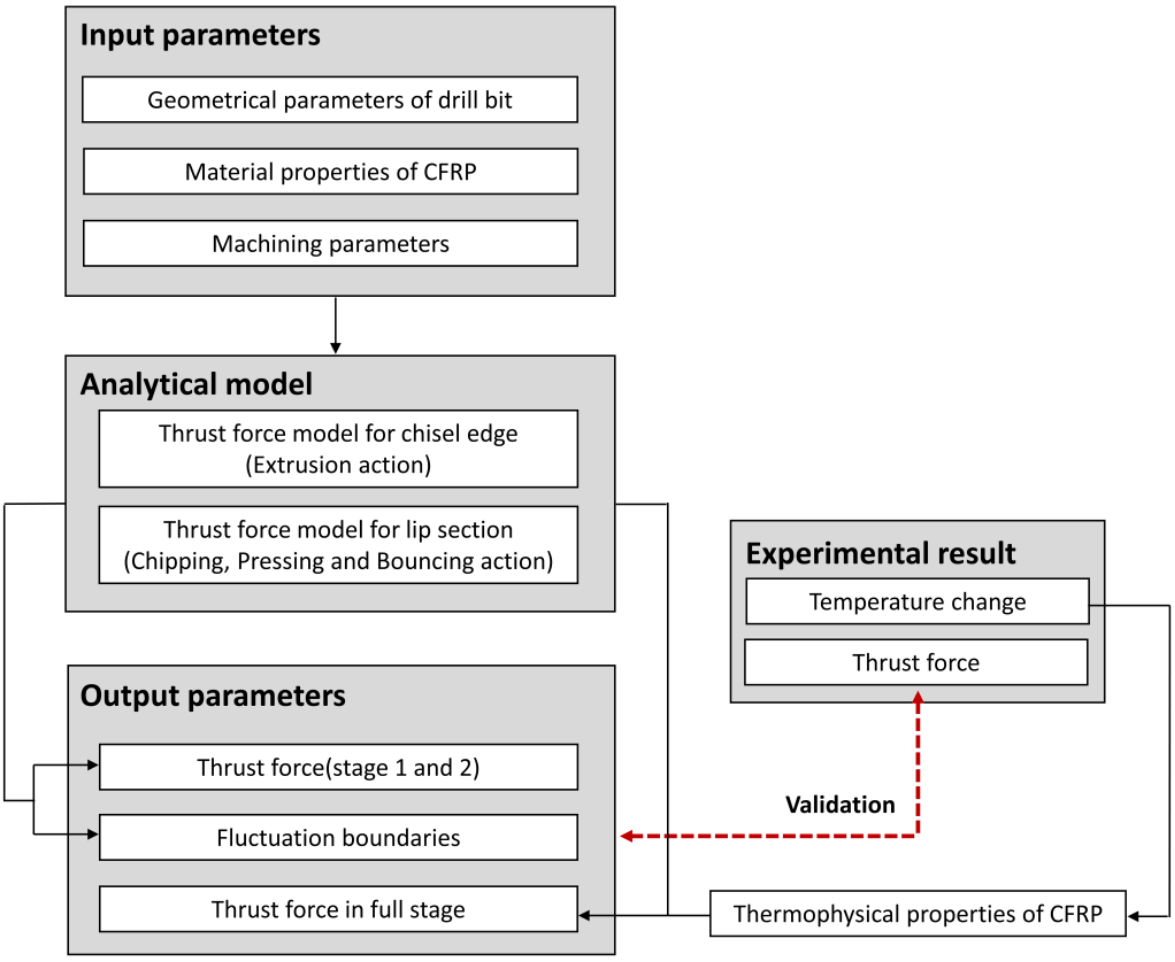

Figure 4-1. Flow chart of analytical modeling process

4.2.1. Forces on the chisel edge

The chisel edge of a drill bit generates an extruding force at the CFRP surface. Figure 2 shows a cross-section of the force distribution along the plane B–B, and defines some geometric parameters.

Guo et al. [99] and Cheng et al. [102] described the force generated by the extruding action of the chisel edge. The elemental cutting force dF_{chi} can be resolved into two parts: (a) dF_{chl} represents the generated thrust force and (b) dF_{chr} represents the generated torque. The elemental force dF_{cha} responsible for generating the thrust force is defined by Eq. (4-1)

$$dF_{chi} = \frac{E_3}{1-v^2}\left(k_{ch}w + \frac{fnt}{2}\right)\tan\gamma_w \cos\gamma_f \tag{4-1}$$

where E_3 is the Young's modulus of the CFRP in the transverse direction, v_{13} is the Poisson's ratio, w is the thickness of the chisel edge, K_{ch} is the chisel edge coefficient (which is assumed to be 0.004), n is the speed of rotation (s^{-1}), f is the feed rate, and t is the time in seconds. γ_w is half of the chisel edge angle and γ_f is the feed rate angle, as described by Eqs. (4-2) and (4-3), respectively.

$$\gamma_f = \tan^{-1}\left(\frac{f}{2\pi r_{chi}}\right) \tag{4-2}$$

$$\gamma_w = \tan^{-1}\left(\tan\left(\frac{\varepsilon_d}{2}\right)\sin(\psi)\right) \tag{4-3}$$

where $\varepsilon_d / 2$ is half of drill bit point angle. r_{chi} is the chisel edge radius, which is given by Eq. (4-4)

$$r_{chi} = w / \sin(180 - \psi) \tag{4-4}$$

where ψ is the chisel edge rake angle (123.7°).

The elementary force given in Eq. (1) can be integrated over the entire region of the chisel edge geometry to find the total thrust force, as described by Eq. (4-5).

$$F_{cha} = \int_{-w/\sin(180-\psi)}^{w/\sin(180-\psi)} \frac{E}{1-v^2}\left(k_{ch}w + \frac{fnt}{2}\right)\tan\gamma_w \cos\gamma_f dr \tag{4-5}$$

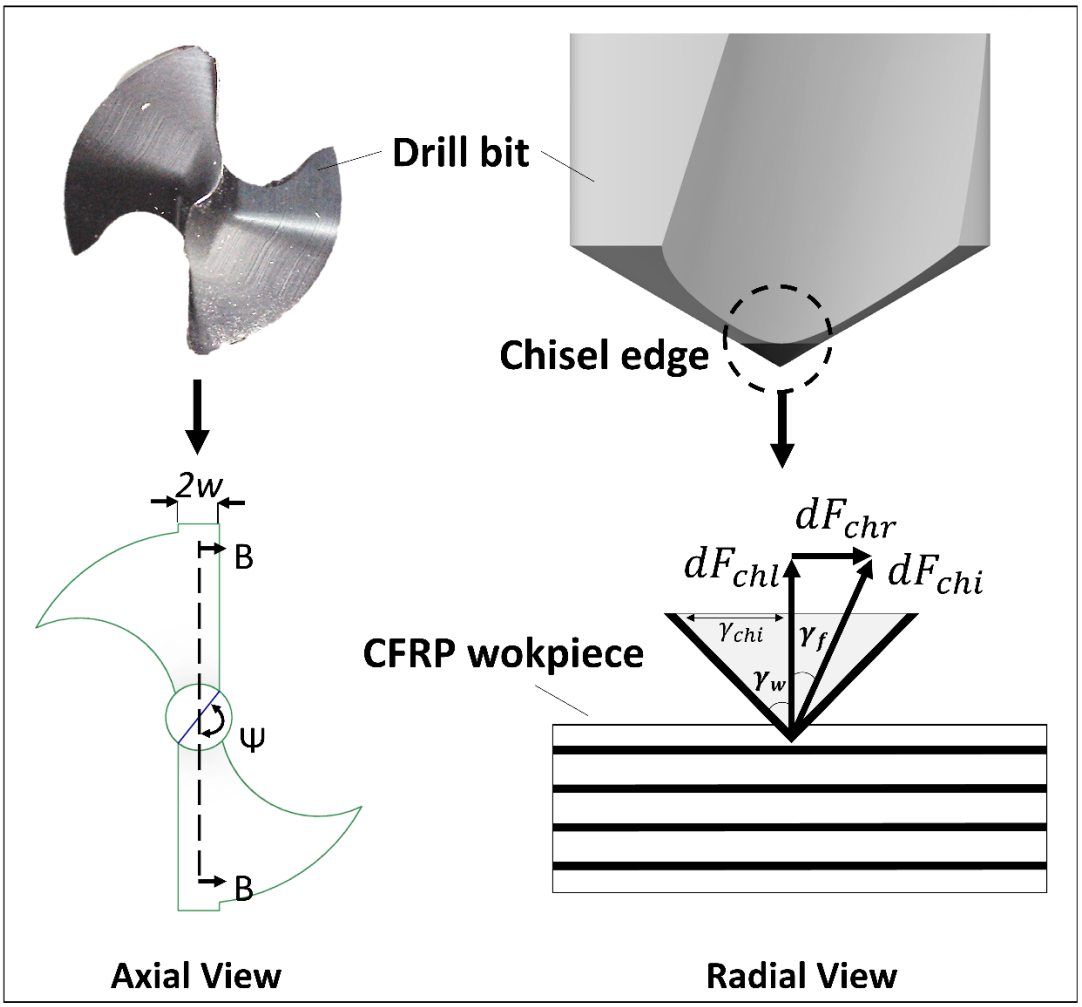

Figure 4-2. Force on the chisel edge in axial and radial view

4.2.2. Forces on the cutting lips

The forces on the drill lip were modeled by mapping the forces generated by the orthogonal cutting system onto the drilling coordinate system, and accounting for the cutting lip angle. As shown in Figure 4, the force generated by the small cutting edge, *dh*, of the drill lip can be resolved with two components: dF_x represents the orthogonal cutting force, and dF_y represents the orthogonal thrust force. When the cutting edge of the drill lip is small, the lip can be described more simply as a number of orthogonal cutting edges, where each edge has different cutting parameters. Zhang et al. [100] reported that orthogonal cutting of a unidirectional composite can be divided into chipping (dF_{y1}), pressing

(dF_{y2}), and bouncing (dF_{y3}) forces. Therefore, the total thrust force in this region, dF_y, is the sum of these three forces (i.e., $dF_y = dF_{y1} + dF_{y2} + dF_{y3}$). The three components are discussed in more detail in the following section.

Region 1: Chipping region

The forces generated in the chipping region are primarily caused by material removal. The vertical thrust force generated in this region is described by dF_{y1} as given by Eq. (4-6).

$$dF_{y1} = \tau_1 a_c \frac{\cos\phi \tan(\phi + \beta - \gamma_0) - \sin\phi}{\tau_1 / \tau_2 \cos(\theta - \phi)\sin\theta - \sin(\theta - \phi)\cos\theta} dh \tag{4-6}$$

where the τ_1 is the shear strength perpendicular to the fiber direction, τ_2 is the shear strength parallel to the fiber direction, θ is the equivalent fiber orientation, a_c is the cutting thickness, β is the friction angle of the tool rake face of the tool, and ϕ is the shear angle of the lip section cutting component, as given by

$$\phi = \tan^{-1}\left(\frac{\cos\gamma_0}{1 - \sin\gamma_0}\right) \tag{4-7}$$

γ_0 is the cutting lip rake angle, which is described by Eq. (4-8)

$$\gamma_0 = \tan^{-1}\frac{(r\cos\phi_1 \tan\theta_r)}{(R_1 \sin(\varepsilon_d / 2) - w\cos(\varepsilon_d / 2)\tan\theta_r)} - \tan^{-1}\left(\frac{\sin\phi_1 \cos(\varepsilon_d / 2)}{\cos\phi_1}\right) \tag{4-8}$$

where, θ_r is the helix angle of the drill bit that varies along the cutting lip and ϕ_1 is the web angle normal to the drill bit axis. Then, θ_r and ϕ_1 are represented by Eqs. (4-9) and (4-10), respectively.

$$\theta_r = \tan^{-1}((\tan\theta_h) r(t) / R_1) \tag{4-9}$$

$$r(t) > r_{chi} \tag{4-10}$$

θ_h is the given helix angle of the drill bit, and dh is an element of the cutting lip section.

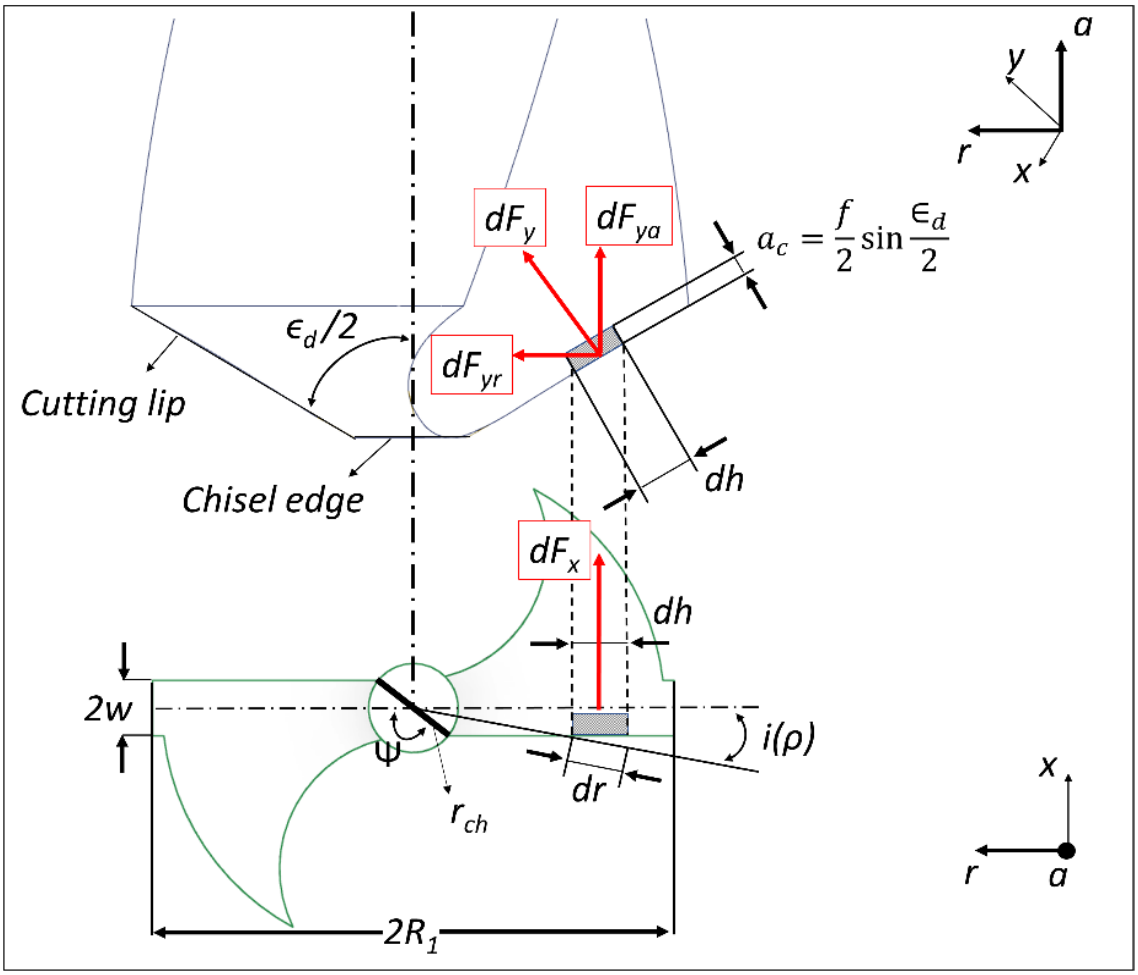

Figure 4-3. Illustration of the drill lip components in axial and radial direction

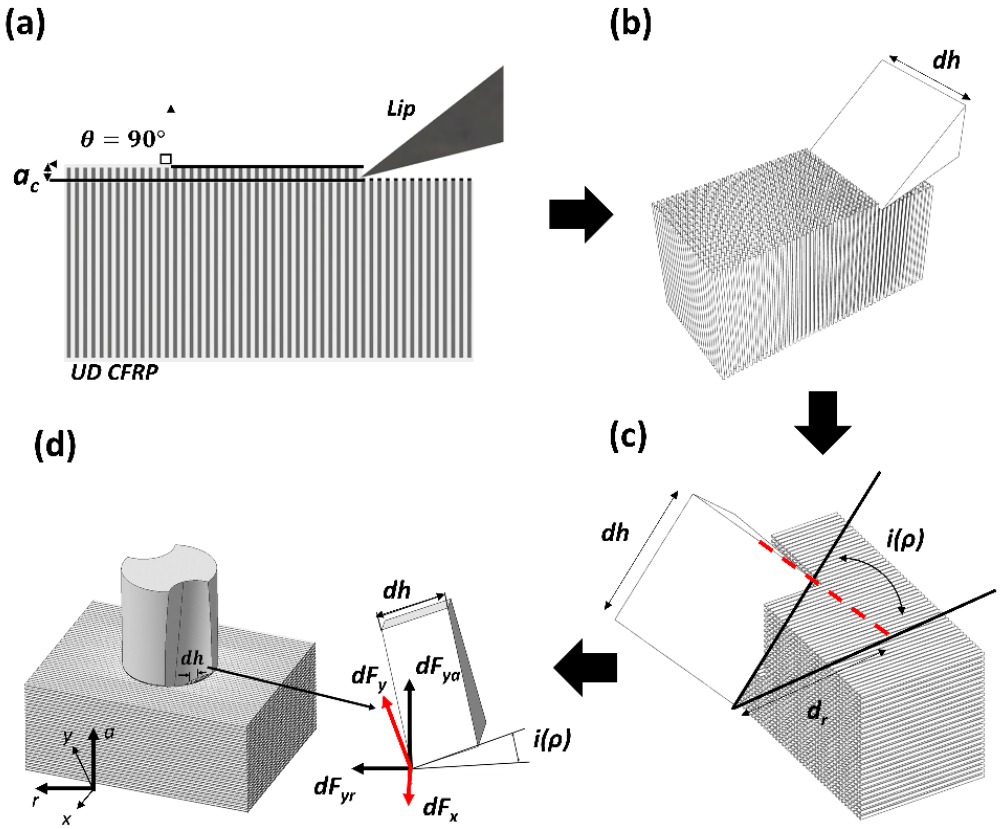

Figure 4-4. Force components and transformation to the drill bit coordinate

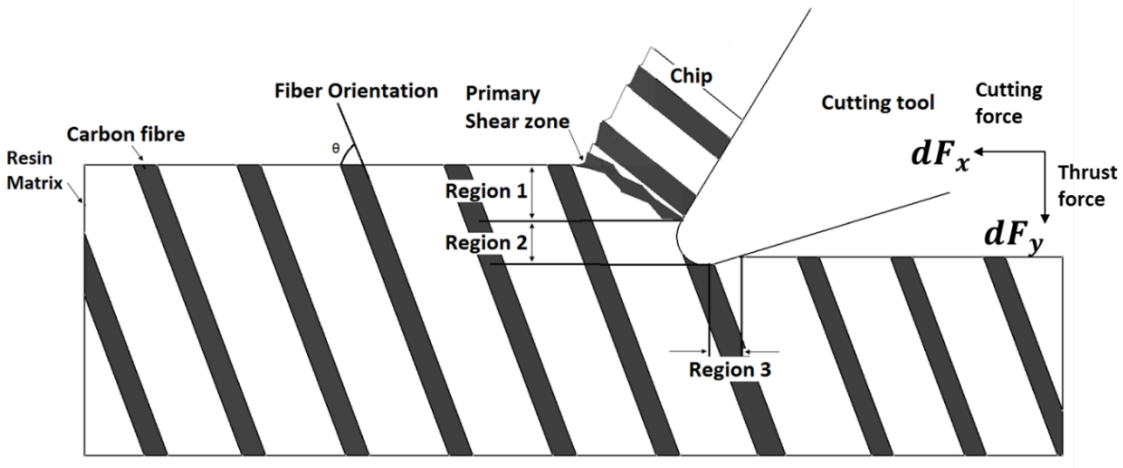

Figure 4-5. Schematic of the orthogonal cutting a unidirectional CFRP

Region 2: Pressing region

Pressing forces are produced by the filleted region of the cutting lip. The vertical force generated by pressing the differential element *dh* is represented by dF_{y2}, as given in Eq. (4-11)

$$dF_{y2} = \frac{r_e \pi E_3^*}{8(1-\nu_3^2)}(\cos\theta - \mu \sin\theta)dh \tag{4-11}$$

where r_e is the cutting lip fillet radius (assumed to be 0.0018 μm), and μ is the friction coefficient between the tool and the workpiece, which is assumed to be 0.8 in this study. E_3^* was calculated using Eq. (4-12), i.e., $E_3^* = E_{\theta p}$ owing to the angle between the cutting lip and fiber orientation.

$$E_{\theta p} = (\frac{\cos^4\theta p}{E_1} + \frac{\sin^4\theta p}{E_3} + (\frac{1}{4})(\frac{1}{G_{13}} - \frac{2\nu_{13}}{E_1})\sin^2 2\theta_p)^{-1} \tag{4-12}$$

where θ_p = 67.5° when the fiber orientation angle θ = 90° with respect to the cutting lip, and θ_p = 90° when θ = 0°.

Region 3: Bouncing region

Bouncing forces are generated at the tool–workpiece. The vertical force generated as the tool bounces is described by dF_{y3}, which is given in Eq. (4-13)

$$dF_{y3} = \frac{1}{2} r_e E_3^* \cos^2\alpha dh \tag{4-13}$$

where α is the tool clearance angle (11°) and $E_3^* = E_{\theta p}$, as the angle between the drill lip and composite fiber direction is 67.5°.

Therefore, the total vertical force generated by the cutting lip is described by dF_y, where

$$dF_y = dF_{y1} + dF_{y2} + dF_{y3} \tag{4-14}$$

As discussed, the orthogonal cutting system force, dF_y, must be transformed into the drilling component forces; dF_{ya} is the thrust force and dF_{yr} is the vertical drill axis force. The drill is symmetrical around the drill axis; thus, dF_{yr} is cancelled-out, so that dF_{ya} is the thrust force generated during the drilling process. Similarly, the cutting force component, dF_x, can be resolved into two components, dF_{xr} and dF_{xz}, where dF_{xr} is cancelled-out such that dF_{xz} is the torque generated during drilling.

$$dF_{ya} = (dF_{y1} + dF_{y2} + dF_{y3})dh \tag{4-15}$$

The element *dh* can be transformed to a radial coordinate system using the incline angle, as described by Eq. (4-16)

$$dh = \cos(i(\rho))dr \tag{4-16}$$

where $\rho = r(t)/R_1$, and R_1 is the maximum drill bit radius, as shown in Figure 4-3.

As given in Figure 4-6,

$$w = \frac{r(t)}{\sin(\varepsilon_d/2)}\sin(i(\rho)) \tag{4-17}$$

$$i(\rho) = \sin^{-1}(\frac{w}{\rho R_1}\sin(\varepsilon_d/2)) \tag{4-18}$$

Hence,

$$\cos(i(\rho)) = [1-\sin^2(i(\rho))]^{\frac{1}{2}} = [1-\frac{w^2\sin^2(\varepsilon_d/2)}{\rho^2 R_1^2}]^{\frac{1}{2}} = [1-\frac{w^2\sin^2(\varepsilon_d/2)}{2\rho^2 R_1^2}] \tag{4-19}$$

The following equation is derived by substituting the value of $\cos(i(\rho))$ into Eq. (4-16)

$$dh = [1-\frac{w^2\sin^2(\varepsilon_d/2)}{2\rho^2 R_1^2}]R_1 d\rho \tag{4-20}$$

Then, the thrust force of the differential element *dh* is calculated by combining Eqs. (4-15) and (4-20)

$$dF_{ya} = (dF_{y1} + dF_{y2} + dF_{y3})(1 - \frac{w^2 \sin^2(\varepsilon_d / 2)}{2\rho^2 R_1^2}) R_1 d\rho \tag{21}$$

Limits can be applied, so that the total thrust force generated by the cutting lip section is calculated as follows :

$$F_{lip-total} = 2\int_{a_1}^{b_1} dF_{ya} \sin(\varepsilon_d / 2) \tag{4-22}$$

The integration limits given in Eq. (4-22) are dependent on the effective radius of the chisel and drill bit. The radius of the cutting lip starts at the chisel edge radius, and increases to its maximum value R_1, at which the cutting lip is fully engaged in a drilling operation. Hence, $r(t)$ is a time-dependent parameter, as described by Eq. (4-23) and shown in Figure 4-6.

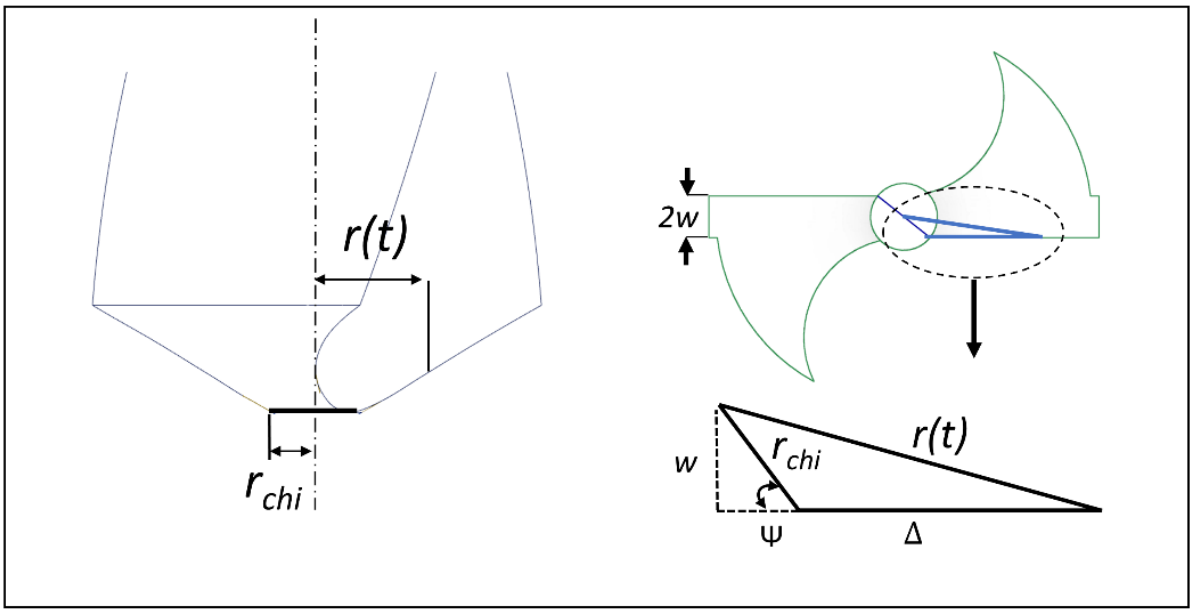

Figure 4-6. The dimensions of the time-dependent radius, r(t), during the drilling process

$$r(t) = \sqrt{(w / \sin(180 - \psi))^2 + \Delta^2 + 2w\Delta / \sin(180 - \psi)\sqrt{1 - \sin^2(180 - \psi)}} \tag{4-23}$$

where Δ is the time interval given by Eq. (4-24), and n and f are the tool rotation and feed speed, respectively.

$$\Delta = \frac{fnt}{\cos(\varepsilon_d / 2)} \tag{4-24}$$

The time-dependent chisel edge radius is used as the upper limit after normalization, as described by

$$b_1 = \frac{r(t)}{R_1} \tag{4-25}$$

The lower limit of the integral in Eq. (4-22) is then given by

$$a_1 = \frac{w}{R_1 \sin\phi} = \frac{r_{chi}}{R_1} \tag{4-26}$$

The equivalent fiber orientation, θ, during the cutting operation is described by

$$\theta = \cos^{-1}(\cos(\theta_0) * \cos(i(\rho))) \tag{4-27}$$

where $i(\rho)$ is the incline angle, and θ_0 is the fiber angle at 0° and 90°.

$$F_{total} = F_{cha} + F_{lip-total} \tag{4-28}$$

The expected force generated during the drilling process until the drill exited the material was calculated using Eq. (4-28). Upon exit from the material, the force was calculated by reversing the limits used to solve Eq. (4-28).

4.2.3. Thermo-physical modeling of CFRP drilling process

When drilling, the friction between the drill bit and workpiece increases their respective temperatures [128, 139, 178]. CFRP materials are abrasive and hard, and have a low thermal conductivity; thus, the resulting temperature can be high enough to reduce the mechanical properties of the composite laminate. Therefore, the thrust force generated throughout stage 3 decreases gradually until the drilling process enters stage 4. Empirical models of the thermophysical properties of CFRP composites at high temperatures have been proposed by several researchers. Fei et al. [139, 140] used an exponential model that accounted for fiber content, resin softening, and decomposition of the mechanical properties:

$$\frac{P(T)}{P_0} = (1-V_f)\exp[-k_1(\frac{T-T_0}{T_g})^3] + V_f \exp[-k_2(\frac{T-T_0}{T_d})^3] \quad (29)$$

where $P(T)$ and P_0 represent the mechanical properties at the process and room temperature, respectively. V_f is the fiber volume fraction of the CFRP composite, and T_g and T_d are the glass transition and decomposition temperatures, respectively. The constants k_1 and k_2 are 1.155 and 0.552, respectively, as identified by the authors. The drilling process temperature was measured experimentally, and the temperature behaviors were included in the empirical model so that the mechanical properties of the composite laminates could be modeled accurately. [139]

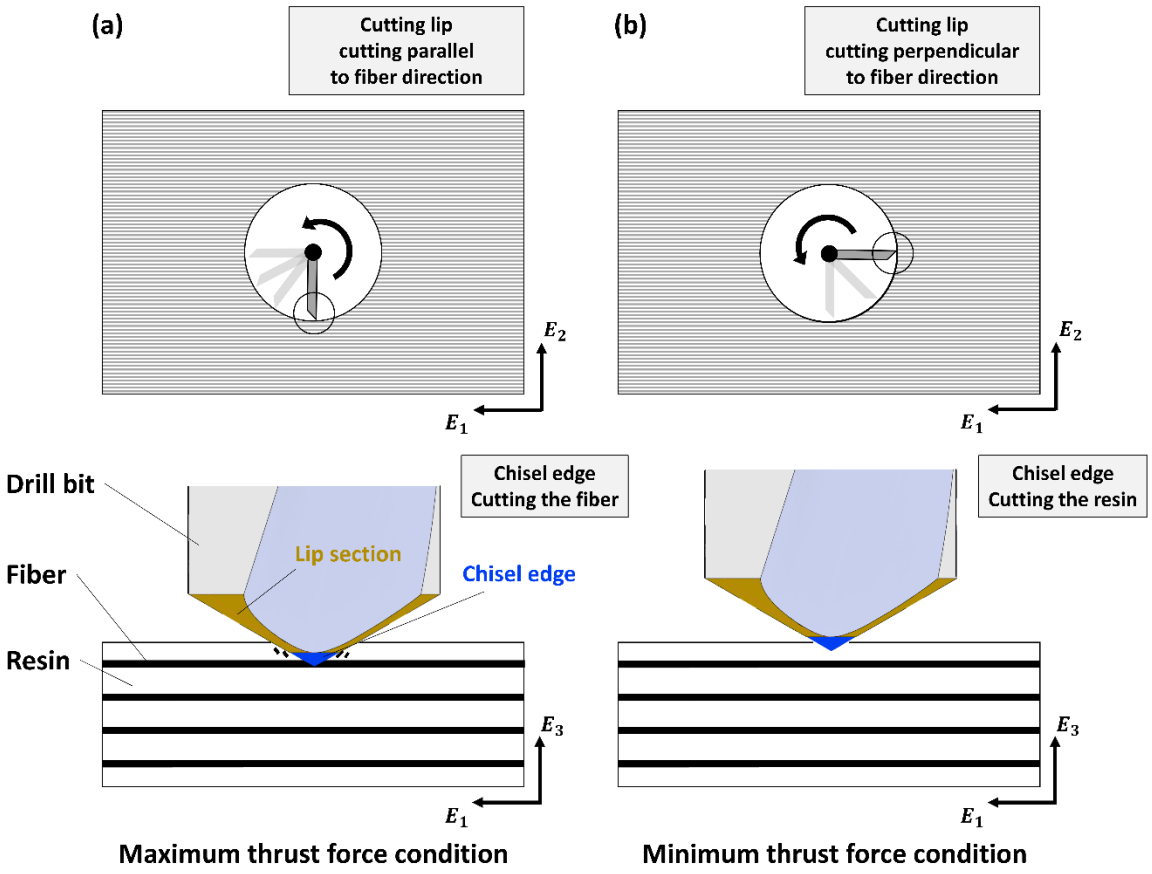

Figure 4-7. Force fluctuation mechanisms. (a) The maximum force occurs when the angle between the cutting lip and fiber is 0° (θ0 = 0°), and (b) the minimum thrust force occurs when the angle between the cutting lip and fiber is 90° (θ0 = 90°)

4.2.4. Fluctuation modeling for drilling process

Unlike homogeneous materials, the thrust force generated when drilling composite laminates fluctuates in a sinusoidal manner. As the drill bit rotates, the chisel edge progresses downward, and the drill lip cuts simultaneously; thus, the force variation incorporates both mechanisms and can be modeled if the minimum and maximum thrust force are known. The maximum thrust force can be obtained by summing Eqs. (4-5) and (4-22), which is described by Eq. (4-28).

It was assumed that the minimum thrust force was generated when the chisel edge interacted with the resin of the CFRP composite, and the angle between the cutting lip and fiber was θ_0 = 90°. Figure 7 shows the conditions under which the maximum and minimum thrust forces are generated. Here, E_1 is the Young's modulus parallel to the fiber direction, and E_2 and E_3 are the Young's moduli perpendicular to the fiber direction in a unidirectional composite. If E_3 is applied to Eq. (4-5) as the Young's modulus of the resin (E_r =2.5 Mpa), and the value of E_3^* discussed in Section 2.2 is used as the value of E_3 in Eq. (4-22) (owing to the 90° angle between the cutting lip and fiber direction), the minimum thrust force can be calculated using Eq. (4-28). Equations (4-30) and (4-31) describe the relevant parameters when the maximum and minimum force are generated. The total fluctuation over a 90° rotation of the drill bit is given in Eq. (4-32)

$$Maximum\ \ thrust\ \ force = F_{total}: \begin{bmatrix} chisel\_edge = E_3; \\ Lip\_region = E_3; \\ \theta_0 = 0; \end{bmatrix} \tag{4-30}$$

$$Minimum\ \ thrust\ \ force = F_{total}: \quad \begin{bmatrix} chisel\_edge = E_r; \\ Lip\_region = E_3^*; \\ \theta_0 = 90; \end{bmatrix} \tag{4-31}$$

$$Thrust\ force(N) = Maximum\ force - \left[\left(Maximum\ force - Minimum\ force \right) \times \cos\left(\frac{n\pi t}{30} \right) \right] \tag{4-32}$$

where $\frac{n\pi t}{30}$ varies from 0° to 90°, and is repeated to obtain the force curve over the duration of the drilling process.

4.3. Validation of analytical model

The experimental thrust forces values obtained were then compared with the predicted mean thrust force of the model at the end moment of stage 2. The comparison between the experimental thrust force and the predicted thrust force is shown in the figure. 4-8. which shows the efficacy of the present model for predicting the mean thrust force. It can be seen from the figure. that the thrust force values of the material which has higher fiber volume fraction has generated the higher thrust force during drilling process in both experimental and predict results. The minimum and the maximum percentage of error for USN 150Y was 12% to 29%; for USN 150B was 19% to 36% and for USN 150E was from 16% to 33% respectively. This might have occurred because of the variation in the predicted material properties with that of the actual one, which was obtained using the rule of mixture. The difference in the experimental and predicted values might have also occurred because of other uncontrollable environmental factors like vibration of the tool, rigidity of the machine tool, defects in the material, design of fixture and, voids in the specimen etc.

4.3.1. Thrust force curve for full stages of drilling process

The representative experimental result for the full stages of drilling process is shown in figure 4-9., which has performed in spindle speed of 7000RPM, feed of 0.02mm/rev with the material of USN

150(57%). The drilling process of CFRP and the thrust force change can be divided into 4 stages: stage1(chisel edge enter stage), stage2(lip section enter stage), stage3(full engagement), and stage4(exit stage). Drilling time along the stages are calculated based on cutting condition and geometry of drill bit. In Fig. 11. raw data of thrust force are averaged through moving filter of 20 to compare each force curves clearly eliminating unpredictable noise. The validation result showed good agreement between the predicted and experimental thrust forces, displaying similar trends through the whole stages figure 4-9. shows the thrust force curves in the spindle speed of 5000RPM, and feed of 0.02mm/rev regarding to different fiber volume fractions in the same manner of figure 4-10.

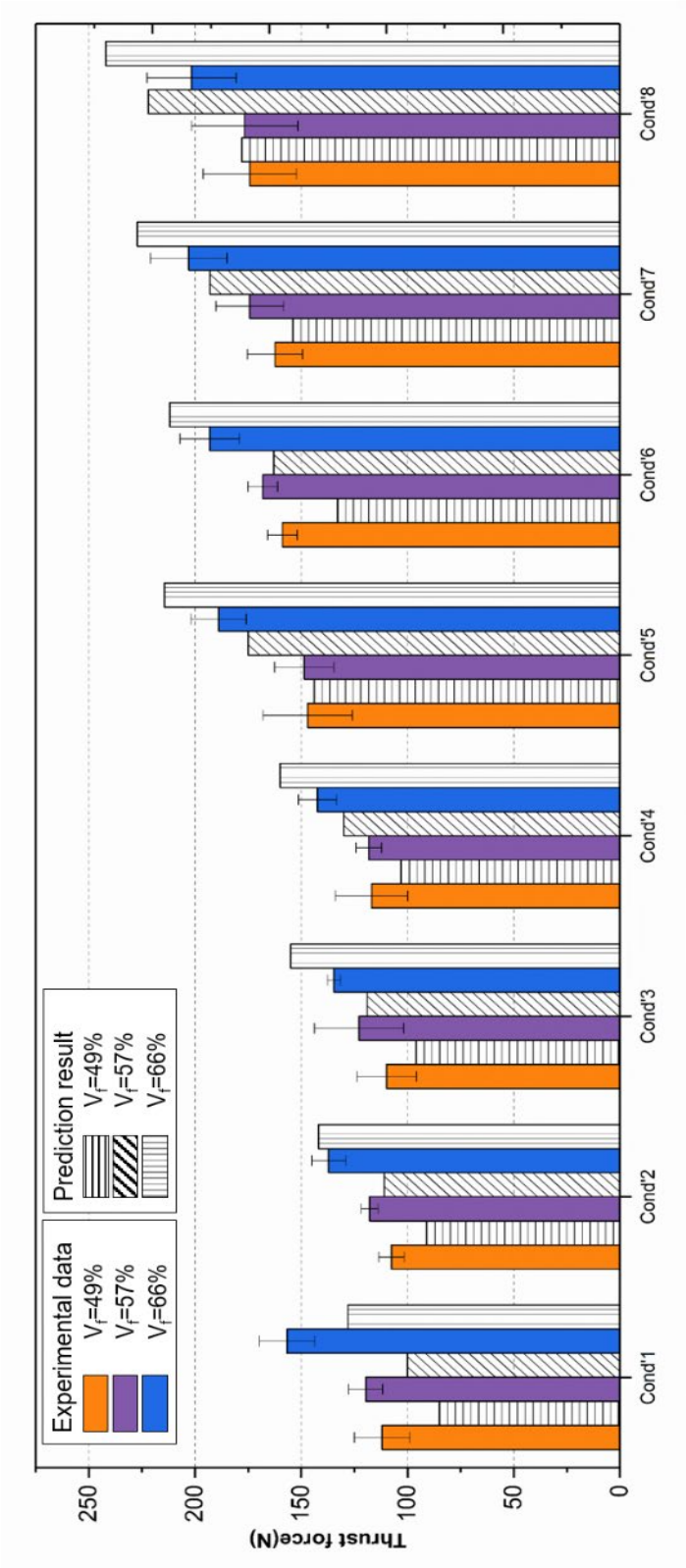

Figure 4-8. The experimental and predictive result of the thrust force according to varying drilling conditions and fiber volume fractions

Table. 4-1 shows the thrust force values at the specific time which divided into 12 points as shown in Fig. 4-8. In the comparison result of fiber volume fraction of 49%, the maximum error magnitude occurred at the time of 2633 msec. At the time point of 1054 msec, thrust force reaches maximum value where the drill bit fully engaged to the material, and from the time point of 2096 msec, drill bit starts to exit the material. During the stage3 (1054~2096msec), thrust force has decreased about 26.5N and 19.7N in the experimental and prediction results respectively. It appears that reduction of the thrust force is mainly due to the softening effect by the heat from the drilling process. Hence, the change of thermophysical properties of material has considered to the prediction model. The elevation of temperature was 85℃ and strength reduction of material was calculated as 28% by the Eq. (4-29). Reduction of the thrust force during stage 3 showed difference between the experimental and prediction result; the overall curve trend showed good agreement. The predicted thrust force curves in figure 4-10(b,c) also showed good agreement that do not deviate significantly from the experimental thrust force curves.

Table 4-1. Thrust force change with specific time

Time [msec]	Thrust force[N] (Experiment)			Thrust force[N] (Prediction)			Error magnitude[%]		
	V_f=49%	V_f=57%	V_f=66%	V_f=49%	V_f=57%	V_f=66%	V_f=49%	V_f=57%	V_f=66%
253	37.2	39.4	50.1	47.1	45.2	52.6	21.2	6.4	4.7
527	59.5	66.1	86.4	67.4	68.3	80.2	11.9	3.2	7.7
780	82.4	95.3	117.6	89.5	94.4	110.2	7.8	1.1	6.7
1054	115.4	124.3	149.6	113.4	125.8	144.8	2.0	1.2	3.3
1317	112.8	123.2	136.0	112.5	123.7	143.4	0.2	0.3	5.1
1570	112.2	119.7	138.1	109.1	120.1	138.5	2.7	0.4	0.3
1833	100.7	104.6	135.4	102.2	111.2	128.6	1.9	5.9	5.5
2096	88.9	85.3	115.3	93.7	100.7	116.0	5.3	15.2	0.4
2370	59.3	68.4	78.7	69.2	75.5	87.2	14.4	9.4	9.7
2633	35.5	38.7	54.4	46.3	48.1	57.2	23.9	19.5	5.2
2897	23.1	20.9	30.2	22.1	24.4	30.6	4.5	14.3	0.2

4.3.2. Thrust force fluctuation

Predicted and experimental cutting forces during stage 1 to 2 with the fluctuation boundaries are described in figure 4-11. Maximum and minimum boundary lines are demonstrated for the three different fiber volume fractions in the identical cutting conditions. In the validation results, boundary lines showing predicted maximum and minimum thrust force of the model shows a trend similar to the boundary of the thrust force results obtained by the experiment. Most of errors appear at the end of stage 1 in every condition; extruding action of chisel edge occurs rapid increase of thrust force in very short time. At the time passed 200msec from the start point, maximum and minimum thrust force of experiment results are 38.4N and 13.7N respectively in figure 4-11(a). When the prediction results are 44.4N and 22.3N respectively. These deviations could be attributed due to the non-controllable factors like vibration of the machine tool, impact between tool and the fiber, etc. However, the main reason is regarded as that the model cannot completely implement the complex geometry of the drill bit.

Table 4-2. Elevated temperature and varying mechanical properties in feed of 0.02mm/rev

Cutting condition	Fiber volume fraction (%)	Temperature elevation (℃)	Varying mechanical properties			
			E_1 (GPa)	E_3, E_2 (GPa)	τ_1 (Mpa)	τ_2 (Mpa)
5000RPM	49	85.2	101	5.7	66	45
	57	89.3	119	6.9	77	55
	66	84.6	144	9.1	89	67
7000RPM	49	95.5	91	5.1	60	41
	57	93.8	112	6.5	72	51
	66	97.1	134	8.5	83	63

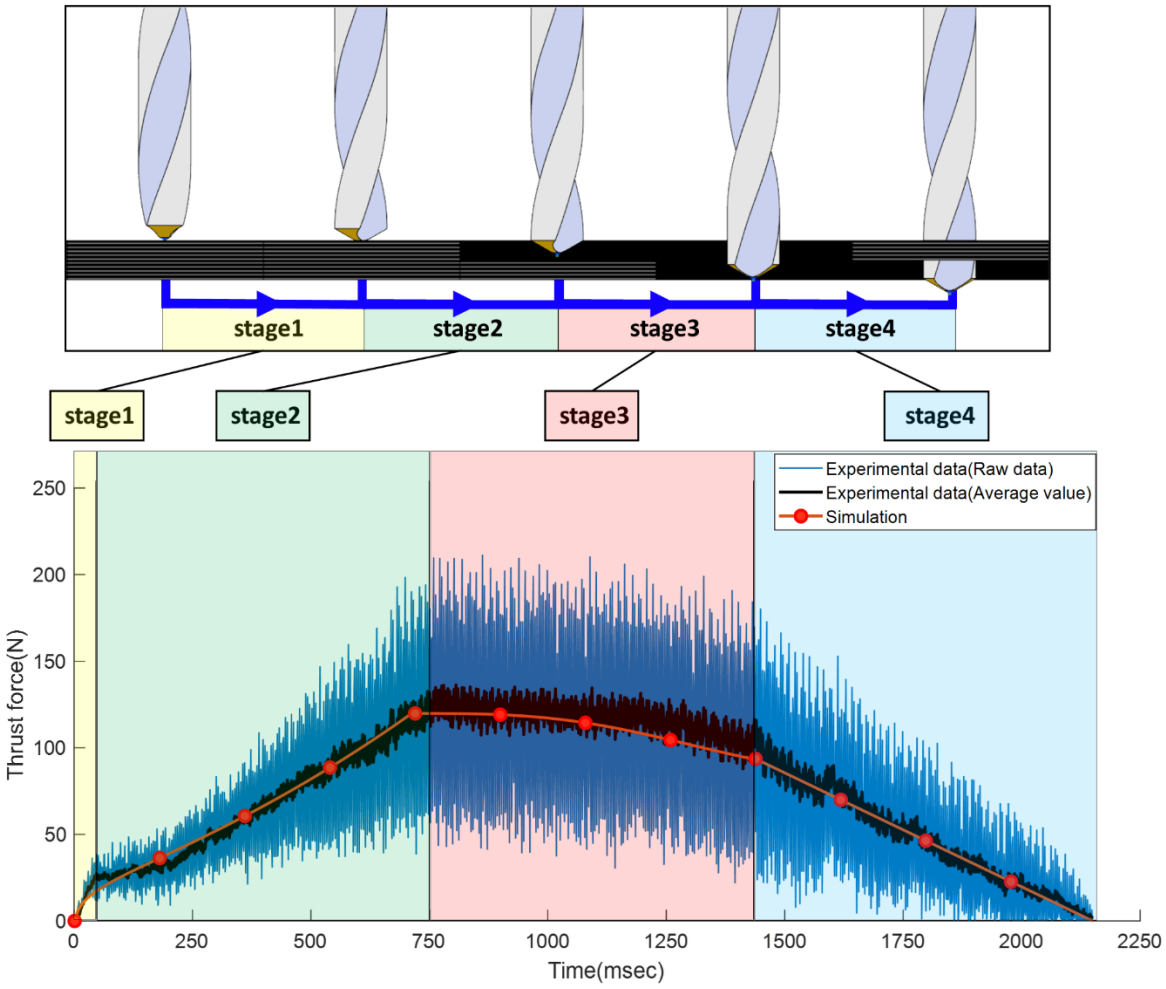

Figure 4-9. Thrust force results for whole drilling stages for both experiment and simulation

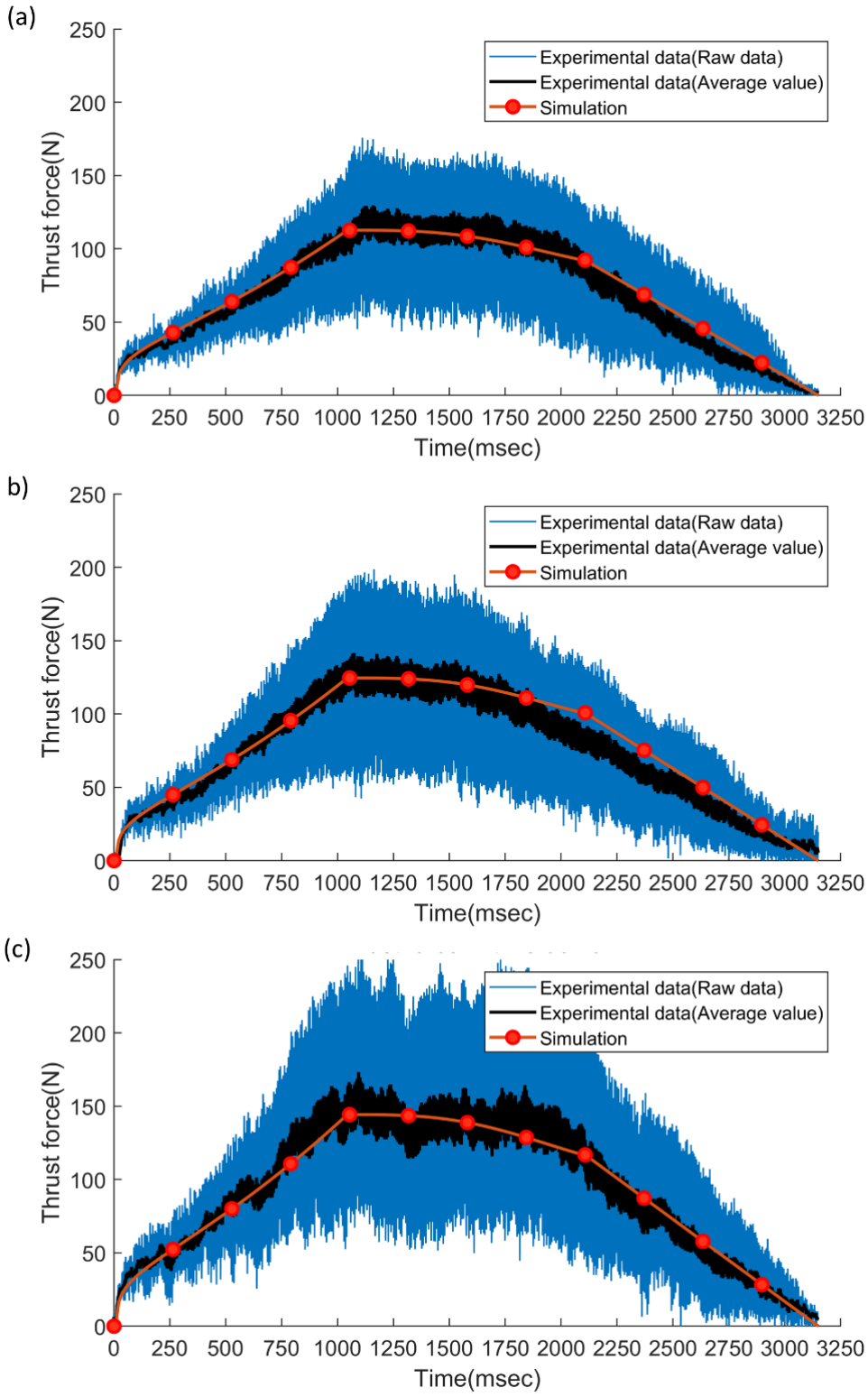

Figure 4-10. Thrust force results for whole drilling stages for both experiment and simulation with the spindle speed f at 5,000 rpm, and a feed of 0.02 mm per revolution for (a) Vf = 49%, (b) Vf = 57%, and (c) Vf = 66%.

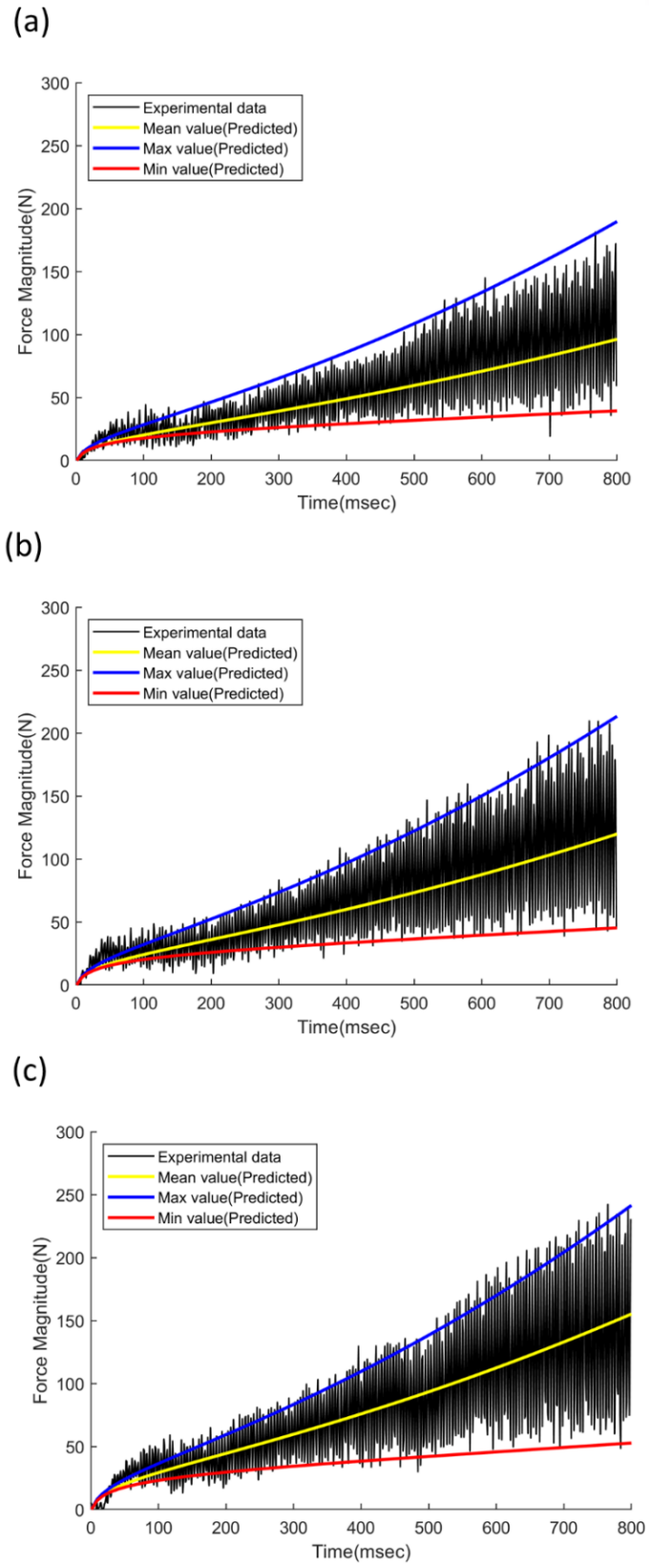

Figure 4-11. The experimental and predicted fluctuation for a spindle speed of 7,000 rpm and a feed of 0.02 mm/rev for (a) Vf = 49%, (b) Vf = 57%, and (c) Vf = 66%.

4.3. Conclusions

An analytical thrust force model that describes the drilling of unidirectional CFRP laminates has been proposed. In this model, the thrust forces are assumed to be the sum of forces generated by the extrusion actions of the chisel edge, and the cutting mechanism of the cutting lip of the drill bit. The model accounts for the material properties of CFRP, the drill bit geometry, and the cutting conditions. In addition to the instantaneous thrust force at a specific point, the model was used to calculate the thrust force throughout the entire drilling process. Here, properties such as the thermophysical behavior and fiber volume fraction of the material were considered. The following conclusions can be drawn from the proposed model and experimental validation:

- ✓ The model was developed by describing the cutting lip as a number of orthogonal cutting operations, and by incorporate chipping, pressing, and bouncing phenomena. Also, the incorporation of true geometric parameters during model development contributed to both the accurate calculation of the mean thrust force and showed proper agreement with the experimental data.

- ✓ The thrust force fluctuations that occurred during the CFRP drilling process were predicted by calculating the maximum and minimum thrust force through careful selection of the material properties. In addition, the thrust force variation according to the fiber volume fraction was anticipated using the proposed model. Although a greater thrust force was generated for the specimen with a high fiber volume fraction, the change in force generation for lower fractions was limited, which was attributed to the nonlinearity of the material properties across such a narrow range.

- ✓ The thrust force during the whole drilling process was calculated by accounting for the thermophysical properties of the CFRP composite materials, and was validated in the time-domain. The modeled data captured trend with the experimental results at specific time points, across all stages.

5. Numerical modeling of CFRP drilling process

5.1. Introduction

Although there have been many developed analytical models to calculate the cutting forces, however, some studies have shown that numerical model plays a key role in the analysis of mechanisms for drilling process and the prediction of damage in the workpiece. [22, 35, 111-113, 117-124, 127, 136, 137, 164, 179] This work presents an investigation of the delamination of carbon fiber reinforced plastics (CFRP) composites laminates during the drilling process. When drilling the CFRP laminates, delamination is one of the severe defects that degrade the quality of CFRP products. Therefore, we developed the finite element model of CFRP drilling process to simulate the thrust force and the damages generated in the cohesive zone between the interface of laminates. Drilling simulation and tests were conducted to analyze effect of feed, spindle speed, and back-up plate on delamination as well as the thrust force. Prior to the delamination investigation, simulated thrust force results were validated by the experimental results. Delamination of the FE model were assessed by the evaluating damage criterion value of cohesive zone between the composite laminate plies. Computational tomography (CT) image was acquired and processed into quantified delamination factor to validate the simulation results. This work is based on the published journal paper by Seo et al. [180]

5.2. FE model development

Figure 5-1 shows the complete numerical modeling process for delamination prediction. Results of FE model were thrust force and damage variable for cohesive surfaces. At first, when the FE model was set and calculated thrust force of drilling process was validated using measured data to ensure reliability of the FE model. In the second stage, damage variable values were acquired for each cohesive surface that implies the level of damage of each node. Damaged area of the simulation model was analyzed with the measured damaged area acquired from micro CT scanning according to the damage variable values. Two-dimensional delamination factor was applied for assessment which has

been the common evaluation method to define the damage degree of delamination. Subsequently, adjusted damage values were then used to derive the confirmed delamination factor.

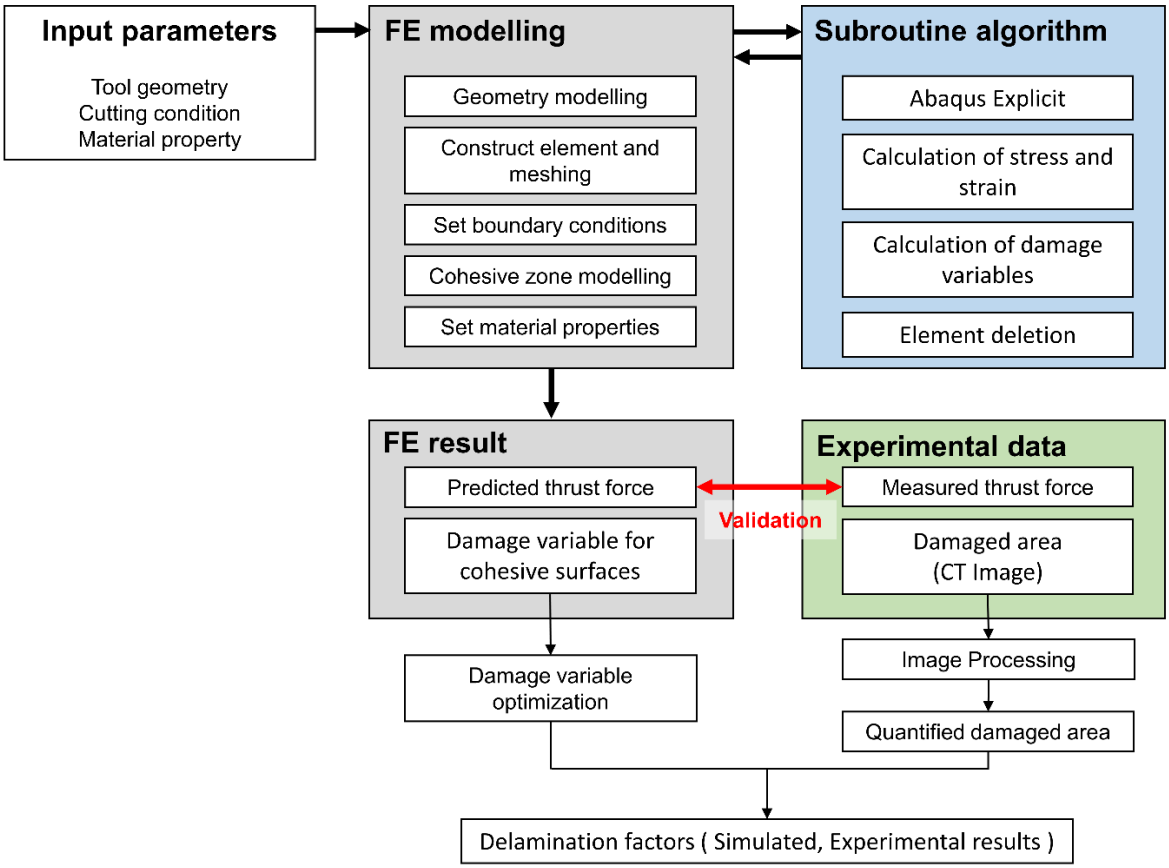

Figure 5-1. Flow chart of drilling delamination prediction for CFRP

5.2.1. FE model setup

Commercial FEM software ABAQUS/Explicit was used to simulate the drilling process of CFRP composite laminates. Summarized information about the FE model is shown in figure 5-2.

5.2.2. Preprocessing of finite element model

The drilling FE model consisted of drill bit, workpiece, and fixture as shown in figure 5-2(b). The composite workpiece used in this work was fabricated by 14 plies of unidirectional carbon fiber fabric. The dimensions of composite workpiece in the FE model were 20mm X 20mm X 3.003 mm.

Plies in the FE model were stacked in sequence of $[(0/90)_3/0]_s$ and cohesive surfaces with thickness of 0.010mm were implemented between the ply interfaces. The dimensions of drill bit used in the FE model are described in the table 5-1. The fixture beneath the CFRP workpiece has the dimensions of 20mm X 20mm X 2mm with the hole which has diameter of 12mm. Jig and the drill bit of FE model were considered as the rigid as it have higher elastic modulus than CFRP workpieces to save the computational time.

The C3D8R element was applied to mesh the CFRP composite laminates, which is the 8-node brick element. The dimensions of element were 0.15mm X 0.15mm X 0.15mm. The C3D6 element was utilized to mesh the drill bit part1 with the refined global size of 0.39mm X 0.39mm. The element type of part2 was swept type which had rectangular shape with global size of 0.39mm X 0.39mm to reduce the computational load.

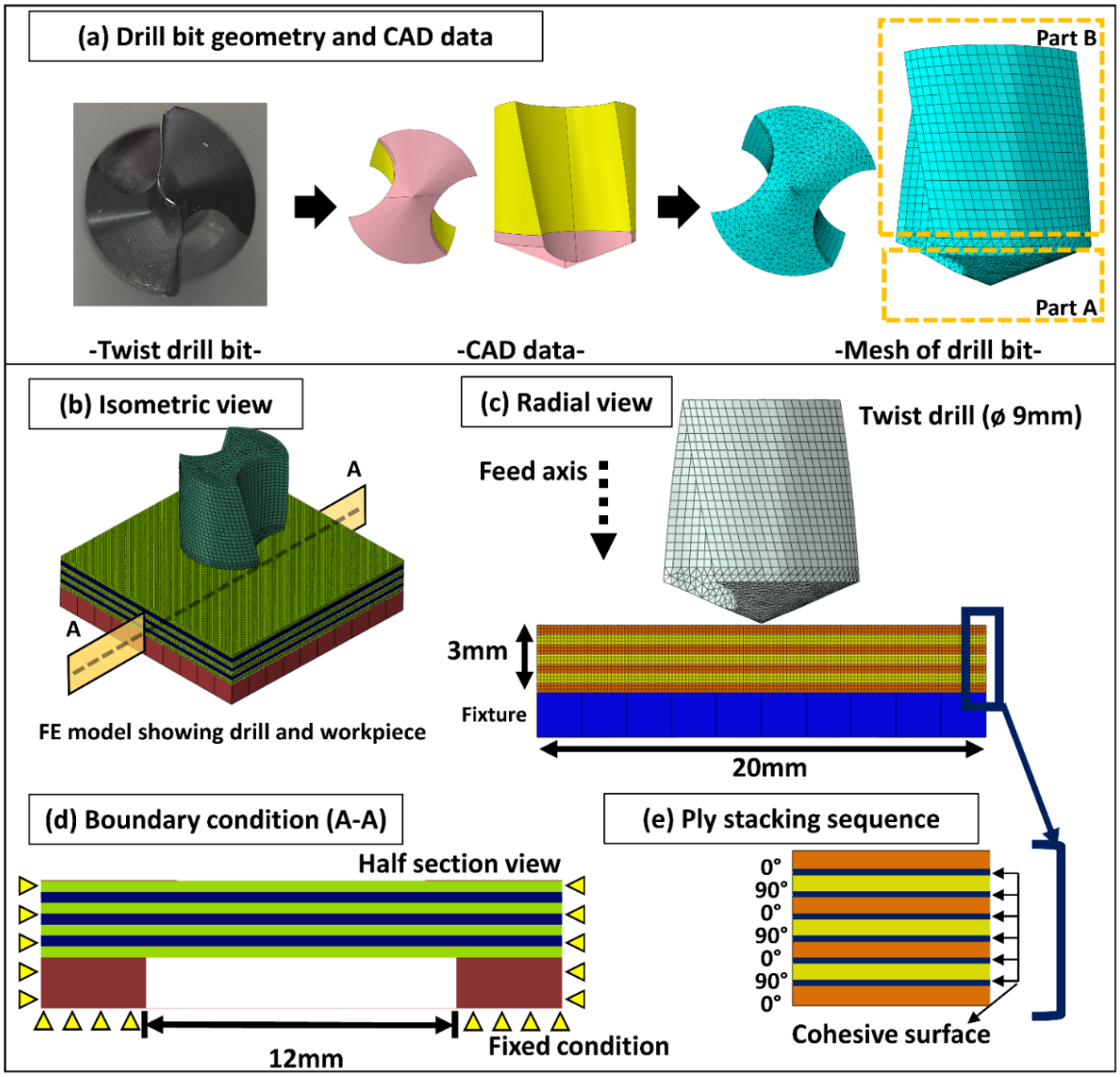

Figure 5-2. FE model setup for (a) Drill bit (b) Isometric view (c) Radial view with dimensions (d) boundary condition with half section view (e) ply stacking sequence with the cohesive surfaces

5.2.3 Material modelling

Material properties of composite laminate were defined by user-defined material subroutine (VUMAT) with solid elements which was well established by previous studies. [18, 25, 28, 33, 35, 39, 48, 107-110, 122, 128, 164, 181] The elastic properties of composite layers were shown in table 5-3 which includes the values of failure for inter-laminar damage, elastic stiffness, strength and fracture energy. Damage evolution was implemented by the power law in mixed-mode. Cohesive surfaces were adapted to the interfaces of composite layers based on traction-separation behavior. In addition, Hanshin damage model was

extended to the 3D composite damage model with the help of VUMAT and applied to the composite laminates to predict fiber failure modes. [182] Puck's model was also used to predict matrix failure mode of composite laminate during CFRP drilling process.

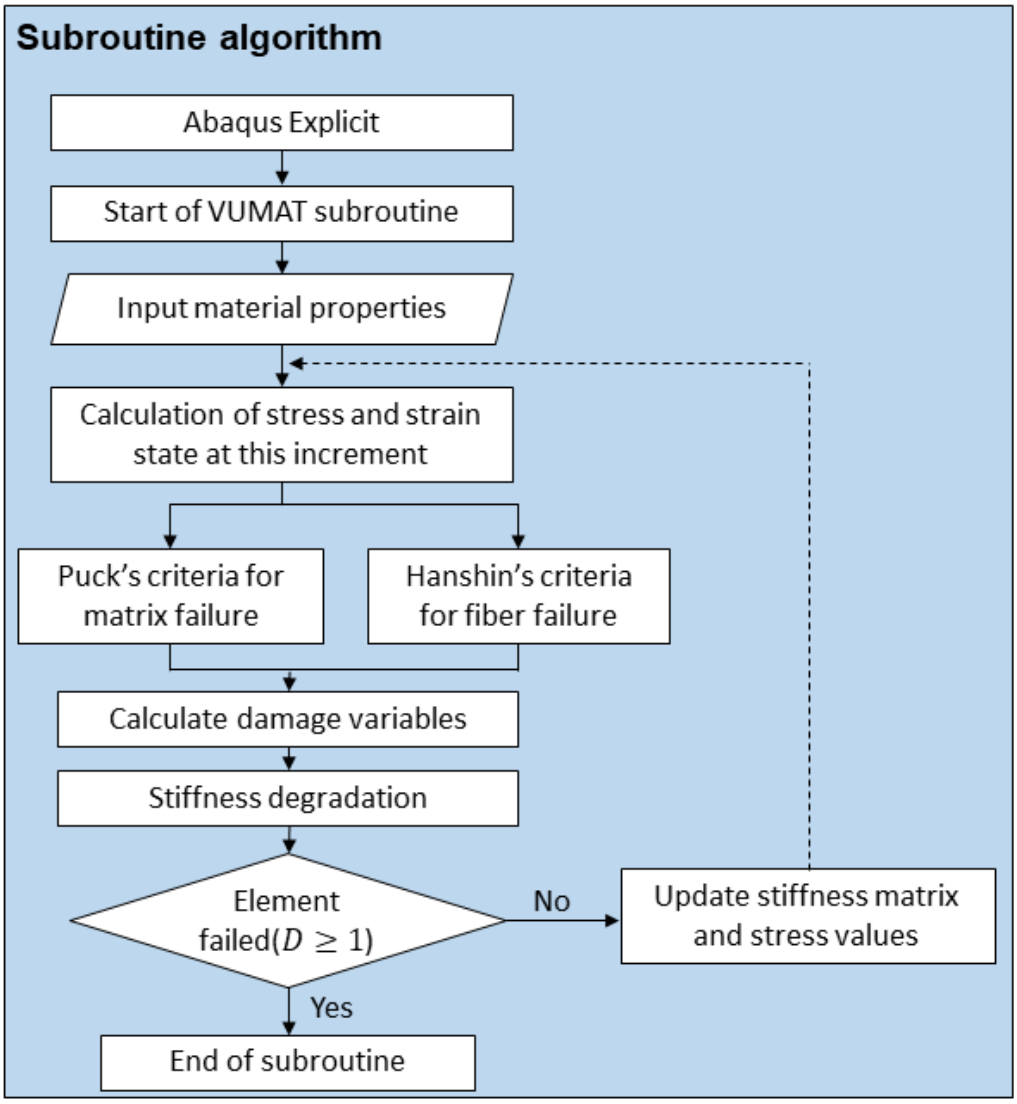

Figure 5-3. Subroutine algorithm (VUMAT) used in the FE model

Hanshin's criteria for failure in elastic fibers is defined in the following equation:

[Fiber tensile failure ($\sigma_{11} \geq 0$)]

$$\left(\frac{\sigma_{11}}{S_{11}}\right)^2 + \left(\frac{\sigma_{11}}{S_{12}}\right)^2 + \left(\frac{\sigma_{11}}{S_{13}}\right)^2 = 1, \quad d_{ft} = 1 \tag{1}$$

[Fiber compressive failure ($\sigma_{11} \geq 0$)]

$$\left(\frac{\sigma_{11}}{X_{1c}}\right)^2 = 1, \quad d_{fc} = 1 \tag{2}$$

Puck's criteria for failure in elastic fibers is defined in the following equation:

[Matrix failure]

$$\left[\left(\frac{\sigma_{11}}{2X_{1t}}\right)^2 + \left(\frac{\sigma_{22}^2}{|X_{2t}X_{2c}|}\right) + \left(\frac{\sigma_{12}}{S_{12}}\right)^2\right] + \sigma_{22}\left(\frac{1}{X_{2t}} + \frac{1}{X_{2c}}\right) = 1 \tag{3}$$

$$\sigma_{22} + \sigma_{33} > 0, \quad d_{mt} = 1$$

$$\sigma_{22} + \sigma_{33} < 0, \quad d_{mc} = 1$$

Where σ_{11}, σ_{22}, σ_{33}, and σ_{12} denotes components of the effective stress tensors., d_{fc}, d_{mt}, and d_{mc} are the damage variables related to failure modes of fiber tension and compression and matrix tension and compression. X_{1t} and X_{2t} are the tensile strength in longitudinal and transverse direction when X_{1c} and X_{2c} are the compressive strength in longitudinal and transverse direction with respect to carbon fibers. S_{11}, S_{12}, and S_{13} are the shear strength in 1-2, 2-3 and 1-3 planes. Strength properties used in the FE simulation are listed in Table 5-1.

Table 5-1. Strength properties used in FE model

X_{1t}	840MPa
$X_{2t} = X_{3t}$	50MPa
X_{1c}	570MPa
$X_{2c} = X_{3c}$	70MPa
S_{12}	72MPa
$S_{13} = S_{23}$	100MPa

Damage on the cohesive surfaces were regarded as the value that denotes on the level delamination in this work. The quadratic nominal stress criterion was adapted to the FE model which assumes damage of interface initiate when the nominal stress ratios reaches a value of one. Expression adapted to the cohesive surfaces are shown in below:

$$\left[\frac{t_n}{t_n^o}\right]^2 + \left[\frac{t_s}{t_s^o}\right]^2 + \left[\frac{t_t}{t_t^o}\right]^2 = 1 \tag{4}$$

Where t_n, t_s, and t_t are the components of the normal and shear tractions at the cohesive surface. t_n^o, t_s^o, and t_t^o means the peak values of the nominal stresses when the deformation is purely normal to the cohesive interface or purely in the first or the second shear directions, respectively.

The damage evolution with the potential, based on fracture energies which was based on mixed-mode was used to a power law fracture criterion with the following equation:

$$\left[\frac{G_n}{G_n^c}\right]^\beta + \left[\frac{G_s}{G_s^c}\right]^\beta + \left[\frac{G_t}{G_t^c}\right]^\beta = 1 \tag{5}$$

Where G_n, G_s and G_t are the instantaneous fracture energies at normal and shear directions. G_n^c, G_s^c, and G_t^c represents the critical values of the fracture energies required to initiate failure in the normal and the first or the second shear directions, respectively. The cohesive interface was defined by a traction-separation law with mode-I failure as shown in figure 5-4.

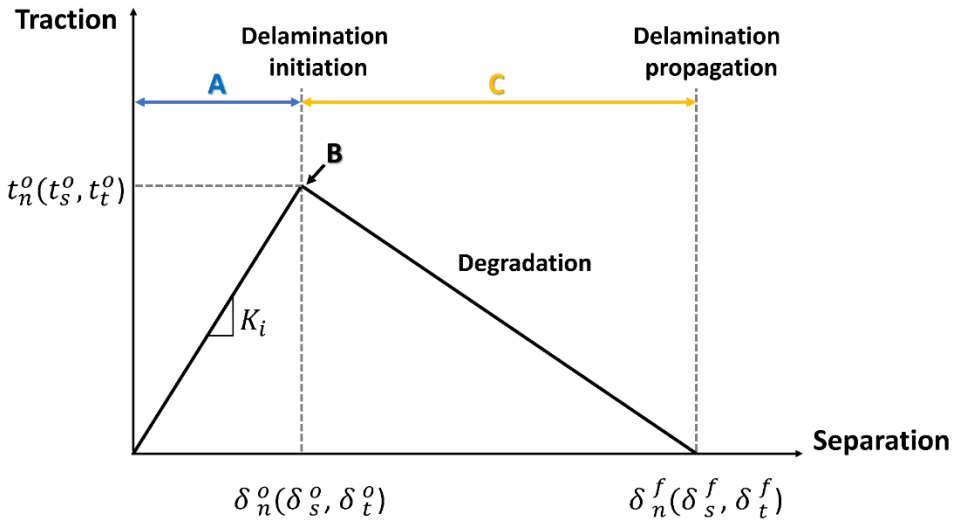

Figure 5-4. Traction-separation response in cohesive interface

The section A in the figure implies linear elastic behavior by the stiffness of the normal and the two shear directions (K_n, K_s and K_t), and curve constantly increases till it reach to the peak point. Section B of the figure describes damage initiation criterion, where t_n, t_s, and t_t are the peak value that denotes the separation point. In section 3, damage evolution occurs where material stiffness is degraded once the initiation criterion is reached as in the section 2. A scalar damage variable, D, represents the overall damage of the cohesive interface which evolves from 0 to 1 as below:

$$D = \frac{\delta_m^f(\delta_m^{\max} - \delta_m^o)}{\delta_m^{\max}(\delta_m^f - \delta_m^o)} \tag{6}$$

In above equation, $\delta_m^{\max}$ is the maximum value of the effective displacement occurred during the process. δ_m^f and δ_m^o are the effective displacement at complete failure and at damage initiation, respectively.

The relationship between traction (t_i), damage variable (D), stiffness (K_i), and displacement (δ_i) for the normal and two shear directions are shown in equation below:

$$t_i = (1-D)K_i\delta_I, \quad i = n, s, t \tag{7}$$

Effective displacement is the combination of normal and shear deformations as equation below:

$$\delta_m = \sqrt{\langle \delta_n \rangle^2 + \delta_s^2 + \delta_t^2} \tag{8}$$

The cohesive properties used in the FE model were listed in the table 5-2.

Table 5-2. Cohesive properties used in FE model

K_n	1GPa
$K_s = K_t$	1GPa
G_n^c	0.2N/mm
$G_s^c = G_t^c$	1N/mm
t_n	10MPa
$t_s = t_t$	20MPa
β	1

5.3. Results and Discussion

5.3.1. FE simulation results

From the FE simulation, Stress-strain state, deformation of material and damage values at the cohesive interfaces were acquired. CSDMG was the damage criterion representing the damage level of cohesive interface which accounts for the delamination of the composite laminate. Figure 5-5 shows the FE simulation conducted for the drilling process in the cutting condition of spindle speed of 5000RPM, and feed rate of 200mm/min. The axial view of the 7th cohesive surface and the half section view of the FE model were illustrated in the figure 5-5 according to the process time. The 7th cohesive surface in the FE model was regarded as the interface of the composite layer which affected by the push-out delamination. Fully damaged elements in the cohesive surface were deleted when the drill bit engaging to the surface. The cohesive surface starts to take damage from the center as the drill bit enters the CFRP material, and damaged area gradually increased from the point where the chisel edge contacts

the interface. For the evaluation of delamination factor of material, the damaged area of cohesive surface at the end of the process were assessed as the delaminated area.

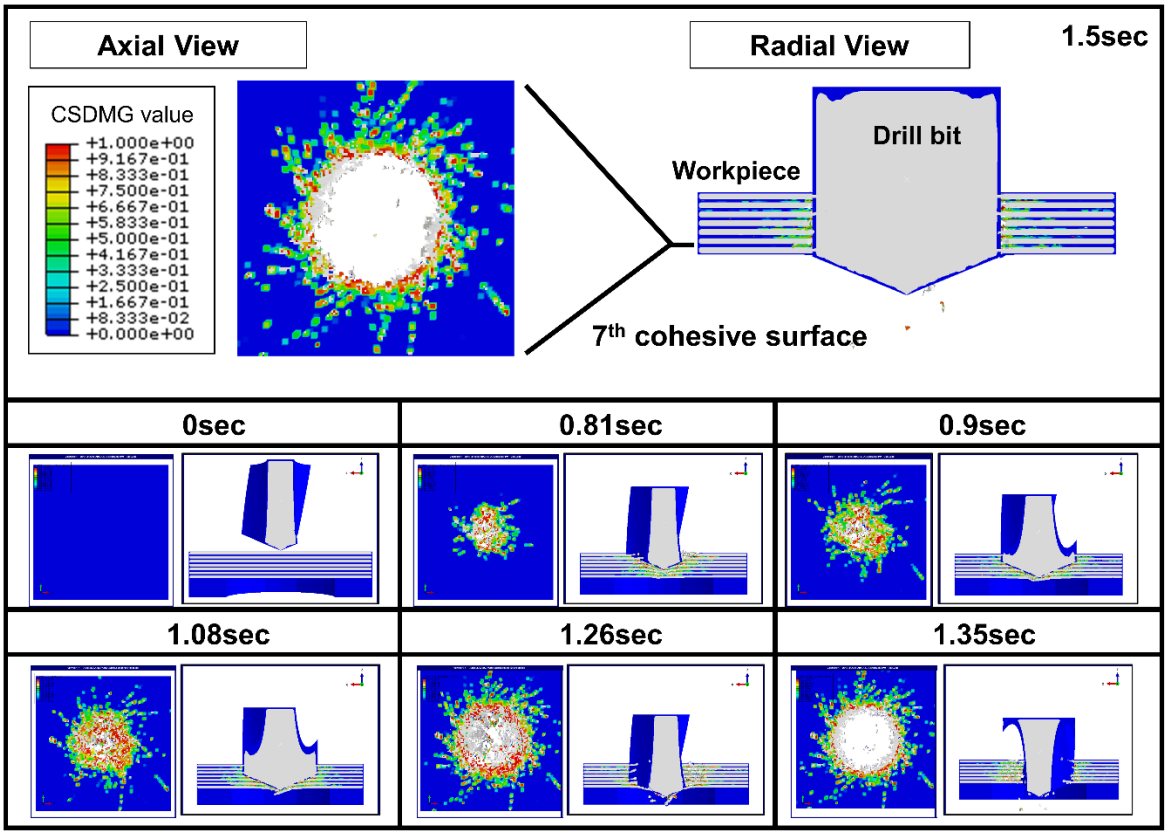

Figure 5-5. FE simulation results at cohesive surface in time domain

5.4. Validation of Finite Element model

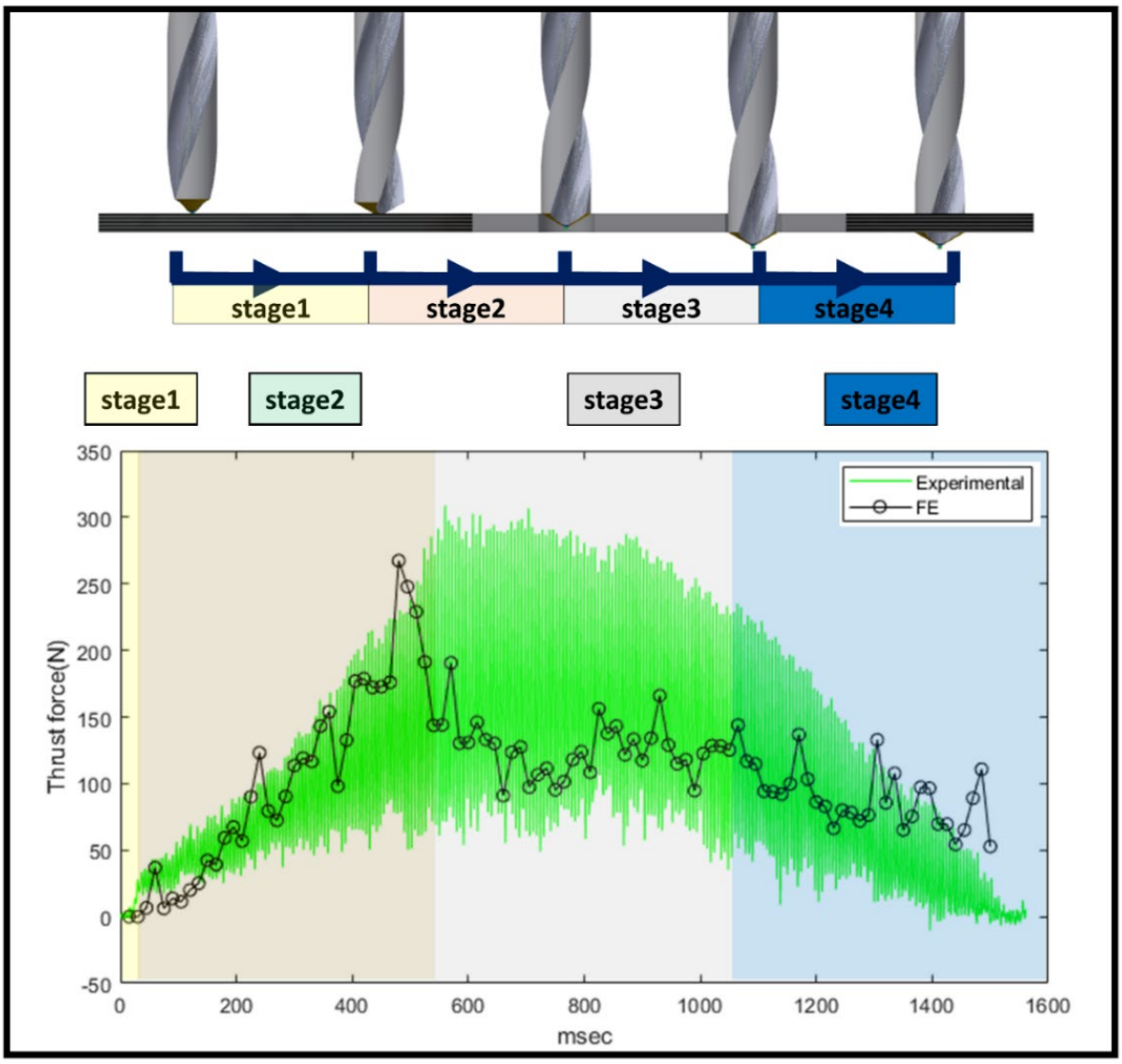

Figure 5-6. Both experimental result and FE simulation thrust force for whole drilling stages of carbon fiber reinforced plastic

The data in figure 5-6 are the experimental and simulation thrust force results according to the drilling stage. During drilling with the twist drill bit, stage 1 corresponds to when the chisel edge of the drill bit generates a thrust force. In stage 2, the thrust force increases to its maximum value as the chisel edge and lip of the bit gradually engage the composite laminate. The bit fully engages with the material at stage 3 and force decreases as the bit exits from the material at stage 4. The FE results were smoothed using a 25-point moving average window so that force curves could be compared more easily. The

There was good agreement between the simulated and experimental thrust forces, and similar behaviors were observed in stages 1 and 2. The maximum thrust force was the critical thrust force affecting the delamination of composite laminate

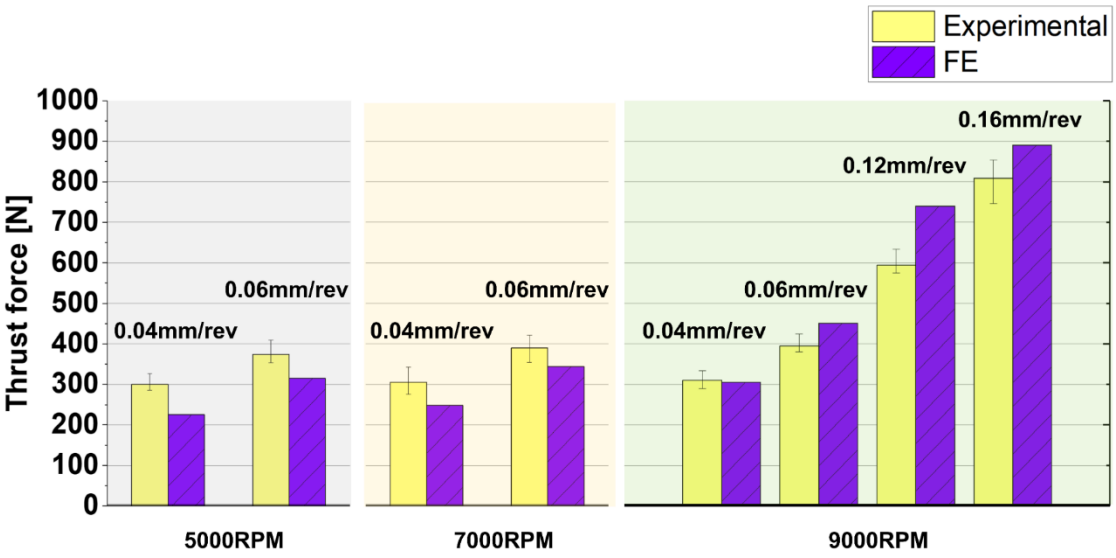

Figure 5-7. Comparison of the experimental and finite element (FE) simulation results for the thrust force under various drilling conditions

The maximum forces at the end of stage 2 were compared between the FE model and experimental results under different machining conditions to validate the FE model, as shown in figure 5-7. The experimental thrust forces generated under the same feed rate conditions had similar trends to those reported in previous studies. However, the FE results were slightly overestimated as spindle speed increased. With a spindle speed of 9,000 RPM, the thrust force increased significantly with feed rate. The maximum error was 33.3%, which occurred at a spindle speed of 5,000 RPM and feed rate of 0.04 mm/rev. The error rates with a spindle speed of 9,000 RPM were 1.6, 12.4, 19.7, and 9.1%; thus, the FE results showed good agreement with the experimental results.

Delamination generated on the cohesive surface was assessed as illustrated in the figure 5-8. FE model were developed under both condition with the back-up plate and without back-up plate.

Delamination generated on the surface of the composite laminates were inspected by the micro CT scanning and scanned image were processed by the VG studio and MATLAB. Thick-slab image of the workpiece were cropped to the size fit for analyze the damaged area. Brightness of cropped images were adjusted, and images were binarized to capture the overall damaged area. Damaged area of the drilled workpiece was measured and delamination factor for each machining condition was calculated to compare with the FE results. CSDMG results of FE model with the back-up plate shows similar visualized contour to the scanned image while difference in the visualized contour were found in the condition without back-up plate. The significant damage propagation along the fiber orientation direction was observed in the workpiece without the back-up plate while the damage on the workpiece reinforced with the back-up plate were restricted as the back-up plate support the composite laminates from bending. Damaged area was restricted to the diameter of the hole in the back-up plate which was 12mm in the experiment, rather, damage was propagated around the hole not to the fiber orientation direction.

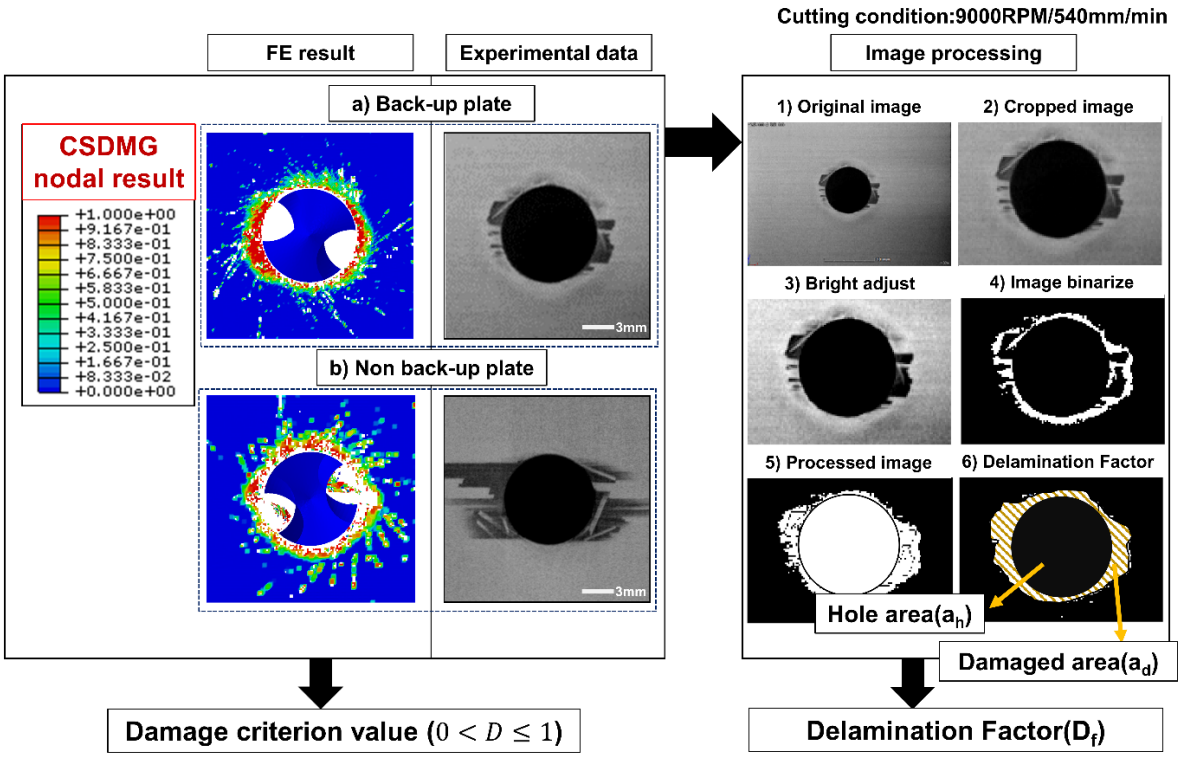

Figure 5-8. FE simulation and experimental result comparison for assessing damage on the surface considering presence of back up plate and image processing technique to quantify damage on the drilled

workpiece

Stress contour of the FE results were common method to assess the delamination from the previous studies. [18, 28, 108, 109, 183] Figure 5-9 shows the von mises stress contour of FE results with and without the back-up plate in spindle speed of 9000RPM and feed rate of 540mm/min. Stress contour results showed good agreement to the scanned image from the experiment as damaged area were adjacent to the hole in the figure 5-9(a) while stress spreads among fiber orientation direction in the figure 5-9(b). However, the stress contour had limitation that quantification as the delamination factor was difficult. To assess the delamination in the quantified value, delamination factor in this work was calculated with the following equation below:

$$D_f = \frac{a_d + a_h}{a_h} \tag{5-1}$$

Delamination factors of the experimental and FE results were compared in the figure 5-8. We tried to investigate the damage characteristics under the extremely high feed conditions in both with back-up plate and without back-up plate using both experiment and FE results in this section. Delamination factors were concentrated around the 1.4 and slightly increased according to the feed condition while the back-up plate was attached to workpiece. Feed over 0.10 mm/rev were the very fast speed condition in the drilling process which are rarely used in the industries. However, delamination factors without back-up plate were gradually increased as the feed speed were faster from the experiment. The delamination factor of 0.18mm/rev was increased 189.7% from the 0.02mm/rev. Delamination factors was 23.7% increased in average as feed increase with 0.02mm/rev.

FE result in figure 5-10 showed the delamination factor assessed under CSQUADCRT criterion which specify a damage initiation based on the quadratic traction-interaction criterion of damaged area of the cohesive surface. The delamination factors of CSQUADCRT results were much higher than the results of experimental delamination factors which showed big errors that cannot be accepted.

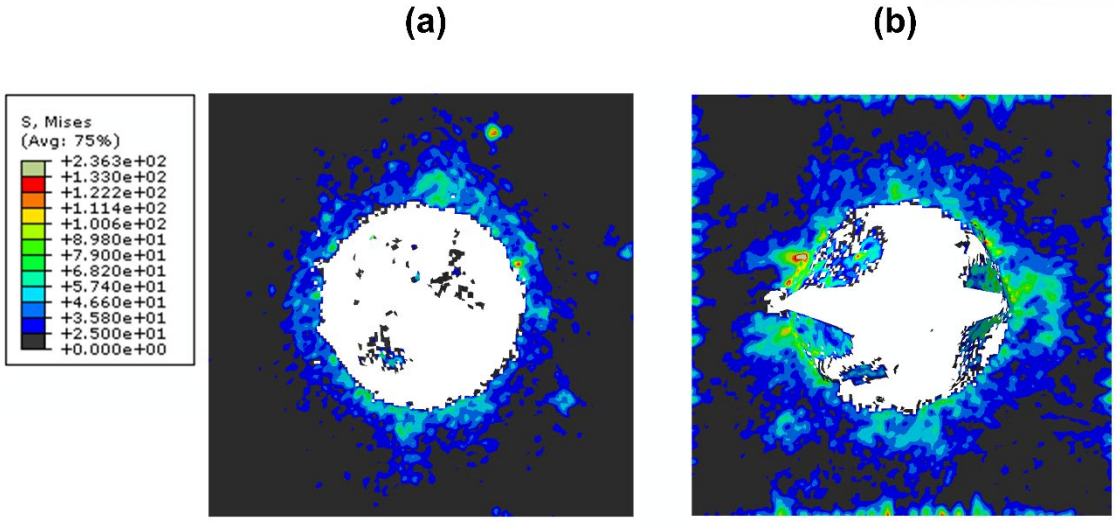

Figure 5-9. Von mises stress contour of the exit surface of composite laminates with a) back-up plate and b) without back-up plate

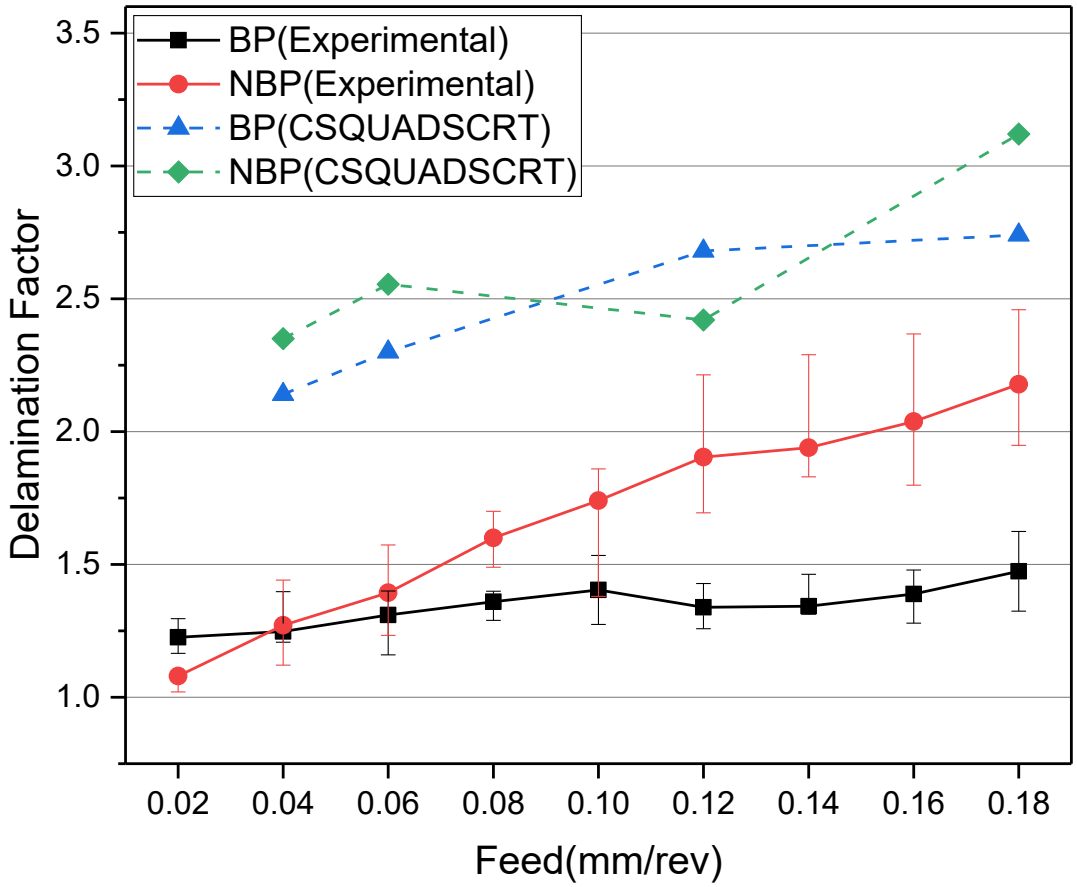

Figure 5-10. Delamination factors of experimental and simulation results of CSDMG and CSQUADSCRT criterion with the condition of a) back-up plate, b) Non-back up plate

However, CSDMG was one of the damage criterion that corresponds to scalar degradation for cohesive surface of composite laminates (CSDMG=0 stands for undamaged condition and CSDMG=1 for complete failure). CSDMG criterion have advantage that damaged area was calculated as a scalar value between 0 to 1 in terms of damage variables. When the CSQUADCRT criterion only divided the damaged and undamaged area as shown in figure 5-11.

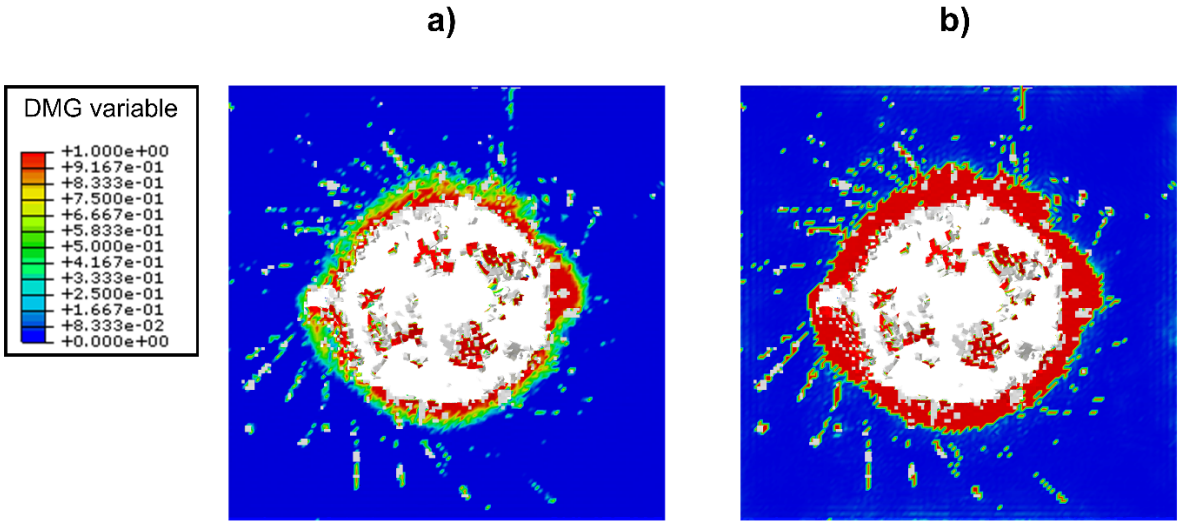

Figure 5-11. Damage contour of the exit surface of composite laminates with a) CSDMG and b) CSQUADCRT criterion

The limitation in the accurate prediction of delamination factor was occurred when implementing damage criterion analysis. There could be many factors responsible for the error of simulation, one reason was the mesh size. Due to the complexity of the geometry and moving process of drill bit, mesh size was restricted to for the computational time. There was also a reason that the feed and rotating condition of drill bit used in the FE model were extremely fast which influenced nonlinear effect, stabilization, and contact problems causing undesirable large deformation as well as the non-convergence. From the FE contour in figure 5-11, damaged area of cohesive surface spread widely in a whirlwind shape due to the rotation of the drill bit. Among them, the specific damaged area was away from the damaged area adjacent to the hole, and those were the one of reasons of simulation error.

Delamination factors of experiment and FE were analyzed according to the minimum damage values under spindle speed of 9000RPM and feed rate of 360mm/min as shown in figure 5-13, Figure 5-14 and 5-15 show the result of delamination factor according to the minimum damage criterion value at the cutting condition of spindle speed of 9000RPM and feed rate of 540mm/min and 1080mm/min. Those results illustrate how the delamination factor changes according to the minimum damage values. Therefore, by controlling the appropriate minimum damage value, prediction accuracy of delamination factors would be increased. For the FE results with back up plate, we can see that the minimum damage value over 0.8 meets the delamination factor from the experiment. On the other hand, delamination factor results of experiment without the back-up plate were higher than the results with the back-up plate that the appropriate minimum damage values were relatively smaller.

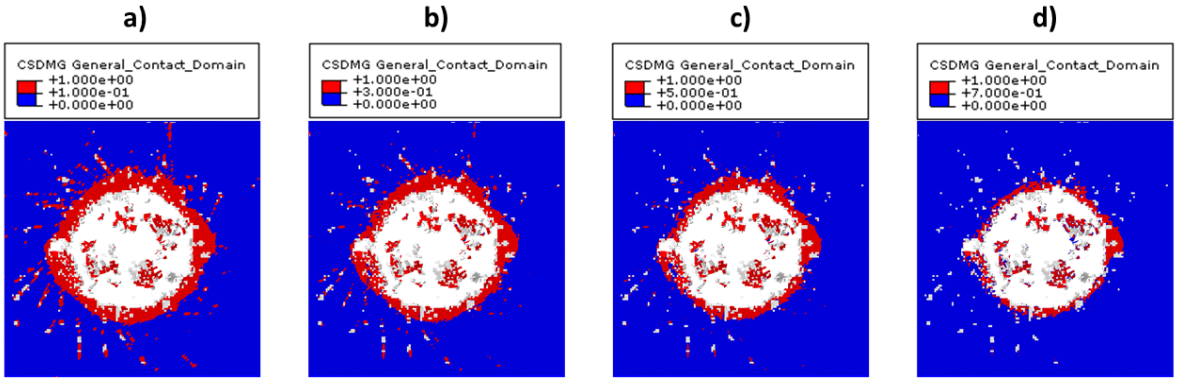

Figure 5-12. Delamination change according to the minimum damage value(Dmin); (a) Dmin=0.1, (b) Dmin=0.3, (c) Dmin=0.5, and (d) Dmin=0.7

From the damage results using CSDMG criterion, cohesive surface could be contoured by arrays of damage variables between 0 to 1 as shown in figure 5-11(a). The node with scalar value between 0 to 1 can be considered as 'damage initiated and in progress' based on damage evolution model as shown in figure 5-4. The delaminated zone was calculated using FE results of cohesive surface for each cutting condition with the developed MATLAB code. The node under damage value of D_{min}, was ignored when calculating the delaminated zone as shown in figure 5-12. As the D_{min} value increases

gradually, delamination area decreases. It means that damage was not progressed enough to be delaminated of exit ply.

Controlling the minimum damage value($D_{\min}$), delamination factors according to the feed were analyzed as shown in figure 5-12. Delamination factors of the FE results showed good agreement when the minimum damage value was 0.9 in figure 5-13a). The maximum error from the comparison was at the feed condition of 0.12mm/rev and it was 10.1% when the average percentage error was 5.32%. In case of condition for without back-up plate, appropriate minimum damage value was 0.8. It showed good agreement for low feed condition when the magnitude of error increased as the faster the feed. Maximum percentage error occurred in the feed condition of 0.18mm/rev, and it was 19.6%. Average percentage error for the overall conditions was 9.17%.

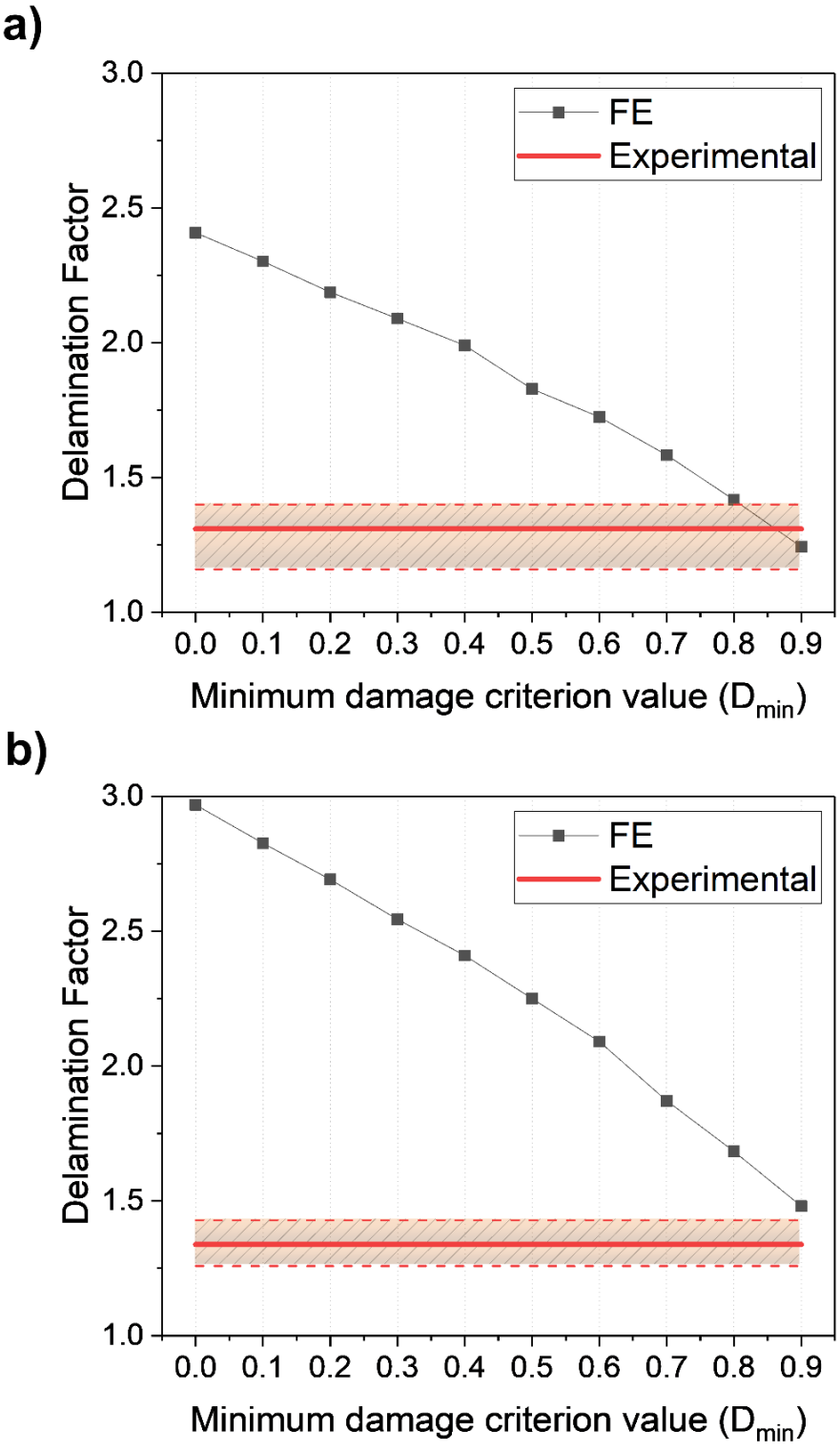

Figure 5-13. . Delamination factor results of FE simulation according to the minimum damage criterion value with back-up plate at cutting condition of a) 9000RPM and 540mm/min of federate and b) 9000RPM and 1080mm/min

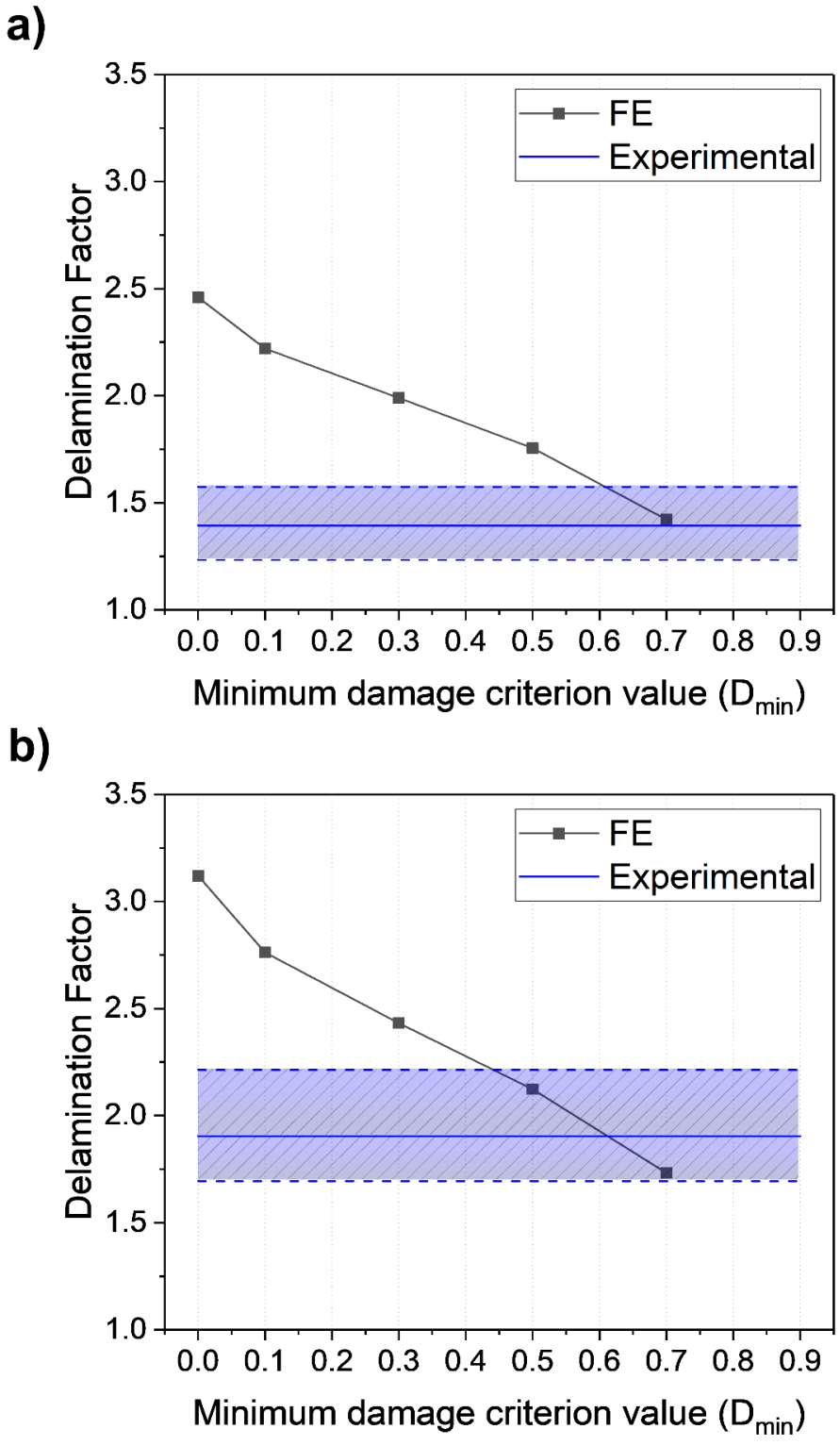

Figure 5-14. Delamination factor results of FE simulation according to the minimum damage criterion value without back-up plate at cutting condition of a) 9000RPM and 540mm/min of federate and b) 9000RPM and 1080mm/min

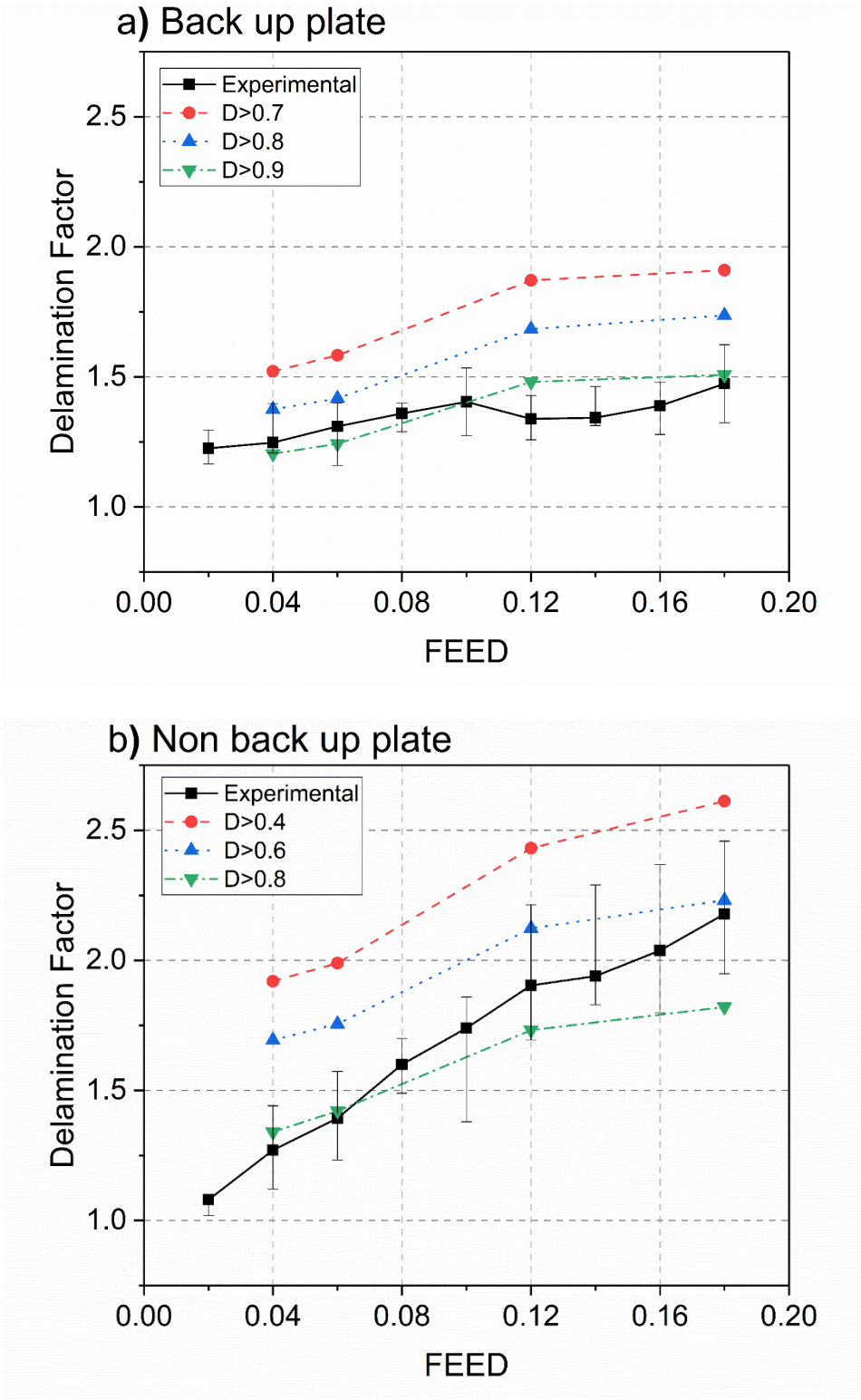

Figure 5-15. Delamination factor results according to the feed and damage value in the presence of a) back up plate and b) without back-up plate

Cutting conditions (spindle speed, feed), tool geometry, and presence of back up material are the key cutting parameters determining cutting forces and delamination for drilling process as reported by previous researches. [4, 21, 26, 33, 36, 47, 82-87, 89, 91-93, 123, 132, 183-190] Feed rate has been the mostly investigated condition and in general, feed rate and delamination factor have proportional relationship. Increase of drill diameter also increase the thrust forces negatively affect to the delamination of workpiece, meanwhile the spindle speed rarely affects the thrust force and delamination. [191-196] In this study, drill diameter was fixed condition when the spindle speed and feed rate were controlled for the cutting condition. When comparing the experimental results, the discrepancy of the thrust force results at fixed feed (0.04mm/rev, and 0.06mm/rev) with different spindle speed (5000RPM,7000RPM, and 9000RPM) was very small as shown in figure 5-7., which have similar trend to previous studies[4, 86, 90].

However, it was observed that FE thrust force results were gradually increased as the spindle speed increase in both feed conditions (0.04mm/rev, and 0.06mm/rev), and showed some discrepancy to the experimental results. While the predictive results for relatively slow cutting speeds were under-estimated, when the predictive results at 9000RPM were over estimated as the feed rate increase. Possible reasons for the error are inadequate modeling of friction coefficient and element-deletion criteria for material damage models. Friction coefficient in the FE model was constant value which cannot perfectly realize cutting tool and workpiece behavior. Other reason is due to lack of accurate geometrical model of cutting tool when the cutting edge radius highly affect the cutting force results during drilling simulation. The other major reason could be the lack of accurate strength and failure model and properties for high-strain behavior of CFRP composites when the information of strengths and failure energies achieved from uniaxial tensile test. Other minor reasons could be the mesh size; due to the complexity of the geometry and movement of the drill bit, we restricted the mesh size to save computational time. Also, the feed rates and spindle speeds of the bit used in the FE model were extremely fast, which caused nonlinear effects and stabilization and contact problems, and thus undesirably large deformations, as well as non-convergence.

Based on the thrust force validation, delamination analysis was conducted on the spindle speed of

9000RPM with varying feed conditions. As the most of delamination on CFRPs during drilling is occurred due to thrust forces acting at exit of holes, backup plate well prevented delamination of workpiece. The effect of backup plate to the delamination during the CFRP drilling process could be observed by drilling experiment and simulating the drilling process with and without the backup plate. Delamination factors from the experimental results in without backup plate conditions follow the same trends that have been reported by previous researches which increase as the feed elevated as shown in figure 5-9. [46, 133, 165] However, in the case of delamination factor results with backup plate, delamination factors (Df) were hard to exceed 1.56 which could be calculated by using eq. (5-1) assuming the maximum diameter of damage area was 12mm, and the diameter of hole was 9mm.

In the case of experiment and simulation conducted with backup plate, appropriate damage value was 0.9. FE results shows the damage is propagated beyond the hole diameter of backup plate. However, the damages occurred outside of hole of backup plate can be considered as a damage was just initiated. It can be seen that the strong damage which could be considered as delaminated actually occurred within the hole of backup plate. Therefore, it showed moderate agreement to experimental data when dmin=0.9 as shown in figure 5-11.

However, in the case of non-backup plate condition, dmin between 0.6 to 0.8 showed moderate agreement. Since there was no support to prevent the bending deformation of exit ply of composite laminate, delamination spreads further according to the feed rate. When the feed rate was relatively slow, the value of dmin=0.8 showed god agreement, but it can be seen that the deviation increases as the feed rate elevated. This denotes that delamination spreads more destructively in high strain rate condition that increases as the feed rate elevated. [33, 36, 40, 128-130, 135, 164, 184, 190, 195, 197-202] High d_{min} value implies that delamination occurred when damage progressed to completely failure condition. Conversely, low dmin value means that delamination occurs even where damage begins to initiated. Therefore, during CFRP drilling under backup plate condition, damages propagated to the hole diameter of backup plate and energies focused on the inside the hole of backup plate that make complete failure of exit ply. Under non-backup plate condition, damages propagated freely parallel to the fiber

orientation. Degree of damage is weaker as the distance from the hole increases. However, when the feed rate is high, it can be seen that the delamination occurred even where the damage was weakly progressed.

5.5. Conclusions

The Finite Element(FE) model that describes the drilling of multi-directional CFRP laminates has been proposed. In this model, the thrust forces, and damage in cohesive surface are simulated to predict the delamination. Delamination of the composite laminates was assessed by micro Computational Tomography(CT) scanning with thick-slab image method. Scanned images of exit surface of composite laminates were processed by the Matlab code for quantification as delamination factor. Delamination factor of FE model was evaluated according to the damage value of CSDMG damage criterion in ABAQUS/Explicit with comparison to common stress contour plat and CSQUADCRT damage criterion. Minimum damage values were presented for the higher accuracy of the delamination prediction using FE model of ABAQUS. The following conclusions can be drawn from the proposed model and experimental validation:

- ✓ The FE model was developed by the ABAQUS/Explicit considering the CFRP composite laminate properties by implementing user-defined material subroutine (VUMAT) and cohesive surface to demonstrate interface characteristics of inter-laminar properties of composite laminates.

- ✓ The thrust forces of FE model were compared to experimental result to validate the feasibility of FE model for delamination assessment. Percentage error in the spindle speed of 9000RPM was the 1.6%, 12.4%, 19.7%, and 9.1%, respectively, and FE results showed good agreement with the experimental results.

- ✓ Delamination factors were analyzed in both with back-up plate, and without back-up plate conditions to investigate the damage behavior of the exit surface of composite laminates. Damage value of CSDMG criterion was controlled to observe delamination growth and showed good agreement with appropriate the minimum damage value.

6. Concluding Remarks

6.1. Overall Conclusions

This thesis mainly focused on the development of predictive model for drilling process of carbon fiber reinforced polymer composites using analytical, and numerical simulation. Experimental investigation has been conducted to find influence of process parameters, and major parameters affecting the quality of the holes were studied. Thrust force and delamination were simulated using the predictive models, and validation showed good agreement. This thesis can be summarized as follows.

1) Experimental investigation on process parameters to the drilling process

Increased fiber volume fraction contributes to the increase of strength for both inter-laminar and fiber orientation, and it causes the thrust force increases under same cutting conditions. Feed of the drilling process also strongly affects the thrust force and delamination of the machined hole. Delamination factors were calculated with the processed images, and it showed proportional relation to the feed conditions, but the effect of the spindle speed was insignificant. Backplate during the drilling process prevent the delamination propagation, and delamination area was restricted to the diameter of the backplate. In addition, micro drilling process tests were conducted according to the drilling process types. Among various drilling types, machined hole with vibration assisted drilling showed the best performance. However, effect of the micro drilling process was low due to the size effect of the drill bit.

2) Development of analytical predictive model for CFRP drilling process

The model was developed by describing the cutting lip as a number of orthogonal cutting operations, and by incorporate chipping, pressing, and bouncing phenomena. Also, the incorporation of true geometric parameters during model development contributed to both the accurate calculation of the mean thrust force and showed proper agreement with the experimental data. The thrust force fluctuations that occurred during the CFRP drilling process were predicted by calculating the maximum and minimum thrust force through careful selection of the material properties. The thrust force during

the whole drilling process was calculated by accounting for the thermophysical properties of the CFRP composite materials, and was validated in the time-domain. The modeled data captured trend with the experimental results at specific time points, across all stages.

3) Development of numerical predictive model for CFRP drilling process

We have proposed an FE model of the drilling of multi-directional CFRP laminate. In this model, the thrust forces and damage in a cohesive surface are simulated to predict delamination. Delamination was assessed by micro CT using thick-slab images. Scans of the exit surface of the composite laminate were processed by MATLAB to obtain the D_f. In the FE model, D_f was evaluated according to the CSDMG damage criterion using Abaqus/Explicit software, and the results were compared against the FE stress contour plots and CSQUADSCRT values. An FE model of CFRP composite laminate properties was developed in Abaqus/Explicit software using a user-defined material subroutine (VUMAT) and cohesive surfaces. The interface characteristics and inter-laminar properties were analyzed to investigate the damage behavior of exit ply of composite laminate. The thrust forces calculated by the FE model were compared to the experimental results to validate the performance of the model for assessing delamination. The error rates at a spindle speed of 9,000 RPM were 1.6, 12.4, 19.7, and 9.1% The CSDMG damage criterion was used to assess delamination growth. With an appropriate value of minimum damage variable, there was good agreement with the experimental results. In case of, drilling with backup plate, appropriate damage value was 0.9 and average error of simulation model was 5.32%. In the condition of non-backup plate, appropriate damage value was 0.8 and average error of simulation model was 9.17%.

6.2. Path Forward

1) Delamination suppression during the machining process of composite materials

Although various predictive model simulating the delamination have been studied with the good agreement, research for the prevention and suppression of the delamination are essential for the industrial application. In the light of the experimental results in chapter 2, it was found that the effects of the fixture design and backplate during the drilling process was significant. Through this idea, CFRP stacked with the soft materials have been manufactured and drilling tests were conducted. Initial test showed meaningful prevention of the delamination of the machined hole with low increase of cutting force. Effective soft materials will be designed, and assessment of the effect will be tested according to the various cutting conditions.

2) Prediction of defect and process optimization based on the artificial intelligence model

Although existing predictive model and proposed models can simulate the mechanical behaviors of composite materials during the machining process, above methods have some disadvantages. Analytical model is only adaptable for the expert, and application of the model is restricted to the specific machining environment. In case of the numerical model, the biggest drawback is the analysis time. In case of the proposed model, it took about 2 days. Prediction and optimization model based on artificial intelligence can be good alternative to predicting complex behavior of CFRP drilling process. Therefore, appropriate deep learning and optimization model for the machining process of composite materials will be developed to predict defect and find optimal conditions in various machining environment.

REFERENCES

1. Chandrasekharan, V.; Kapoor, S.; DeVor, R., A mechanistic approach to predicting the cutting forces in drilling: with application to fiber-reinforced composite materials. **1995**.
2. Chen, W.-C., Some experimental investigations in the drilling of carbon fiber-reinforced plastic (CFRP) composite laminates. *International Journal of Machine Tools and Manufacture* **1997,** *37* (8), 1097-1108.
3. Paulo Davim, J.; Reis, P.; Conceição António, C., Drilling fiber reinforced plastics (FRPs) manufactured by hand lay-up: influence of matrix (Viapal VUP 9731 and ATLAC 382-05). *Journal of Materials Processing Technology* **2004,** *155-156*, 1828-1833.
4. Campos Rubio, J.; Abrao, A. M.; Faria, P. E.; Correia, A. E.; Davim, J. P., Effects of high speed in the drilling of glass fibre reinforced plastic: Evaluation of the delamination factor. *International Journal of Machine Tools and Manufacture* **2008,** *48* (6), 715-720.
5. Holmes, M., Carbon fibre reinforced plastics market continues growth path. *Reinforced Plastics* **2013,** *57* (6), 24-29.
6. Jacob, A., Carbon fibre and cars – 2013 in review. *Reinforced Plastics* **2014,** *58* (1), 18-19.
7. Davim, J. P.; Reis, P.; António, C. C., Experimental study of drilling glass fiber reinforced plastics (GFRP) manufactured by hand lay-up. *Composites Science and Technology* **2004,** *64* (2), 289-297.
8. Santiuste, C.; Sánchez-Sáez, S.; Barbero, E., A comparison of progressive-failure criteria in the prediction of the dynamic bending failure of composite laminated beams. *Composite Structures* **2010,** *92* (10), 2406-2414.
9. Liu, D.; Tang, Y.; Cong, W. L., A review of mechanical drilling for composite laminates. *Composite Structures* **2012,** *94* (4), 1265-1279.
10. Santiuste, C.; Miguélez, H.; Soldani, X., Out-of-plane failure mechanisms in LFRP composite cutting. *Composite Structures* **2011,** *93* (11), 2706-2713.
11. Wang, K.; Young, B.; Smith, S. T., Mechanical properties of pultruded carbon fibre-reinforced polymer (CFRP) plates at elevated temperatures. *Engineering Structures* **2011,** *33* (7), 2154-2161.
12. Ashrafi, S. A.; Sharif, S.; Yazid, Y. M.; Davoudinejad, A., Assessment of Hole Quality and Thrust Force when Drilling CFRP/Al Stack Using Carbide Tools. *Applied Mechanics and Materials* **2012,** *234*, 28-33.
13. Karpat, Y.; Bahtiyar, O.; Değer, B., Milling Force Modelling of Multidirectional Carbon Fiber Reinforced Polymer Laminates. *Procedia CIRP* **2012,** *1*, 460-465.
14. Khashaba, U. A., Drilling of polymer matrix composites: A review. *Journal of Composite Materials* **2012,** *47* (15), 1817-1832.
15. Krishnaraj, V.; Prabukarthi, A.; Ramanathan, A.; Elanghovan, N.; Senthil Kumar, M.; Zitoune, R.; Davim, J. P., Optimization of machining parameters at high speed drilling of carbon fiber reinforced plastic (CFRP) laminates. *Composites Part B: Engineering* **2012,** *43* (4), 1791-1799.
16. Pecat, O.; Rentsch, R.; Brinksmeier, E., Influence of milling process parameters on the surface integrity of CFRP. *Procedia Cirp* **2012,** *1*, 466-470.
17. Davim, J. P., *Machining composites materials*. John Wiley & Sons: 2013.
18. Isbilir, O.; Ghassemieh, E., Numerical investigation of the effects of drill geometry on drilling induced delamination of carbon fiber reinforced composites. *Composite Structures* **2013,** *105*, 126-133.
19. Panchagnula, K. K.; Palaniyandi, K., Drilling on fiber reinforced polymer/nanopolymer composite laminates: a review. *Journal of Materials Research and Technology* **2018,** *7* (2), 180-189.
20. Hegde, S.; Satish Shenoy, B.; Chethan, K. N., Review on carbon fiber reinforced polymer (CFRP) and their mechanical performance. *Materials Today: Proceedings* **2019,** *19*, 658-662.
21. Abrão, A. M.; Rubio, J. C. C.; Faria, P. E.; Davim, J. P., The effect of cutting tool geometry on thrust force and delamination when drilling glass fibre reinforced plastic composite. *Materials & Design* **2008,** *29* (2), 508-513.
22. Singh, I.; Bhatnagar, N.; Viswanath, P., Drilling of uni-directional glass fiber reinforced plastics: Experimental and finite element study. *Materials & Design* **2008,** *29* (2), 546-553.

23. Shyha, I.; Soo, S. L.; Aspinwall, D.; Bradley, S., Effect of laminate configuration and feed rate on cutting performance when drilling holes in carbon fibre reinforced plastic composites. *Journal of Materials Processing Technology* **2010,** *210* (8), 1023-1034.
24. Pyo Jung, J.; Woo Kim, G.; Yong Lee, K., Critical thrust force at delamination propagation during drilling of angle-ply laminates. *Composite Structures* **2005,** *68* (4), 391-397.
25. Durão, L. M. P.; de Moura, M. F. S. F.; Marques, A. T., Numerical simulation of the drilling process on carbon/epoxy composite laminates. *Composites Part A: Applied Science and Manufacturing* **2006,** *37* (9), 1325-1333.
26. Grilo, T. J.; Paulo, R. M. F.; Silva, C. R. M.; Davim, J. P., Experimental delamination analyses of CFRPs using different drill geometries. *Composites Part B: Engineering* **2013,** *45* (1), 1344-1350.
27. El-Sonbaty, I.; Khashaba, U. A.; Machaly, T., Factors affecting the machinability of GFR/epoxy composites. *Composite Structures* **2004,** *63* (3-4), 329-338.
28. Kubher, S.; Gururaja, S.; Zitoune, R., Numerical Modeling of Exit-Ply Delamination During Drilling of CFRPs Considering Thermal Effects. *International Journal for Computational Methods in Engineering Science and Mechanics* **2019,** *19* (6), 383-389.
29. Seo, J.; Banerjee, N.; Kim, Y.; Kim, D. C.; Park, H. W., Experimental and analytical investigation of the drilling forces of the carbon fiber reinforced plastics including thermal effects. *Journal of Manufacturing Processes* **2020,** *58*, 1126-1137.
30. Faraz, A.; Biermann, D.; Weinert, K., Cutting edge rounding: An innovative tool wear criterion in drilling CFRP composite laminates. *International Journal of Machine Tools and Manufacture* **2009,** *49* (15), 1185-1196.
31. Iliescu, D.; Gehin, D.; Gutierrez, M. E.; Girot, F., Modeling and tool wear in drilling of CFRP. *International Journal of Machine Tools and Manufacture* **2010,** *50* (2), 204-213.
32. Park, K.-H.; Beal, A.; Kim, D.; Kwon, P.; Lantrip, J., Tool wear in drilling of composite/titanium stacks using carbide and polycrystalline diamond tools. *Wear* **2011,** *271* (11-12), 2826-2835.
33. Khashaba, U. A., Drilling of polymer matrix composites: A review. *Journal of Composite Materials* **2013,** *47* (15), 1817-1832.
34. Wang, X.; Kwon, P. Y.; Sturtevant, C.; Kim, D.; Lantrip, J., Tool wear of coated drills in drilling CFRP. *Journal of Manufacturing Processes* **2013,** *15* (1), 127-135.
35. Che, D. M.; Saxena, I.; Han, P. D.; Guo, P.; Ehmann, K. F., Machining of Carbon Fiber Reinforced Plastics/Polymers: A Literature Review. *J Manuf Sci E-T Asme* **2014,** *136* (3).
36. Feito, N.; Diaz-Alvarez, J.; Diaz-Alvarez, A.; Cantero, J. L.; Miguelez, M. H., Experimental Analysis of the Influence of Drill Point Angle and Wear on the Drilling of Woven CFRPs. *Materials (Basel)* **2014,** *7* (6), 4258-4271.
37. Ramirez, C.; Poulachon, G.; Rossi, F.; M'Saoubi, R., Tool Wear Monitoring and Hole Surface Quality During CFRP Drilling. *Procedia CIRP* **2014,** *13*, 163-168.
38. Feito, N.; Milani, A. S.; Muñoz-Sánchez, A., Drilling optimization of woven CFRP laminates under different tool wear conditions: a multi-objective design of experiments approach. *Structural and Multidisciplinary Optimization* **2015,** *53* (2), 239-251.
39. Feito, N.; Diaz-Álvarez, J.; López-Puente, J.; Miguelez, M. H., Numerical analysis of the influence of tool wear and special cutting geometry when drilling woven CFRPs. *Composite Structures* **2016,** *138*, 285-294.
40. Gaugel, S.; Sripathy, P.; Haeger, A.; Meinhard, D.; Bernthaler, T.; Lissek, F.; Kaufeld, M.; Knoblauch, V.; Schneider, G., A comparative study on tool wear and laminate damage in drilling of carbon-fiber reinforced polymers (CFRP). *Composite Structures* **2016,** *155*, 173-183.
41. Poulachon, G.; Outeiro, J.; Ramirez, C.; André, V.; Abrivard, G., Hole Surface Topography and Tool Wear in CFRP Drilling. *Procedia CIRP* **2016,** *45*, 35-38.
42. Attanasio, A.; Faini, F.; Outeiro, J. C., FEM Simulation of Tool Wear in Drilling. *Procedia CIRP* **2017,** *58*, 440-444.
43. Caggiano, A.; Centobelli, P.; Nele, L.; Teti, R., Multiple Sensor Monitoring in Drilling of CFRP/CFRP Stacks for Cognitive Tool Wear Prediction and Product Quality Assessment. *Procedia*

CIRP **2017,** *62*, 3-8.
44. Rimpault, X.; Chatelain, J. F.; Klemberg-Sapieha, J. E.; Balazinski, M., Tool wear and surface quality assessment of CFRP trimming using fractal analyses of the cutting force signals. *CIRP Journal of Manufacturing Science and Technology* **2017,** *16*, 72-80.
45. Jamshidi, M.; Rimpault, X.; Balazinski, M.; Chatelain, J.-F., Fractal analysis implementation for tool wear monitoring based on cutting force signals during CFRP/titanium stack machining. *The International Journal of Advanced Manufacturing Technology* **2020,** *106* (9-10), 3859-3868.
46. Ranjan, J.; Patra, K.; Szalay, T.; Mia, M.; Gupta, M. K.; Song, Q.; Krolczyk, G.; Chudy, R.; Pashnyov, V. A.; Pimenov, D. Y., Artificial Intelligence-Based Hole Quality Prediction in Micro-Drilling Using Multiple Sensors. *Sensors (Basel)* **2020,** *20* (3).
47. Gaitonde, v.; Karnik, S.; Rubio, J. C.; Correia, A. E.; Abrao, A.; Davim, J. P., Analysis of parametric influence on delamination in high-speed drilling of carbon fiber reinforced plastic composites. *Journal of materials processing technology* **2008,** *203* (1-3), 431-438.
48. López-Puente, J.; Zaera, R.; Navarro, C., Experimental and numerical analysis of normal and oblique ballistic impacts on thin carbon/epoxy woven laminates. *Composites Part A: Applied Science and Manufacturing* **2008,** *39* (2), 374-387.
49. Rajasekaran, T.; Palanikumar, K.; Vinayagam, B. K., Application of fuzzy logic for modeling surface roughness in turning CFRP composites using CBN tool. *Production Engineering* **2011,** *5* (2), 191-199.
50. Kara, F.; Aslantas, K.; Çiçek, A., ANN and multiple regression method-based modelling of cutting forces in orthogonal machining of AISI 316L stainless steel. *Neural Computing and Applications* **2014,** *26* (1), 237-250.
51. Luiz Lara Oliveira, T.; Zitoune, R.; Ancelotti Jr, A. C.; Cunha Jr, S. S. d., Smart machining: Monitoring of CFRP milling using AE and IR. *Composite Structures* **2020,** *249*.
52. Geier, N.; Davim, J. P.; Szalay, T., Advanced cutting tools and technologies for drilling carbon fibre reinforced polymer (CFRP) composites: A review. *Composites Part A: Applied Science and Manufacturing* **2019,** *125*.
53. Schmidt, C.; Hocke, T.; Denkena, B., Artificial intelligence for non-destructive testing of CFRP prepreg materials. *Production Engineering* **2019,** *13* (5), 617-626.
54. Cuomo, S.; De Simone, M. E.; Andreades, C.; Ciampa, F.; Meo, M., Machine learning for impact detection on composite structures. *Materials Today: Proceedings* **2020**.
55. Caggiano, A.; Rimpault, X.; Teti, R.; Balazinski, M.; Chatelain, J.-F.; Nele, L., Machine learning approach based on fractal analysis for optimal tool life exploitation in CFRP composite drilling for aeronautical assembly. *CIRP Annals* **2018,** *67* (1), 483-486.
56. Fu, R.; Jia, Z.; Wang, F.; Jin, Y.; Sun, D.; Yang, L.; Cheng, D., Drill-exit temperature characteristics in drilling of UD and MD CFRP composites based on infrared thermography. *International Journal of Machine Tools and Manufacture* **2018,** *135*, 24-37.
57. Hrechuk, A.; Bushlya, V.; Ståhl, J.-E., Hole-quality evaluation in drilling fiber-reinforced composites. *Composite Structures* **2018,** *204*, 378-387.
58. Kim, D.-H.; Kim, T. J. Y.; Wang, X.; Kim, M.; Quan, Y.-J.; Oh, J. W.; Min, S.-H.; Kim, H.; Bhandari, B.; Yang, I.; Ahn, S.-H., Smart Machining Process Using Machine Learning: A Review and Perspective on Machining Industry. *International Journal of Precision Engineering and Manufacturing-Green Technology* **2018,** *5* (4), 555-568.
59. Kim, D. M.; Kim, D. Y.; Banerjee, N.; Park, H. W., Predictive modeling for the cryogenic cooling condition of the hard turning process. *The International Journal of Advanced Manufacturing Technology* **2018,** *99* (9-12), 2877-2891.
60. Li, H.; Qin, X.; Huang, T.; Liu, X.; Sun, D.; Jin, Y., Machining quality and cutting force signal analysis in UD-CFRP milling under different fiber orientation. *The International Journal of Advanced Manufacturing Technology* **2018,** *98* (9-12), 2377-2387.
61. Rimpault, X.; Chatelain, J.-F.; Klemberg-Sapieha, J.-E.; Balazinski, M., Fractal Analysis of Cutting Force and Acoustic Emission Signals During CFRP Machining. *Procedia CIRP* **2016,** *46*, 143-146.

62. Shetty, N.; Herbert, M. A.; Shetty, R.; Shetty, D. S.; Vijay, G. S., Soft computing techniques during drilling of bi-directional carbon fiber reinforced composite. *Applied Soft Computing* **2016,** *41*, 466-478.
63. Shunmugesh, K.; Panneerselvam, K., Machinability study of Carbon Fiber Reinforced Polymer in the longitudinal and transverse direction and optimization of process parameters using PSO–GSA. *Engineering Science and Technology, an International Journal* **2016,** *19* (3), 1552-1563.
64. Wang, C.; Cheng, K.; Rakowski, R.; Greenwood, D.; Wale, J., Comparative studies on the effect of pilot drillings with application to high-speed drilling of carbon fibre reinforced plastic (CFRP) composites. *The International Journal of Advanced Manufacturing Technology* **2016,** *89* (9-12), 3243-3255.
65. Abhishek, K.; Datta, S.; Mahapatra, S. S., Optimization of MRR, Surface Roughness, and Maximum Tool-Tip Temperature during Machining of CFRP Composites. *Materials Today: Proceedings* **2017,** *4* (2), 2761-2770.
66. Abhishek, K.; Kumar, V. R.; Datta, S.; Mahapatra, S. S., Parametric appraisal and optimization in machining of CFRP composites by using TLBO (teaching–learning based optimization algorithm). *Journal of Intelligent Manufacturing* **2017,** *28* (8), 1769-1785.
67. Sorrentino, L.; Turchetta, S.; Bellini, C., In process monitoring of cutting temperature during the drilling of FRP laminate. *Composite Structures* **2017,** *168*, 549-561.
68. Rimpault, X.; Balazinski, M.; Chatelain, J.-F., Fractal Analysis Application Outlook for Improving Process Monitoring and Machine Maintenance in Manufacturing 4.0. *Journal of Manufacturing and Materials Processing* **2018,** *2* (3).
69. Song, K. H.; Lee, D. Y., The State of the Art in Monitoring Technology of Machining Operations. *Journal of the Korean Society for Precision Engineering* **2018,** *35* (3), 293-304.
70. Pahuja, R.; Ramulu, M., Surface quality monitoring in abrasive water jet machining of Ti6Al4V–CFRP stacks through wavelet packet analysis of acoustic emission signals. *The International Journal of Advanced Manufacturing Technology* **2019,** *104* (9-12), 4091-4104.
71. Romoli, L.; Lutey, A. H. A., Quality monitoring and control for drilling of CFRP laminates. *Journal of Manufacturing Processes* **2019,** *40*, 16-26.
72. Pahuja, R.; Mamidala, R., Quality monitoring in milling of unidirectional CFRP through wavelet packet transform of force signals. *Procedia Manufacturing* **2020,** *48*, 388-399.
73. Serin, G.; Sener, B.; Ozbayoglu, A. M.; Unver, H. O., Review of tool condition monitoring in machining and opportunities for deep learning. *The International Journal of Advanced Manufacturing Technology* **2020,** *109* (3-4), 953-974.
74. Yashiro, T.; Ogawa, T.; Sasahara, H., Temperature measurement of cutting tool and machined surface layer in milling of CFRP. *International Journal of Machine Tools and Manufacture* **2013,** *70*, 63-69.
75. Che, D.; Saxena, I.; Han, P.; Guo, P.; Ehmann, K. F., Machining of Carbon Fiber Reinforced Plastics/Polymers: A Literature Review. *Journal of Manufacturing Science and Engineering* **2014,** *136* (3).
76. Dix, M.; Wertheim, R.; Schmidt, G.; Hochmuth, C., Modeling of drilling assisted by cryogenic cooling for higher efficiency. *CIRP Annals* **2014,** *63* (1), 73-76.
77. Lauro, C. H.; Brandão, L. C.; Baldo, D.; Reis, R. A.; Davim, J. P., Monitoring and processing signal applied in machining processes – A review. *Measurement* **2014,** *58*, 73-86.
78. Xu, J.; Mkaddem, A.; El Mansori, M., Recent advances in drilling hybrid FRP/Ti composite: A state-of-the-art review. *Composite Structures* **2016,** *135*, 316-338.
79. Morkavuk, S.; Köklü, U.; Bağcı, M.; Gemi, L., Cryogenic machining of carbon fiber reinforced plastic (CFRP) composites and the effects of cryogenic treatment on tensile properties: A comparative study. *Composites Part B: Engineering* **2018,** *147*, 1-11.
80. Geng, D.; Liu, Y.; Shao, Z.; Lu, Z.; Cai, J.; Li, X.; Jiang, X.; Zhang, D., Delamination formation, evaluation and suppression during drilling of composite laminates: A review. *Composite Structures* **2019,** *216*, 168-186.
81. Kim, J.; Kim, Y.-B.; Seo, J. W.; Park, H. W., Deburring drilled holes in CFRP composites with

large pulsed electron beam (LPEB) irradiation. *Journal of Manufacturing Processes* **2019,** *40*, 68-75.
82. Marques, A. T.; Durão, L. M.; Magalhães, A. G.; Silva, J. F.; Tavares, J. M. R. S., Delamination analysis of carbon fibre reinforced laminates: Evaluation of a special step drill. *Composites Science and Technology* **2009,** *69* (14), 2376-2382.
83. Voß, R.; Henerichs, M.; Rupp, S.; Kuster, F.; Wegener, K., Evaluation of bore exit quality for fibre reinforced plastics including delamination and uncut fibres. *CIRP Journal of Manufacturing Science and Technology* **2016,** *12*, 56-66.
84. Nikbakht, M.; Yousefi, J.; Hosseini-Toudeshky, H.; Minak, G., Delamination evaluation of composite laminates with different interface fiber orientations using acoustic emission features and micro visualization. *Composites Part B: Engineering* **2017,** *113*, 185-196.
85. Mohan, N. S.; Kulkarni, S. M.; Ramachandra, A., Delamination analysis in drilling process of glass fiber reinforced plastic (GFRP) composite materials. *Journal of Materials Processing Technology* **2007,** *186* (1-3), 265-271.
86. Davim, J.; Rubio, J.; Abrao, A., A novel approach based on digital image analysis to evaluate the delamination factor after drilling composite laminates. *Composites Science and Technology* **2007,** *67* (9), 1939-1945.
87. Tsao, C. C.; Hocheng, H.; Chen, Y. C., Delamination reduction in drilling composite materials by active backup force. *CIRP Annals* **2012,** *61* (1), 91-94.
88. Kourra, N.; Warnett, J. M.; Attridge, A.; Kiraci, E.; Gupta, A.; Barnes, S.; Williams, M. A., Metrological study of CFRP drilled holes with x-ray computed tomography. *The International Journal of Advanced Manufacturing Technology* **2015,** *78* (9-12), 2025-2035.
89. Haeger, A.; Schoen, G.; Lissek, F.; Meinhard, D.; Kaufeld, M.; Schneider, G.; Schuhmacher, S.; Knoblauch, V., Non-destructive Detection of Drilling-induced Delamination in CFRP and its Effect on Mechanical Properties. *Procedia Engineering* **2016,** *149*, 130-142.
90. Karnik, S. R.; Gaitonde, V. N.; Rubio, J. C.; Correia, A. E.; Abrão, A. M.; Davim, J. P., Delamination analysis in high speed drilling of carbon fiber reinforced plastics (CFRP) using artificial neural network model. *Materials & Design* **2008,** *29* (9), 1768-1776.
91. Abhishek, K.; Datta, S.; Mahapatra, S. S., Optimization of thrust, torque, entry, and exist delamination factor during drilling of CFRP composites. *The International Journal of Advanced Manufacturing Technology* **2014,** *76* (1-4), 401-416.
92. Melentiev, R.; Priarone, P. C.; Robiglio, M.; Settineri, L., Effects of Tool Geometry and Process Parameters on Delamination in CFRP Drilling: An Overview. *Procedia CIRP* **2016,** *45*, 31-34.
93. Giasin, K.; Ayvar-Soberanis, S., An Investigation of burrs, chip formation, hole size, circularity and delamination during drilling operation of GLARE using ANOVA. *Composite Structures* **2017,** *159*, 745-760.
94. Saoudi, J.; Zitoune, R.; Mezlini, S.; Gururaja, S.; Seitier, P., Critical thrust force predictions during drilling: Analytical modeling and X-ray tomography quantification. *Composite Structures* **2016,** *153*, 886-894.
95. Matsumura, T.; Tamura, S., Cutting Force Model in Drilling of Multi-layered Materials. *Procedia CIRP* **2013,** *8*, 182-187.
96. Santiuste, C.; Díaz-Álvarez, J.; Soldani, X.; Miguélez, H., Modelling thermal effects in machining of carbon fiber reinforced polymer composites. *Journal of Reinforced Plastics and Composites* **2013,** *33* (8), 758-766.
97. Shahrajabian, H.; Farahnakian, M., Modeling and multi-constrained optimization in drilling process of carbon fiber reinforced epoxy composite. *International Journal of Precision Engineering and Manufacturing* **2013,** *14* (10), 1829-1837.
98. Langella, A.; Nele, L.; Maio, A., A torque and thrust prediction model for drilling of composite materials. *Composites Part A: Applied Science and Manufacturing* **2005,** *36* (1), 83-93.
99. Guo, D. M.; Wen, Q.; Gao, H.; Bao, Y. J., Prediction of the cutting forces generated in the drilling of carbon-fibre-reinforced plastic composites using a twist drill. *Proceedings of the Institution of Mechanical Engineers, Part B: Journal of Engineering Manufacture* **2011,** *226* (1), 28-42.
100. Zhang, L. C.; Zhang, H. J.; Wang, X. M., A Force Prediction Model for Cutting Unidirectional

Fibre-Reinforced Plastics. *Machining Science and Technology* **2001,** *5* (3), 293-305.
101. Karpat, Y.; Bahtiyar, O.; Değer, B.; Kaftanoğlu, B., A mechanistic approach to investigate drilling of UD-CFRP laminates with PCD drills. *CIRP Annals* **2014,** *63* (1), 81-84.
102. Cheng, H.; Li, Y.; Zhang, K. F.; Luo, B., An Efficient Model for Trust Force Dynamic Analysis in Drilling of CFRP/AL Stack. *Applied Mechanics and Materials* **2012,** *249-250*, 263-269.
103. Meng, Q.; Zhang, K.; Cheng, H.; Liu, S.; Jiang, S., An analytical method for predicting the fluctuation of thrust force during drilling of unidirectional carbon fiber reinforced plastics. *Journal of Composite Materials* **2014,** *49* (6), 699-711.
104. Cheng, H.; Zhang, K.; Wang, N.; Luo, B.; Meng, Q., A novel six-state cutting force model for drilling-countersinking machining process of CFRP-Al stacks. *The International Journal of Advanced Manufacturing Technology* **2016,** *89* (5-8), 2063-2076.
105. Maegawa, S.; Morikawa, Y.; Hayakawa, S.; Itoigawa, F.; Nakamura, T., Mechanism for changes in cutting forces for down-milling of unidirectional carbon fiber reinforced polymer laminates: Modeling and experimentation. *International Journal of Machine Tools and Manufacture* **2016,** *100*, 7-13.
106. Sahraie Jahromi, A.; Bahr, B., An analytical method for predicting cutting forces in orthogonal machining of unidirectional composites. *Composites Science and Technology* **2010,** *70* (16), 2290-2297.
107. Phadnis, V. A.; Makhdum, F.; Roy, A.; Silberschmidt, V. V., Experimental and Numerical Investigations in Conventional and Ultrasonically Assisted Drilling of CFRP Laminate. *Procedia CIRP* **2012,** *1*, 455-459.
108. Feito, N.; López-Puente, J.; Santiuste, C.; Miguélez, M. H., Numerical prediction of delamination in CFRP drilling. *Composite Structures* **2014,** *108*, 677-683.
109. Qi, Z.; Zhang, K.; Cheng, H.; Liu, S., Numerical simulation for delamination during drilling of CFRP/AL stacks. *Materials Research Innovations* **2015,** *19* (sup6), S6-98-S6-101.
110. Zitoune, R.; Krishnaraj, V.; Collombet, F.; Le Roux, S., Experimental and numerical analysis on drilling of carbon fibre reinforced plastic and aluminium stacks. *Composite Structures* **2016,** *146*, 148-158.
111. Ramesh, M. V.; Seetharamu, K. N.; Ganesan, N.; Sivakumar, M. S., Analysis of machining of FRPs using FEM. *Int J Mach Tool Manu* **1998,** *38* (12), 1531-1549.
112. Mahdi, M.; Zhang, L. C., A finite element model for the orthogonal cutting of fiber-reinforced composite materials. *Journal of Materials Processing Technology* **2001,** *113* (1-3), 373-377.
113. Usui, S.; Wadell, J.; Marusich, T., Finite Element Modeling of Carbon Fiber Composite Orthogonal Cutting and Drilling. *Procedia CIRP* **2014,** *14*, 211-216.
114. Smolenicki, D.; Boos, J.; Kuster, F.; Roelofs, H.; Wyen, C. F., In-process measurement of friction coefficient in orthogonal cutting. *CIRP Annals* **2014,** *63* (1), 97-100.
115. Cheng, H.; Gao, J.; Kafka, O. L.; Zhang, K.; Luo, B.; Liu, W. K., A micro-scale cutting model for UD CFRP composites with thermo-mechanical coupling. *Composites Science and Technology* **2017,** *153*, 18-31.
116. Abena, A.; Soo, S. L.; Essa, K., Modelling the orthogonal cutting of UD-CFRP composites: Development of a novel cohesive zone model. *Composite Structures* **2017,** *168*, 65-83.
117. Wu, M.; Gao, Y.; Cheng, Y.; Wang, B.; Huo, T., Carbon Fiber Composite Materials Finite Element Simulation Analysis of Cutting Force. *Procedia CIRP* **2016,** *56*, 109-114.
118. Phadnis, V. A.; Roy, A.; Silberschmidt, V. V., Finite element analysis of drilling in carbon fiber reinforced polymer composites. *Journal of Physics: Conference Series* **2012,** *382*.
119. Isbilir, O.; Ghassemieh, E., Finite Element Analysis of Drilling of Carbon Fibre Reinforced Composites. *Applied Composite Materials* **2011,** *19* (3-4), 637-656.
120. Phadnis, V. A.; Roy, A.; Silberschmidt, V. V., A Finite Element Model of Ultrasonically Assisted Drilling in Carbon/Epoxy Composites. *Procedia CIRP* **2013,** *8*, 141-146.
121. Shetty, N.; Shahabaz, S. M.; Sharma, S. S.; Divakara Shetty, S., A review on finite element method for machining of composite materials. *Composite Structures* **2017,** *176*, 790-802.
122. Wang, G.-D.; Melly, S. K., Three-dimensional finite element modeling of drilling CFRP composites using Abaqus/CAE: a review. *The International Journal of Advanced Manufacturing*

Technology **2017,** *94* (1-4), 599-614.
123. Al-wandi, S.; Ding, S.; Mo, J., An approach to evaluate delamination factor when drilling carbon fiber-reinforced plastics using different drill geometries: experiment and finite element study. *The International Journal of Advanced Manufacturing Technology* **2017,** *93* (9-12), 4043-4061.
124. Giasin, K.; Ayvar-Soberanis, S.; French, T.; Phadnis, V., 3D Finite Element Modelling of Cutting Forces in Drilling Fibre Metal Laminates and Experimental Hole Quality Analysis. *Applied Composite Materials* **2016,** *24* (1), 113-137.
125. Santiuste, C.; Soldani, X.; Miguélez, M. H., Machining FEM model of long fiber composites for aeronautical components. *Composite Structures* **2010,** *92* (3), 691-698.
126. Rentsch, R.; Pecat, O.; Brinksmeier, E., Macro and micro process modeling of the cutting of carbon fiber reinforced plastics using FEM. *Procedia Engineering* **2011,** *10*, 1823-1828.
127. Chakladar, N. D.; Pal, S. K.; Mandal, P., Drilling of woven glass fiber-reinforced plastic—an experimental and finite element study. *The International Journal of Advanced Manufacturing Technology* **2011,** *58* (1-4), 267-278.
128. Diaz-Alvarez, J.; Olmedo, A.; Santiuste, C.; Miguelez, M. H., Theoretical Estimation of Thermal Effects in Drilling of Woven Carbon Fiber Composite. *Materials (Basel)* **2014,** *7* (6), 4442-4454.
129. Eneyew, E. D.; Ramulu, M., Experimental study of surface quality and damage when drilling unidirectional CFRP composites. *Journal of Materials Research and Technology* **2014,** *3* (4), 354-362.
130. Turki, Y.; Habak, M.; Velasco, R.; Aboura, Z.; Khellil, K.; Vantomme, P., Experimental investigation of drilling damage and stitching effects on the mechanical behavior of carbon/epoxy composites. *International Journal of Machine Tools and Manufacture* **2014,** *87*, 61-72.
131. Feito, N.; Diaz-Álvarez, A.; Cantero, J. L.; Rodríguez-Millán, M.; Miguélez, H., Experimental analysis of special tool geometries when drilling woven and multidirectional CFRPs. *Journal of Reinforced Plastics and Composites* **2015,** *35* (1), 33-55.
132. Kumar, D.; Singh, K. K.; Zitoune, R., Experimental investigation of delamination and surface roughness in the drilling of GFRP composite material with different drills. *Advanced Manufacturing: Polymer & Composites Science* **2016,** *2* (2), 47-56.
133. Li, Z.; Yang, D.; Hao, W.; Wu, T.; Wu, S.; Li, X., A novel technique for micro-hole forming on skull with the assistance of ultrasonic vibration. *J Mech Behav Biomed Mater* **2016,** *57*, 1-13.
134. Geng, D.; Zhang, D.; Li, Z.; Liu, D., Feasibility study of ultrasonic elliptical vibration-assisted reaming of carbon fiber reinforced plastics/titanium alloy stacks. *Ultrasonics* **2017,** *75*, 80-90.
135. Karam, E. C.; Hawileh, R. A.; El Maaddawy, T.; Abdalla, J. A., Experimental investigations of repair of pre-damaged steel-concrete composite beams using CFRP laminates and mechanical anchors. *Thin-Walled Structures* **2017,** *112*, 107-117.
136. Phapale, K.; Ahire, A.; Singh, R., Experimental characterization and finite element modeling of critical thrust force in cfrp drilling. *Machining Science and Technology* **2017,** *22* (2), 249-270.
137. Wang, G.-D.; Melly, S. K.; Li, N., Using dampers to mitigate thrust forces during carbon-fibre reinforced polymer drilling: Experimental and finite element evaluation. *Journal of Reinforced Plastics and Composites* **2017,** *37* (1), 60-74.
138. Perret, O.; Lebée, A.; Douthe, C.; Sab, K., Experimental determination of the equivalent-layer shear stiffness of CLT through four-point bending of sandwich beams. *Construction and Building Materials* **2018,** *186*, 1132-1143.
139. Xu, J.; Li, C.; Dang, J.; El Mansori, M.; Ren, F., A Study on Drilling High-Strength CFRP Laminates: Frictional Heat and Cutting Temperature. *Materials (Basel)* **2018,** *11* (12).
140. Zhou, F.; Zhang, J.; Song, S.; Yang, D.; Wang, C., Effect of temperature on material properties of carbon fiber reinforced polymer (CFRP) tendons: experiments and model assessment. *Materials* **2019,** *12* (7), 1025.
141. Brinksmeier, E.; Janssen, R., Drilling of Multi-Layer Composite Materials consisting of Carbon Fiber Reinforced Plastics (CFRP), Titanium and Aluminum Alloys. *CIRP Annals* **2002,** *51* (1), 87-90.
142. Chowdhury, F. H.; Hosur, M. V.; Jeelani, S., Studies on the flexural and thermomechanical properties of woven carbon/nanoclay-epoxy laminates. *Materials Science and Engineering: A* **2006,**

421 (1-2), 298-306.
143. Attaran, A.; Majid, D. L.; Basri, S.; Mohd Rafie, A. S.; Abdullah, E. J., Structural optimization of an aeroelastically tailored composite flat plate made of woven fiberglass/epoxy. *Acta Mechanica* **2007,** *196* (3-4), 161-173.
144. Shenghu, C.; Zhis, W. U.; Xin, W., Tensile Properties of CFRP and Hybrid FRP Composites at Elevated Temperatures. *Journal of Composite Materials* **2009,** *43* (4), 315-330.
145. Iliescu, D.; Gehin, D.; Iordanoff, I.; Girot, F.; Gutiérrez, M. E., A discrete element method for the simulation of CFRP cutting. *Composites Science and Technology* **2010,** *70* (1), 73-80.
146. Rahmé, P.; Landon, Y.; Lachaud, F.; Piquet, R.; Lagarrigue, P., Analytical models of composite material drilling. *The International Journal of Advanced Manufacturing Technology* **2010,** *52* (5-8), 609-617.
147. Karpat, Y.; Bahtiyar, O., Energy Based Investigation of Process Parameters While Drilling Carbon Fiber Reinforced Polymers. *Procedia CIRP* **2016,** *46*, 59-62.
148. Geier, N.; Szalay, T., Optimisation of process parameters for the orbital and conventional drilling of uni-directional carbon fibre-reinforced polymers (UD-CFRP). *Measurement* **2017,** *110*, 319-334.
149. Leo Kumar, S. P., State of The Art-Intense Review on Artificial Intelligence Systems Application in Process Planning and Manufacturing. *Engineering Applications of Artificial Intelligence* **2017,** *65*, 294-329.
150. Ojo, S. O.; Ismail, S. O.; Paggi, M.; Dhakal, H. N., A new analytical critical thrust force model for delamination analysis of laminated composites during drilling operation. *Composites Part B: Engineering* **2017,** *124*, 207-217.
151. Davim, J. P.; Reis, P., Drilling carbon fiber reinforced plastics manufactured by autoclave—experimental and statistical study. *Materials & Design* **2003,** *24* (5), 315-324.
152. Karpat, Y.; Bahtiyar, O., Comparative Analysis of PCD Drill Designs During Drilling of CFRP Laminates. *Procedia CIRP* **2015,** *31*, 316-321.
153. Karpat, Y.; Bahtiyar, O., Tool geometry based prediction of critical thrust force while drilling carbon fiber reinforced polymers. *Advances in Manufacturing* **2015,** *3* (4), 300-308.
154. Heisel, U.; Pfeifroth, T., Influence of Point Angle on Drill Hole Quality and Machining Forces When Drilling CFRP. *Procedia CIRP* **2012,** *1*, 471-476.
155. Ismail, S. O.; Dhakal, H. N.; Dimla, E.; Popov, I., Recent advances in twist drill design for composite machining: A critical review. *Proceedings of the Institution of Mechanical Engineers, Part B: Journal of Engineering Manufacture* **2016,** *231* (14), 2527-2542.
156. Lopresto, V.; Caggiano, A.; Teti, R., High Performance Cutting of Fibre Reinforced Plastic Composite Materials. *Procedia CIRP* **2016,** *46*, 71-82.
157. Wang, C.; Ming, W.; An, Q.; Chen, M., Machinability characteristics evolution of CFRP in a continuum of fiber orientation angles. *Materials and Manufacturing Processes* **2016,** *32* (9), 1041-1050.
158. Altin Karataş, M.; Motorcu, A. R.; Gökkaya, H., Optimization of machining parameters for kerf angle and roundness error in abrasive water jet drilling of CFRP composites with different fiber orientation angles. *Journal of the Brazilian Society of Mechanical Sciences and Engineering* **2020,** *42* (4).
159. Luo, B.; Li, Y.; Zhang, K.; Cheng, H.; Liu, S., A novel prediction model for thrust force and torque in drilling interface region of CFRP/Ti stacks. *The International Journal of Advanced Manufacturing Technology* **2015,** *81* (9-12), 1497-1508.
160. Mortazavian, S.; Fatemi, A., Effects of fiber orientation and anisotropy on tensile strength and elastic modulus of short fiber reinforced polymer composites. *Composites Part B: Engineering* **2015,** *72*, 116-129.
161. Li, M. J.; Soo, S. L.; Aspinwall, D. K.; Pearson, D.; Leahy, W., Influence of Lay-up Configuration and Feed Rate on Surface Integrity when Drilling Carbon Fibre Reinforced Plastic (CFRP) Composites. *Procedia CIRP* **2014,** *13*, 399-404.
162. Soepangkat, B. O. P.; Norcahyo, R.; Effendi, M. K.; Pramujati, B., Multi-response optimization of carbon fiber reinforced polymer (CFRP) drilling using back propagation neural

network-particle swarm optimization (BPNN-PSO). *Engineering Science and Technology, an International Journal* **2020,** *23* (3), 700-713.
163. Merino-Pérez, J. L.; Royer, R.; Merson, E.; Lockwood, A.; Ayvar-Soberanis, S.; Marshall, M. B., Influence of workpiece constituents and cutting speed on the cutting forces developed in the conventional drilling of CFRP composites. *Composite Structures* **2016,** *140*, 621-629.
164. Marco, M.; Rodriguez-Millan, M.; Santiuste, C.; Giner, E.; Henar Miguelez, M., A review on recent advances in numerical modelling of bone cutting. *J Mech Behav Biomed Mater* **2015,** *44*, 179-201.
165. Liu, L.; Qi, C.; Wu, F.; Yu, F.; Zhu, X., The effect of support on multi-hole drilling for glass fiber-reinforced plastic composite materials. *The International Journal of Advanced Manufacturing Technology* **2017,** *93* (1-4), 953-965.
166. Zhang, Y.; Wu, D.; Chen, K., A theoretical model for predicting the CFRP drilling-countersinking thrust force of stacks. *Composite Structures* **2019,** *209*, 337-348.
167. Amuthakkannan, P.; Manikandan, V.; Jappes, J. W.; Uthayakumar, M., Effect of fibre length and fibre content on mechanical properties of short basalt fibre reinforced polymer matrix composites. *Materials Physics and Mechanics* **2013,** *16* (2), 107-117.
168. Naveen, J.; Jawaid, M.; Amuthakkannan, P.; Chandrasekar, M., Mechanical and physical properties of sisal and hybrid sisal fiber-reinforced polymer composites. In *Mechanical and physical testing of biocomposites, fibre-reinforced composites and hybrid composites*, Elsevier: 2019; pp 427-440.
169. Rahamathullah, I.; Shunmugam, M. S., Mechanistic approach for prediction of forces in micro-drilling of plain and glass-reinforced epoxy sheets. *The International Journal of Advanced Manufacturing Technology* **2014,** *75* (5-8), 1177-1187.
170. Qi, Z.; Zhang, K.; Cheng, H.; Wang, D.; Meng, Q., Microscopic mechanism based force prediction in orthogonal cutting of unidirectional CFRP. *The International Journal of Advanced Manufacturing Technology* **2015,** *79* (5-8), 1209-1219.
171. Anand, R. S.; Patra, K., Mechanistic cutting force modelling for micro-drilling of CFRP composite laminates. *CIRP Journal of Manufacturing Science and Technology* **2017,** *16*, 55-63.
172. Kumar, R.; Agrawal, P. K.; Singh, I., Fabrication of micro holes in CFRP laminates using EDM. *Journal of Manufacturing Processes* **2018,** *31*, 859-866.
173. Grund, D.; Orlishausen, M.; Taha, I., Determination of fiber volume fraction of carbon fiber-reinforced polymer using thermogravimetric methods. *Polymer Testing* **2019,** *75*, 358-366.
174. Olmedo, A.; Santiuste, C.; Barbero, E., An analytical model for the secondary bending prediction in single-lap composite bolted-joints. *Composite Structures* **2014,** *111*, 354-361.
175. Qi, Z.; Zhang, K.; Li, Y.; Liu, S.; Cheng, H., Critical thrust force predicting modeling for delamination-free drilling of metal-FRP stacks. *Composite Structures* **2014,** *107*, 604-609.
176. Vankanti, V. K.; Ganta, V., Optimization of process parameters in drilling of GFRP composite using Taguchi method. *Journal of Materials Research and Technology* **2014,** *3* (1), 35-41.
177. An, Q.; Ming, W.; Cai, X.; Chen, M., Study on the cutting mechanics characteristics of high-strength UD-CFRP laminates based on orthogonal cutting method. *Composite Structures* **2015,** *131*, 374-383.
178. Merino-Pérez, J. L.; Royer, R.; Ayvar-Soberanis, S.; Merson, E.; Hodzic, A., On the temperatures developed in CFRP drilling using uncoated WC-Co tools Part I: Workpiece constituents, cutting speed and heat dissipation. *Composite Structures* **2015,** *123*, 161-168.
179. Liu, H.; Sun, X.; Xu, Y.; Chu, X., A hierarchical multilevel finite element method for mechanical analyses of periodical composite structures. *Composite Structures* **2015,** *131*, 115-127.
180. Seo, J.; Kim, Y.; Kim, D. C.; Park, H. W., Numerical and experimental investigation of the delamination in drilling of the carbon fiber-reinforced plastic composite. *The International Journal of Advanced Manufacturing Technology* **2021**.
181. Santiuste, C.; Rodríguez-Millán, M.; Giner, E.; Miguélez, H., The influence of anisotropy in numerical modeling of orthogonal cutting of cortical bone. *Composite Structures* **2014,** *116*, 423-431.
182. *Abaqus 6.14 User'sManual*. Dassault Systèmes Simulia Corp: Providence, RI.

183. Santiuste, C.; Olmedo, A.; Soldani, X.; Miguélez, H., Delamination prediction in orthogonal machining of carbon long fiber-reinforced polymer composites. *Journal of Reinforced Plastics and Composites* **2012,** *31* (13), 875-885.
184. Singh, A. P.; Sharma, M.; Singh, I., A review of modeling and control during drilling of fiber reinforced plastic composites. *Compos Part B-Eng* **2013,** *47*, 118-125.
185. Chaudhari, A. B.; Chaudhary, V.; Gohil, P.; Patel, K., Investigation of Delamination Factor in High Speed Drilling on Chopped GFRP Using ANFIS. *Procedia Technology* **2016,** *23*, 272-279.
186. Hocheng, H.; Tsao, C. C.; Chen, H. T., Utilizing internal icing force to reduce delamination in drilling composite tubes. *Composite Structures* **2016,** *139*, 36-41.
187. Joshi, S.; Rawat, K.; A.S.S, B., A novel approach to predict the delamination factor for dry and cryogenic drilling of CFRP. *Journal of Materials Processing Technology* **2018,** *262*, 521-531.
188. Sorrentino, L.; Turchetta, S.; Bellini, C., A new method to reduce delaminations during drilling of FRP laminates by feed rate control. *Composite Structures* **2018,** *186*, 154-164.
189. Girot, F.; Dau, F.; Gutiérrez-Orrantia, M. E., New analytical model for delamination of CFRP during drilling. *Journal of Materials Processing Technology* **2017,** *240*, 332-343.
190. Ismail, S. O.; Ojo, S. O.; Dhakal, H. N., Thermo-mechanical modelling of FRP cross-ply composite laminates drilling: Delamination damage analysis. *Composites Part B: Engineering* **2017,** *108*, 45-52.
191. Shan, C.; Lin, X.; Wang, X.; Yan, J.; Cui, D., Defect analysis in drilling needle-punched carbon–carbon composites perpendicular to nonwoven fabrics. *Advances in Mechanical Engineering* **2015,** *7* (8).
192. Wang, C.-Y.; Chen, Y.-H.; An, Q.-L.; Cai, X.-J.; Ming, W.-W.; Chen, M., Drilling temperature and hole quality in drilling of CFRP/aluminum stacks using diamond coated drill. *International Journal of Precision Engineering and Manufacturing* **2015,** *16* (8), 1689-1697.
193. Wang, P.; He, R.; Chen, H.; Zhu, X.; zhao, Q.; Fang, D., A novel predictive model for mechanical behavior of single-lap GFRP composite bolted joint under static and dynamic loading. *Composites Part B: Engineering* **2015,** *79*, 322-330.
194. Yuan, S.; Zhang, C.; Amin, M.; Fan, H.; Liu, M., Development of a cutting force prediction model based on brittle fracture for carbon fiber reinforced polymers for rotary ultrasonic drilling. *The International Journal of Advanced Manufacturing Technology* **2015,** *81* (5-8), 1223-1231.
195. Zarif Karimi, N.; Minak, G.; Kianfar, P., Analysis of damage mechanisms in drilling of composite materials by acoustic emission. *Composite Structures* **2015,** *131*, 107-114.
196. Abhishek, K.; Kumar, V. R.; Datta, S.; Mahapatra, S. S., Application of JAYA algorithm for the optimization of machining performance characteristics during the turning of CFRP (epoxy) composites: comparison with TLBO, GA, and ICA. *Engineering with Computers* **2016,** *33* (3), 457-475.
197. Erkan, Ö.; Işık, B.; Çiçek, A.; Kara, F., Prediction of Damage Factor in end Milling of Glass Fibre Reinforced Plastic Composites Using Artificial Neural Network. *Applied Composite Materials* **2012,** *20* (4), 517-536.
198. Mayuet, P.; Gallo, A.; Portal, A.; Arroyo, P.; Alvarez, M.; Marcos, M., Damaged Area based Study of the Break-IN and Break-OUT Defects in the Dry Drilling of Carbon Fiber Reinforced Plastics (CFRP). *Procedia Engineering* **2013,** *63*, 743-751.
199. Kumar, D.; Singh, K. K., An approach towards damage free machining of CFRP and GFRP composite material: a review. *Advanced Composite Materials* **2014,** *24* (sup1), 49-63.
200. Pecat, O.; Brinksmeier, E., Low Damage Drilling of CFRP/Titanium Compound Materials for Fastening. *Procedia CIRP* **2014,** *13*, 1-7.
201. Bonnet, C.; Poulachon, G.; Rech, J.; Girard, Y.; Costes, J. P., CFRP drilling: Fundamental study of local feed force and consequences on hole exit damage. *International Journal of Machine Tools and Manufacture* **2015,** *94*, 57-64.
202. Sadek, A.; Shi, B.; Meshreki, M.; Duquesne, J.; Attia, M. H., Prediction and control of drilling-induced damage in fibre-reinforced polymers using a new hybrid force and temperature modelling approach. *CIRP Annals* **2015,** *64* (1), 89-92.

ACKNOWLEDGEMENT

When I first came to UNIST with the title of ‘Adult’ in 2009, I never imagined that I would spend my entire 20s here. A little over 10 years have been spent here, a lot has happened, and I have tried to make as many experiences as possible. Since 2009, through the decisions and choices I thought were the best at each moment, I came to this state now, and although there are still some regrets, I feel that I have lived a life that is not over lacking or excessive. I would like to express my gratitude first to my parents who supported me silently and supported me through prayer during this long time. The prayer and support of my sister, brother-in-law, and nephews Dongju and Dongbin were also of great help.

My life as a researcher began as an undergraduate researcher in Prof. Hyung Wook Park's Multiscale Hybrid Manufacturing Lab in the Department of Mechanical Engineering and got the title of Ph.D. in the same space. I respect and appreciate Prof. Hyung Wook Park who has guided and supported me during the long period of undergraduate research students, master's, and doctoral programs. I was able to learn both my professionalism as a researcher and my behavior as a member of society, and I will deeply engrave it in the future. I also thank Prof. Young-Bin Park. He has participated all of my master's and doctoral programs’ committee member, and have always shown an example of respectful scholar. I am also grateful to Prof. Namhun Kim to be my thesis committee member. When I was an undergraduate student, he gave me a chance to expand my knowledge with lab tour in USA. Besides. he always has treated me kindly during undergraduates and graduate period. I am also grateful to Prof. Sang hoon Kang, who was willing to participate as a committee member, although he did not know me well. And the comments during the defense were great help giving me new insights to the research. Lastly, I would like to thank Prof. Hae-Jin Choi of Chung-Ang University for participating my Ph. D defense presentation and advise me from a long distance.

Lastly, I would like to express my gratitude to all of the graduates of Multiscale Hybrid Manufacturing lab, Dr. Eunju Park, Dr. Dongmin Kim, Prof. Jisoo Kim, Prof. Doyoung Kim, and Youngbin Kim and Minji Kim. Also, I would like to say thank you to the current lab members Dr. Biplab K. Deka, Dr. Ankita Hazarika, Hyunmin Park, Ahra Jeon, Hae gu Lee, Yun jae Hwang, Sang min Yang, and Anand Prakash Jaiswal. In particular, I wish Dongchan Kim and Chang hyeon Mun, who are currently dispatched to Canada, to complete their Ph.D program without any problems in the future. I also would like to express my great gratitude to Jaehoon Cha and Jinsik Kim of the ‘Maker lab’ who helped me with my machining experiments and supported me with their techniques for a long time.